Rijksuniversiteit Groningen

Modelling the hydrodynamics of swimming fish, from individuals to infinite schools

Proefschrift

ter verkrijging van het doctoraat in de
Wiskunde en Natuurwetenschappen
aan de Rijksuniversiteit Groningen
op gezag van de
Rector Magnificus, dr. E. Sterken,
in het openbaar te verdedigen op
maandag 26 september 2011
om 13.15 uur

door

Daniel Alexander Peter Reid

geboren op 26 september 1978
te Westeremden

Promotor	:	Prof. dr. C. K. Hemelrijk
Copromotor	:	Dr. J. T. Padding
Beoordelingscommissie	:	Prof. dr. J. J. Videler
		Prof. dr. G. Gompper
		Prof. dr. Ir. J. van Leeuwen

ISBN: 978-90-367-5122-3
ISBN: 978-90-367-5123-0 (electronic version)

CONTENTS

SAMENVATTING

Dit proefschrift richt zich op het bestuderen van de hydrodynamica van vissen die zwemmen door hun lichaam gestaag te golven. Hiertoe wenden wij een computer model (de zogeheten Multiparticle Collision Dynamics methode) en een meta-analyse van gepubliceerde data over de kinematica van zwemmende vissen aan.

In het computermodel worden het water en zijn dynamica gesimuleerd door middel van miljoenen deeltjes, die rondbewegen en met elkaar botsen. Uit dit gedrag op de microschaal ontstaat op de macroschaal gedrag dat hydrodynamisch klopt. Door niet-bewegende vormen te bestuderen in een kanaal waardoorheen water vloeit ontdekken we dat het toevoegen van lange, staartachtige platen aan de stroomafwaartse zijde van een cylinder de waterweerstand verhoogt bij lage Reynoldsgetallen, maar verlaagt bij hogere Reynoldsgetallen. Dit suggereert dat het alleen voor relatief grote organismen nuttig is om een staart te hebben. Hiernaast bestuderen we de hydrodynamica van vormen die kunnen veranderen van positie, hoek en vorm, namelijk een slaande insectenvleugel (ter validatie van de methode) en een golvende vis. De resultaten komen in beide gevallen overeen met data uit experimenten. We tonen aan dat de veelgebruikte techniek om in simulaties van het zemmen van vissen ze te beperken zodat ze niet kunnen accelereren de resultaten kan beinvloeden. We vinden geen effect van het beperken van acceleratie in de lengterichting. Wanneer echter de acceleratie in de zijdelingse richting voorkomen wordt dan neemt de zwemsnelheid toe, en worden de kracht- en stroompatronen versterkt, zodat zij lijken op die van een vrij-zwemmende vis met een hogere staartslagfrequentie. Ons derde onderzoek betreft oneindig grote scholen van vissen, in verscheidene ruimtelijke configuraties in het computermodel. We bestuderen de configuratie met een ruitvormig rooster die in theorie optimaal is, en een rechthoekige roosterstructuur. Verder simuleren we een oneindig lange stoet (de 'rij') en een oneindig brede 'falanx' om zo de effecten van het hebben van buren in de lengte- dan wel breedterichting te scheiden.

Onze resultaten zijn in enkele opzichten naar verwachting: we bevestigen theoretische voorspellingen dat het hebben van zijdelingse buren de efficiëntie positief beinvloedt, en dat in een dicht opeengepakte ruitstructuur de individuen een gebied met lage stroomsnelheid voor zich vinden. Onverwacht is echter dat deze dichte ruitstructuur in ons model niet optimaal efficiënt is. Interessant genoeg tonen wij ook aan dat in de meeste gevallen het voordelig is qua zwemsnelheid en efficiëntie om direct in het onverstoorde kielzog van een voorganger te zwemmen.

We breiden de inzichten die wij uit onze simulatieonderzoeken hebben opgedaan verder uit door middel van een meta-analyse van de wetenschappelijke literatuur over gestaag zwemmende echte vissen. De grootte van de dataverzameling leidt tot enkele significante bevindingen die ongeacht de vissoort geldig zijn. Met name belangrijk is dat we aantonen dat de achterwaartse snelheid V van de voortstuwende lichaamsgolf verreweg de belangrijkste factor is voor het bepalen van de uiteindelijke zwemsnelheid U. Hiernaast ontdekken we

onder andere nog dat de zogeheten 'slip ratio' (U/V) afhangt van het Reynoldsgetal, wat ook in ons computermodel het geval is.

Samenvattend leidt dit proefschrift tot een beter begrip van de hydrodynamica van gestaag zwemmen door het golven van het lichaam, zowel van enkele zwemmers als van groepen.

SUMMARY

This thesis investigates the hydrodynamics of fish that swim by steady undulation of their body. This is done by means of a computer model (specifically the Multiparticle Collision Dynamics method) and of a meta-analysis of published experimental data.

In the computer model, the water and its dynamics are simulated by means of millions of particles that move and collide. From this behaviour at the micro-scale, correct hydrodynamics emerge at the macro-scale. From studying static shapes in flow in a channel we find that when attaching long tail-like plates, drag increases at low Reynolds numbers but decreases at higher ones, suggesting that tails are only useful for larger organisms. Further, we examine the hydrodynamics of single shapes that change their position, orientation and form: a flapping insect wing (for validation purposes) and an undulating fish. The results of both cases agree with experimental data. We show that the commonly used practice in simulations of fish swimming to constrain the fish from accelerating can influence results. We find no effect of constraint of acceleration in the longitudinal direction. On the other hand, constraint in the lateral direction increases the swimming speed and exaggerates patterns of force and flow, so that they resemble those of unconstrained fish with higher tailbeat frequencies. Our third study concerns infinite schools of fish in several different spatial configurations in the model. We investigate the diamond-shaped lattice that is theoretically optimal and a rectangular lattice. Further, to separate out the effects of longitudinal and lateral neighbours we simulate an infinitely long progression, or 'line' and an infinitely wide 'phalanx'. Our results confirm theoretical predictions that having lateral neighbours is beneficial for efficiency, and that a closely-spaced diamond lattice causes individuals to encounter a low-velocity area ahead of them. Unexpectedly however, the prediction that this pattern of the closely-packed diamond lattice increases efficiency is not borne out by our results. Remarkably we also show that in most cases swimming directly behind a fish in its undisturbed wake is beneficial as regards speed and efficiency.

We extend the insights gained from our simulations by means of a meta-analysis of the scientific literature on steady swimming of real fish. The size of our data set leads to several significant insights that apply across species. Most importantly, we show that the strongest predictor of swimming speed U is the speed V of the rearwards-traveling body wave. Further insights include the fact that the slip ratio U/V is a function of the Reynolds number (which is also the case in our model).

In conclusion, this thesis increases the understanding of steady, undulatory swimming, both alone and in groups.

STRESZCZENIE

Głównym tematem niniejszej pracy doktorskiej jest badanie hydrodynamiki ryb pływających przy pomocy ruchów falistych ciała. W pracy zastosowano model komputerowy (a ściśle metodę Dynamiki Zderzeń Wielocząsteczkowych, Multiparticle Collision Dynamics method) oraz meta-analizę danych eksperymentalnych z publikacji naukowych. W modelu komputerowym woda i jej dynamika są symulowane przy pomocy milionów cząstek, które poruszają się i zderzają ze sobą. Z zachowania cząstek w mikroskali wyłania się poprawna hydrodynamika w makroskali. Symulacje nieruchomych obiektów w strumieniu wody w tunelu pokazały, że przyłączenie długich, podobnych do ogona płyt zwiększa opór przy małych liczbach Reynoldsa, ale zmniejsza go przy większych liczbach Reynoldsa, co sugeruje, że ogon jest przydatny tylko większym organizmom. Dodatkowo badaliśmy pojedyncze obiekty, które zmieniają swoją pozycję, orientację i formę, a ściśle – machające skrzydło owadzie (w celach walidacji metody) i płynącą rybę. Wyniki dla obu przypadków są zgodne z danymi eksperymentalnymi. Pokazaliśmy także, że częsta w symulacjach komputerowych praktyka ograniczania ruchu ryby, tak by nie przyśpieszała, może wpływać na wyniki. Uniemożliwienie przyśpieszenia (zwalniania) ryby w przód nie wpływa znacząco na wyniki, jednak ograniczenie ruchu ryby w bok powoduje, że prędkość ryby do przodu wzrasta, a wzorce sił i przepływu są wyolbrzymione, co przypomina wyniki uzyskane w przypadku swobodnie płynącej ryby, poruszającej się z wyższą częstotliwością uderzeń ogona. Nasz ostatni model bada nieskończone ławice ryb w różnych konfiguracjach. Badaliśmy teoretycznie optymalną siatkę w kształcie rombu oraz siatkę w kształcie prostokąta. Dodatkowo aby oddzielić wpływ sąsiedztwa innych ryb z boku od wpływu sąsiedztwa innych ryb z przodu/tyłu, przeprowadziliśmy symulacje nieskończonej „kolumny" i nieskończonego „szeregu" ryb. Z jednej strony nasze wyniki są zgodne z teoretycznymi przewidywaniami, gdyż pokazują, że posiadanie sąsiadów z boku jest korzystne dla wydajności oraz że ciasny szyk siatki w kształcie rombu powoduje, że osobniki napotykają przed sobą obszar o niskiej prędkości wody. Z drugiej jednak strony zaskakujące jest to, że wyniki nie potwierdzają przewidywania, że ciasny szyk siatki w kształcie rombu zwiększa wydajność. Pokazaliśmy również, co ciekawe, że w większości przypadków płynięcie bezpośrednio za inną rybą w powstałych za nią niezakłóconych wirach jest korzystne, jeśli chodzi o prędkość i wydajność. Aby uzupełnić badania, przeprowadziliśmy meta-analizę opublikowanych danych eksperymentalnych na temat jednostajnego poruszania się rzeczywistych ryb. Dzięki zebraniu dużej ilości danych mogliśmy uzyskać kilka znaczących wyników, które znajdują zastosowanie w przypadku różnych gatunków ryb. Przede wszystkim pokazaliśmy, że najlepszym czynnikiem pozwalającym przewidzieć prędkość pływania ryby (U) jest prędkość fali rozchodzącej się w kierunku tyłu na powierzchni jej ciała (V). Pokazaliśmy także, że współczynnik poślizgu (U/V) zależy od liczby Reynoldsa, co jest zgodne z wynikami naszego modelu. Podsumowując, niniejsza praca doktorska zwiększa wiedzę na temat poruszania się ryb płynących w sposób jednostajny przy pomocy ruchów falistych ciała, zarówno samotnie, jak i w ławicach.

1

INTRODUCTION

The swimming of fish has fascinated humans for ages. The underwater environment, a dense, viscous liquid, is almost entirely alien to ours. Fish propel themselves through it, almost weightless due to their buoyancy. The seemingly effortless ease with which they do so has inspired scientists and engineers, who have spent much time attempting to understand the mechanics of fish propulsion (Gray, 1933; Lighthill, 1960, 1971; Triantafyllou et al., 1993; Barrett and Triantafyllou, 1995). Vertebrate life originated in the ocean, with the first undulatory swimmers such as jawless fish similar to lampreys. Given the long evolutionary history of undulatory swimming, it is reasonable to expect it to be an optimal mode of propulsion. However, which aspect of swimming is optimised, be it speed, manoeuvrability, efficiency, stealth to predators or cost of "construction," remains to be determined.

The majority of species of fish spend some stage of their development in a group of some kind, ranging from drifting clouds of larvae to travelling schools of millions of adults. Living in groups is theorised to have all sorts of advantages, including protection from predators, increased access to mates and greater foraging efficiency (Krause and Ruxton, 2002). A further supposed benefit (and the focus of this thesis) is increased hydrodynamical efficiency.

1.1 EMPIRICAL STUDY OF FISH SWIMMING

Here is presented a brief overview of the history of the empirical study of fish swimming - (for a more thorough overview, see Videler (1993) and Drucker and Summers (2007)).

The earliest scientific discussion of fish swimming comes from Aristotle, who noted the morphological variety across species in number of fins, and argued that many-finned fish (i.e.. possessing paired pectoral and pelvic fins) should propel themselves by flapping their fins, while those with fewer fins should do so through undulating their body. As was the case for many other subjects, Aristotle's ideas on fish swimming remained unquestioned through the middle ages, until Giovanni Borelli in 1680 published *On the Movement of Animals*, a groundbreaking work on biomechanics. He noted that, since the majority of the muscles of fish are found aligned with the spine in the body rather than attached to the fins, it is much more likely that it is the undulating body that does the work when fish swim. There matters rested until the invention of the ciné camera.

The modern study of the swimming of fish through the use of films was spearheaded by the work of Gray (1933). Especially important were his attempts to calculate the forces of swimming such as forwards thrust and rearwards drag from the movements of the fish. These calculations and experiments underlie much of the theory of fish hydrodynamics

of the twentieth century (Lighthill, 1960; Wu, 1961). The most well-known outcome of his work is 'Gray's paradox,' which states that (according to his calculations) dolphins can not produce enough thrust to reach the high speeds at which they swim. This led to the idea that something about undulatory swimming made it extremely efficient, greatly increasing the research on it (Fish, 2006). The paradox was only solved recently, by using the modern Digital Particle Image Velocimetry technique to map the flow around the tail of the dolphin, demonstrating that the force it generates is well in excess of that predicted by Gray (Wei et al., 2008).

The Digital Particle Image Velocimetry technique came into use in 1993, and has greatly improved our understanding of biohydrodynamics. It involves seeding the water with neutrally buoyant particles, and shining a flat sheet of laser light through the area where the flow is of interest. Subsequently, digitised high-speed video of the movement of the particles is analysed, resulting in a two-dimensional vector flow field that is a cross-section of the three-dimensional flow. The technique has been applied over a wide range of scales, from tiny (for example copepods (van Duren et al., 2003)) to large (for example eels (Tytell, 2007)). From these flow fields, inferences can be made about the power and efficiency of swimming (Müller et al., 1997; Tytell and Lauder, 2004). It should be noted however that, as pointed out by Dabiri (2005), for accurate estimations of the forces of swimming and thus the efficiency, the pressure field should also be measured, which is currently not possible.

In this thesis we study fish kinematics only in terms of the undulatory wave that passes rearwards through their body. Of this wave the characteristic length, frequency and amplitude (measured at the tail tip) are most frequently reported. Especially the tailbeat frequency is seen as important, and has been shown to be a major factor in what causes the swimming speed of fish (Bainbridge, 1958; Webb et al., 1984). Rarer are reports of how the amplitude of undulation varies along the body. Using Fourier analysis of digitised films of fish, Videler and Hess showed that the undulation can be described by a multiplication of a sine function that varies with time, and an "envelope" function that varies with the position along the body (Videler and Hess, 1984). This envelope function differs greatly among species. For example, for saithe it is quadratic, with the point on the body of lowest lateral movement behind the head, at approximately 25% of the body length. In contrast, for eels the envelope function is exponential, with a minimum at the head (Gillis, 1998; Tytell and Lauder, 2004) (Fig. 1.1).

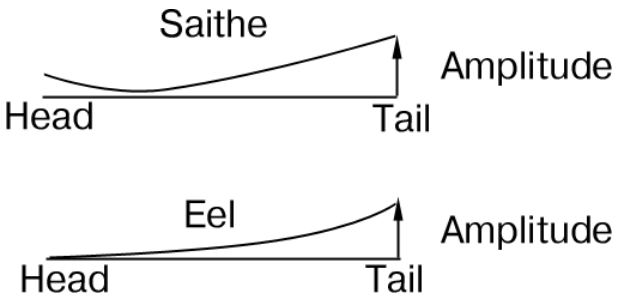

Figure 1.1.: Amplitude envelope functions of saithe and eel.

An important number when discussing hydrodynamical systems is the Reynolds number, which describes the relative importance of inertial and viscous forces, with higher Re indicating higher inertia. It is given by $Re = UL/\nu$, where U is the speed, L is the characteristic size (usually length when discussing fish) and ν is the kinematic viscosity of the fluid.

The most recent thorough overview of how the kinematics of fish swimming are interrelated, as well as their effect on swimming speed, is in John Videler's *Fish Swimming* (Videler, 1993). Since then, much experimental work has been done, but an integration of these results is lacking. We attempt to do so in the final chapter of this thesis.

1.2 THEORETICAL STUDY OF FISH SWIMMING

The swimming of fishes has been studied in models in many different ways, from single fish to groups, from detailed kinematics of individual fish to groups of travelling point particles. However, there is very little work that combines group dynamics with a somewhat realistic embodiment or 'situatedness' of the individuals, for example as regards their mass, size, shape or hydro/aerodynamics. This is unfortunate, because such embodiment strongly affects the mechanics of a system (Pfeifer and Scheier, 1999). For example, realistic flocking behaviour of starlings in a model was only achieved once the individuals were made to follow simple rules of aerodynamics (Hildenbrandt et al., 2010). In this thesis, rather than attempting to add hydrodynamics to already-existing models of flocking, we start with the modelling of hydrodynamics.

Modelling the hydrodynamics of swimming fish greatly improved in the last half century or so, most notably by Sir James Lighthill's Elongated Body Theory (Lighthill, 1960, 1971). This influential theory formed the basis for many experiments as well as calculations based on those experiments, for example to estimate the efficiency. The theory does not take viscosity into account however, and its predictions are largely qualitative.

Since the middle of the 1990s, computational power has advanced sufficiently to allow computer simulations of hydrodynamics on a scale that is sufficient to model fish swimming in detail as regards their complex shape and undulation. The first work of interest was that by Liu et al., who studied the swimming of a tadpole and fish in a computational fluid dynamics model (Liu et al., 1996, 1997). Their work shows the power of simulations to not only allow the study the flow and forces on the swimmers, but also to test several unrealistic situations, for example to make a fish undulate like a tadpole and vice versa. Liu et al. indicated that the swimming mode of the tadpole was uniquely suited to its shape and developmental history: its efficiency and flow field were unaffected by the addition of leg-like stumps, whereas a regular fish suffered greatly reduced efficiency and speed when leg-like stumps were added to it, or when it was made to undulate like the tadpole. Further interesting computational work on the hydrodynamics of swimming is that of Kern & Koumoutsakos who investigated the differences between 2- and 3-dimensional simulations of swimming fish (Kern and Koumoutsakos, 2006). Their results show that simulations in 2 dimensions, while differing in several aspects from the 3-dimensional ones, greatly resemble the experimental results of real fish. Also of great importance is the recent work by Borazjani and Sotiropoulos, whose simulations of swimming lampreys and mackerels

clearly demonstrate the importance of both kinematics and body shape to the efficiency of swimming fish (Borazjani and Sotiropoulos, 2008, 2009, 2010).

1.3 EMPIRICAL STUDY OF FLOW EXPLOITATION

The previous sections addressed the study of single fish in uniform flows. Here we discuss the available empirical evidence that indicates whether and how fish in schools might exploit the wakes of others. There are several indications that they do so. In short, first, fish can sense flows in great detail, second, fish can exploit flows to reduce swimming effort, and third, schools of fish as a whole are more efficient than single fish.

Just as we can feel the strength and direction of a breeze, fish can sense the flows of water. They can do so with great sensitivity and precision, due to a specialised system of sensors, much of which is concentrated (in most fish) in a thin groove along the length of the body, commonly called the lateral line. Through the lateral line fish can sense not only the direction of flows, but also (within a certain distance) their precise point of origin in space (Engelmann et al., 2000). This sensitivity is applied to several purposes. For instance, catfish can track their prey by following their wake (Pohlmann et al., 2001). The lateral line also plays an important part in schooling, as was elegantly shown in a series of experiments by Partridge and Pitcher (1980), who found that blindfolded fish with an intact lateral line could still school, and that fish with intact vision but disabled lateral lines took up different positions relative to their neighbours than entirely intact fish. The lateral line also plays a role in the exploitation of wakes. Rainbow trout whose lateral line was disabled spent much less time in the wake of a cylinder than intact ones did, and were much less likely to display the characteristic wake-exploiting gait reported by Liao et al. (2003b); Liao (2006).

This brings us to the point that fish have clearly been shown to exploit wakes, specifically those of cylinders. The downstream wake of a cylinder in flow at medium to high Reynolds number consists of a series of vortices that are shed alternatingly from the sides of the cylinder, with an area of low velocity zig-zagging between them. This is known as a von Kármán vortex street. Rainbow trout in a flow tank exploited the vortex wake of a cylinder by adopting an unique gait, slaloming between the vortices and moving from side to side much more than they did when swimming outside of the wake. From measurements of the muscle activity of the fish it became clear that this gait in the wake greatly reduced the effort the fish expended to stay in place (Liao et al., 2003b,a). Interestingly, later experiments showed that this reduction in effort may arise passively. When tethered behind the cylinder, a dead (but still flexible) fish would undulate and move upstream due to the buffeting of the vortex wake (Beal et al., 2006).

Fish also exploit the wakes of others when travelling in schools, as shown by experimental evidence dating back to as far as the 1960s (Belyayev and Zuyev, 1969). Fish were shown to decrease their oxygen consumption when swimming in schools, and fish at the rear of the school appeared to have lower tailbeat frequency, which may indicate that they spend less effort (Herskin and Steffensen, 1998). Further, it was demonstrated that fish preferred specific distances to one another, indicating that some positions are better than others (Svendsen et al., 2003). None of these experiments has shown exactly *how* the fish are improving their efficiency, however. For example, no experimental evidence has supported the rigid spatial

structure which is theoretically optimal (Partridge and Pitcher, 1979; Abrahams and Colgan, 1985). The theory of wake exploitation is further outlined below.

1.4 THEORY OF FLOW EXPLOITATION

Regarding the hydrodynamical efficiency of schooling, Weihs has made several predictions, however this theory of hydrodynamics ignores viscosity and the shape of the body of the fish (Weihs, 1973). His first prediction was that for optimal efficiency groups of fish should adopt regular, fixed positions relative to one another, in horizontal, two-dimensional layers. Within these layers, individuals should swim in staggered rows, resulting in diamond-like lattices (Fig. 1.2). The lateral distance between neighbours should be approximately two times the width of their wake, and the longitudinal distance between rows (measured from tail to nose) should be at least 0.7 fish lengths. The second prediction was that lateral neighbours increase an individual's efficiency, and the third that in the diamond lattice structure, lateral neighbours should beat their tails in antiphase to one another (Weihs, 1973, 1975).

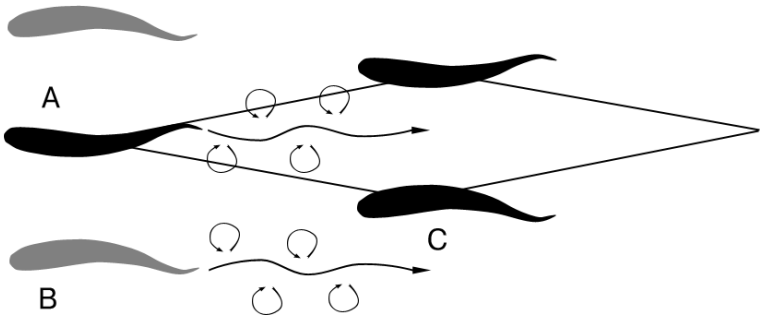

Figure 1.2.: Diamond-shaped spatial structure as predicted to be optimal by Weihs. Lateral neighbours A and C are undulating in antiphase, and trailing fish B is profiting from the area of low velocity between their wakes.

Only very recently have computers become powerful enough to model the hydrodynamics of multiple, undulating fish. To date only a few theoretical studies have investigated hydrodynamical interactions between swimming fish. The two most relevant ones to this thesis were first, a single fish swimming between the wakes of two predecessors (Deng and Shao, 2006) and second, an infinitely wide phalanx of side-by-side fish (Dong and Lu, 2007). Unfortunately, both studies were unbiological as regards either their parametrisation (Deng and Shao, 2006) or the constant, fixed speed of the individuals (Dong and Lu, 2007), making the value of their results unclear. That said, an increase in efficiency was found in both studies: in the case of three fish the third, trailing fish was more efficient and needed to beat its tail less widely, and the fish in an infinite phalanx saved power if they were swimming in phase (Dong and Lu, 2007). Of course, neither a phalanx nor a group of three fish are a test of the predictions of a diamond structure. This thesis aims to be the first true test.

1.5 COMPUTER SIMULATIONS OF HYDRODYNAMICS

Hydrodynamics is described by the Navier-Stokes equations. However, no general solution to these equations exists, and therefore all methods simulating hydrodynamics involve discretisation of time and space in some way. Computer models of hydrodynamics can be roughly divided into two categories based on their methods of discretisation, namely numerical and particle-based simulations. Below they are both briefly described, followed by a description of the method used for our simulations (Multiparticle Collision Dynamics), as well as the reasons why we chose this particular method.

The numerical models solve the Navier-Stokes equations by discretising them onto a spatial grid. It is necessary for such methods to adapt the grid to the shape of whatever object or organism is being simulated (Fig. 1.3). If the object is moving or deforming (as in the case of an undulating fish) the grid needs to be re-adapted frequently, which is a process that is both complex and computationally demanding.

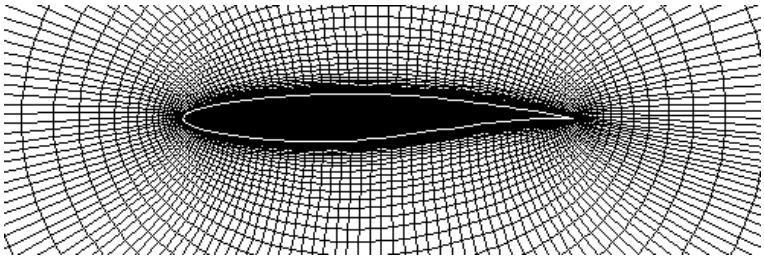

Figure 1.3.: Example of a grid around an airfoil shape, to be used in a numerical simulation of hydrodynamics around it. Note that the grid would need to be entirely recalculated if the airfoil changed shape or position.

The particle-based methods on the other hand discretise hydrodynamics into particles that move and collide. These particles represent small quantities of fluid. This coarse-graining leads to the common term of 'meso-scale' modelling, with its scale lying does between the micro-scale of molecules and the macro-scale of hydrodynamical phenomena such as vortices. From the interactions between particles at the meso-scale, hydrodynamics according to the Navier-Stokes equations emerge at the macro-scale. The particles may be restricted to a grid, such as in the commonly-used Lattice Boltzmann method (Sui et al., 2007), or move freely as in several other methods (Monaghan, 1992; Kajtar and Monaghan, 2008; Malevanets and Kapral, 1998). In case they move freely, the interactions among particles may be smoothed over longer ranges, such as in in the Smoothed Particle Hydrodynamics method (Monaghan, 1992; Kajtar and Monaghan, 2008), or be more local, as in the Multiparticle Collision Dynamics method (Malevanets and Kapral, 1998).

For our simulations of swimming fish we chose to use the Multiparticle Collision Dynamics method. It is a relatively new method, being introduced in the late 1990s. It has been shown to produce hydrodynamics consistent with the Navier-Stokes equations, and numerical expressions for several of its properties such as viscosity and transport coefficients have been

found (Malevanets and Kapral, 1999; Kikuchi et al., 2003; Padding and Louis, 2006). We thus regard the method as reliable and well-understood.

We chose to use the Multiparticle Collision Dynamics method because it has several advantages. Most importantly, the representation of space is continuous, meaning that there is no grid. Therefore smooth, organic shapes (such as of a fish) can be represented in the model. Further, the interaction of the fluid with the fish can be modelled relatively simply through collisions between the fluid particles and the body, in contrast with numerical simulations where special border conditions are required for example at the sharp trailing edges of a fish tail. Another advantage is that the method is computationally very efficient. This efficiency is further increased because the short range of interactions between particles makes the method ideally suited for parallellisation. Therefore we could use the graphics processor of modern graphics cards for much of the fluid-dynamical calculations, which increased the simulation speed by a factor of 10.

1.6 WORK PRESENTED IN THIS THESIS

The aim of this thesis is to increase the understanding the swimming of fish, both singly and in groups. We do so through computer modelling and a meta-analysis of experimental literature.

Our modelling work is presented in chapters 2-4. They proceed in logical order from least to most complex, each representing a step in the implementation process and its careful testing. In chapter 2, we validate our implementation of the Multiparticle Collision Dynamics model for the classic cases of flow past a static square and circular cylinder. Further, we study more complex, biological shapes, including a fish and tadpole (both with and without leg-like growths) and several cylinder shapes with trailing thin plates. We show that the trailing plates increase drag at low Reynolds numbers but decrease drag at higher ones by increasing the suppressing vortex shedding. In chapter 3, we extend the model with moving shapes that change their orientation, position and shape. We validate the model as regards changing orientation and position by comparing the forces of a flapping cross-section of an insect wing in our model against those of both an empirical and a numerically-simulated one. We subsequently simulate undulating fish, measuring their speed, efficiency and forces of thrust and drag for several Reynolds numbers. Our results show that the common practise in simulations to constrain the fish to not accelerate laterally skews the results to resemble those of free fish with a higher tail beat frequency. Finally, in chapter 4, we simulate infinitely-large schools of undulating fish (similar to those of chapter 3) in several different spatial configurations. The spatial configurations we study are the diamond-shaped lattice that Weihs predicted to be optimal (Weihs, 1973) and a rectangular lattice. Further, in order to investigate the effects of longitudinal and lateral neighbours separately we simulate an infinitely long progression, or 'line' and an infinitely wide 'phalanx'. Our results show that swimming directly behind a fish in its undisturbed wake is beneficial as regards speed and efficiency in most cases. Besides, we confirm Weihs' predictions that having lateral neighbours is beneficial for efficiency, and that a closely-spaced diamond lattice causes individuals to encounter a low-velocity area ahead of them. However, his prediction that this would increase efficiency is not borne out by our results.

We expand on the insights gained from our simulation studies by means of a meta-analysis of the scientific literature on steady swimming. The size of our data set results in several new significant insights. Most importantly, we show that the strongest predictor of swimming speed is the speed of the body wave. Further insights include the fact that the slip ratio U/V is a function of the Reynolds number (which is also the case in our model).

2

FLOW AROUND STATIC FISHLIKE SHAPES[1]

Abstract

Empirical measurements of hydrodynamics of swimming fish are very difficult. Therefore, modelling studies may be of great benefit. Here, we investigate the suitability for such a study of a recently developed mesoscale method, namely Multi-Particle Collision Dynamics. As a first step, we confine ourselves to investigations at intermediate Reynolds numbers of objects that are stiff. Due to the lack of empirical data on the hydrodynamics of stiff fish-like shapes we use a previously published numerical simulation of the shapes of a fish and a tadpole for comparison. Because the shape of a tadpole resembles that of a circle with an attached splitter plate, we exploit the knowledge on hydrodynamic consequences of such an attachment to test the model further and study the effects of splitter plates for objects of several shapes at several Reynolds numbers. Further, we measure the angles of separation of flow around a circular cylinder and make small adjustments to the boundary condition and the method to drive the flow. Our results correspond with empirical data and with results from other models.

2.1 INTRODUCTION

Mesoscale models of fluid dynamics have been used to study many phenomena in fields such as physics and biochemistry. Examples include flow around cylinders (Breuer et al., 2000), molecular diffusion (Falck et al., 2004), polymers in flow (Ripoll et al., 2004) and the formation of micelles (Sakai et al., 2000). They have also been applied to study biological systems, mainly at the cellular level, for example red blood cells in flow (Noguchi and Gompper, 2005). In the present paper we test whether a mesoscale model of hydrodynamics, namely Multi-Particle Collision Dynamics (Malevanets and Kapral, 1998, 2000), is suitable to study stiff fish-like shapes in flow. This is part of a long-term project to investigate the hydrodynamics of actively swimming fish, both alone and in a group. We prefer a mesoscale model over the numerical methods derived from the Navier-Stokes equations of flow used for similar problems (Eldredge, 2007; Kelly and Murray, 2000) because it allows us to study the hydrodynamics of any shape without needing to adapt a coordinate grid to it (Liu et al., 1996) or add additional assumptions, such as to impose vorticity (Eldredge, 2007) or to use a

1 PUBLISHED AS: D. A. P. REID, H. HILDENBRANDT, J. T. PADDING, C. K. HEMELRIJK – *"FLOW AROUND FISHLIKE SHAPES STUDIED USING MULTIPARTICLE COLLISION DYNAMICS,"* PHYSICAL REVIEW E, VOL. 79, NO. 4, 046313, 2009.

special boundary condition for edges such as a tail fin (Kelly and Murray, 2000). Further, since it is an off-grid method, it is one of the most suitable mesoscale methods to extend with objects that deform, such as an undulating fish.

The Multi-Particle Collision Dynamics model was introduced by Malevanets and Kapral (1998) and has since been used to investigate a variety of micro-scale hydrodynamic systems (Noguchi and Gompper, 2005; Padding and Louis, 2006; Ripoll et al., 2004; Watari et al., 2007). The model consists of a fluid of particles which move and collide, whereby the collisions conserve both mass and momentum. At the macro scale the system exhibits behaviour that is consistent with the Navier-Stokes laws of hydrodynamics. Expressions for the viscosity and several transport coefficients have been derived (Kikuchi et al., 2003), showing that the model is correct as regards both short- and long-range hydrodynamics.

Although fish swim at high Reynolds numbers of 10^3 up to 10^5 (Videler, 1993), in the present study we confine ourselves to intermediate Reynolds numbers (ie. Re $10 - 110$) which are relevant for fish larvae (Müller et al., 2000). We use these lower Reynolds numbers for two reasons. First, it reduces computational effort, which scales quadratically with the Reynolds number. Second, the comparability to earlier studies at the same Re number of hydrodynamics of a circle and square (Lamura et al., 2001; Lamura and Gompper, 2002).

In this paper we confine ourselves to the study of stiff shapes, with the aim to later extend the model to deformable ones. Because empirical data on hydrodynamic traits of stiff fish are lacking we use other data, namely previously published results of a numerical simulation of a fish and a tadpole (Liu et al., 1996, 1997). Apart from this comparison we note that the shape of a tadpole resembles that of a circle with an attached splitter plate. This resemblance we exploit because much is known about the hydrodynamic effects of splitter plates (Kwon and Choi, 1996). Therefore we examine flow around, and drag of a circle with and without a splitter plate attached to it. We do so for a series of different Re numbers and object shapes. We further verify our implementation for a circular cylinder with a new measurement, namely of the separation angle of flow. Our results confirm the suitability of the model for the study of the hydrodynamics of fish-like shapes.

2.2 METHODS

2.2.1 *System overview*

We investigate the hydrodynamics of objects held in place in a channel. Although the model has been shown to perform well in three dimensions (Allahyarov and Gompper, 2002), we use two-dimensional simulations to reduce computational effort. A schematic overview of the system is shown in Fig. 2.1. The channel has width W and length L. We set these to be the same as those used by Lamura and Gompper (2002), against whose work we compare our results. The width and length are both functions of the cross-section D of the object, with $W = 8 * D$ and $L = 50 * D$. This results in a blockage ratio $B = D/W$ of 0.125 (Lamura et al., 2001). The channel has solid walls at the top and bottom, and is periodic in the x-direction. All objects are represented as polygons so that they may have any shape. We use a relatively

wide system so that the wake of the object will die out before it encounters the object again. Flow goes from left to right. We calculate the Reynolds number as

$$Re = \frac{\rho v_x D}{\mu}, \tag{2.1}$$

where ρ is the fluid density, v_x is the flow speed along the channel centre far away from the object and μ is the dynamic viscosity which consists of two components (Eq. 2.4, see below).

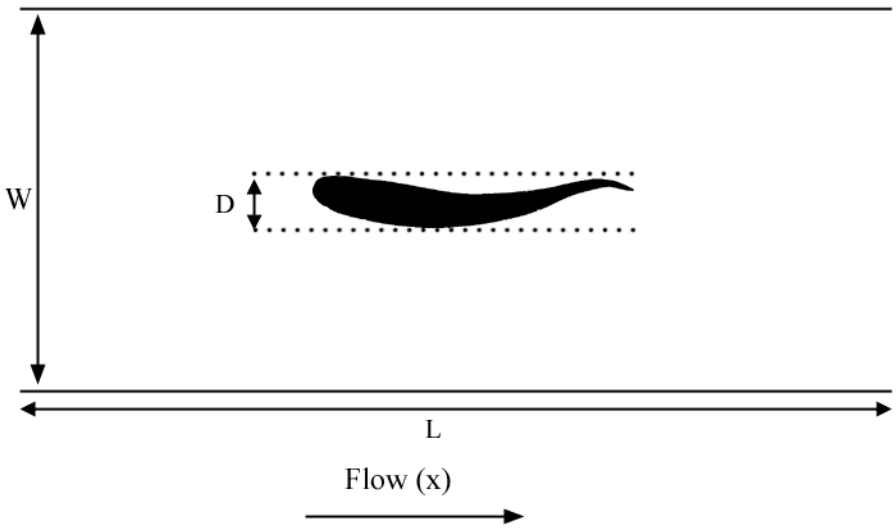

Figure 2.1.: The simulation setup. W is the width of the channel , L is its length (not to scale), D is the object diameter, measured along the width-axis.

2.2.2 *Multi-Particle Collision Dynamics*

The system consists of a two-dimensional homogeneous space containing N identical particles of mass m. The positions $\mathbf{x}_i$ and velocities $\mathbf{v}_i$ of the particles are two-dimensional vectors of continuous variables. Every time step Δt the particles first move and then collide. Moving leads to new positions $\mathbf{x}_i$ according to equation 2.2:

$$\mathbf{x}_i(t + \Delta t) = \mathbf{x}_i(t) + \mathbf{v}_i(t)\Delta t. \tag{2.2}$$

To simulate collisions, a square lattice with mesh size a_0 is used to partition the system. In each lattice cell, all particles simultaneously collide with each other, changing their velocities according to

$$\mathbf{v}_i = \overline{\mathbf{v}} + \omega \cdot (\mathbf{v}_i - \overline{\mathbf{v}}). \tag{2.3}$$

Here $\overline{\mathbf{v}}$ is the mean velocity of the particles in the grid cell and ω is a stochastic rotation matrix that rotates the velocities by either $+\alpha$ or -α (where α is a fixed system parameter), with equal probability. It is the same for all particles within a cell. The rotation procedure can thus be viewed as a coarse-graining of particle collisions over space and time. We set α

to $\frac{\pi}{2}$ for three reasons. Firstly because it is the value used in the studies to which we compare our results (Lamura et al., 2001; Lamura and Gompper, 2002). Secondly because Allahyarov and Gompper (2002) showed that the kinematic viscosity is lowest for this value of α, thus maximising the Reynolds number. Thirdly because rotation by $\frac{\pi}{2}$ is computationally very fast.

An overview of parameter settings is shown in Table 2.1. From these parameters we derive the mean free path, which is the mean distance travelled by a particle before it collides. This path length is given by the expression $l = \Delta t\sqrt{k_B T/m}$, where k_B is the Boltzmann constant, and T is the temperature of the system. If the system temperature and thus the mean free path is low, and $l < a_0$, the same particles will often collide with each other on consecutive time steps, which breaks Galilean invariance. To solve this problem we follow the solution proposed by Ihle and Kroll (2001) and displace the lattice every time step by a vector with x- and y-components which are randomly selected from the interval $[0, a_0]$.

Parameter name	Symbol	Value used
Temperature	$k_B T$	1.0
Lattice cell size	a_0	1.0
Collision rotation angle	α	$\frac{\pi}{2}$
Particle mass	m	1.0
Particles per cell (average)	ρ	10
Time step length	Δt	1.0

Table 2.1.: Parameter values used

An important advantage of this method is that its simplified dynamics has allowed the analytic calculation of several transport properties (Kikuchi et al., 2003). The most important one for this study is the viscosity μ, which consists of 2 components:

$$\mu = \mu_{kin} + \mu_{coll}, \tag{2.4}$$

where μ_{kin} is the kinetic component of the fluid viscosity while μ_{coll} is the collisional component. The simplified equations for the components of the viscosity, omitting parameters that are set to 1 in our simulations, are as follows:

$$\mu_{kin} = \frac{\rho}{2}\left[\frac{\rho}{(\rho - 1 + e^{-\rho})} - 1\right] \tag{2.5}$$

$$\mu_{coll} = \frac{1}{12}(\rho - 1 + e^{-\rho}), \tag{2.6}$$

where ρ is the average number of particles per collision cell. Since we use a density $\rho = 10$, the viscosity in our simulation units is 1.306.

2.2.3 *Boundary Conditions*

At the macroscopic scale of organisms, there should be no slip at the interface between a fluid and a solid. This means that the fluid's tangent velocity to any surface at the interface

should be zero - the so-called no-slip condition. We use two complementary methods from previous implementations of the model to ensure minimum slip, i.e. the virtual particle rule of Lamura and Gompper (2002), and the random-reflect boundary condition (Inoue et al., 2001; Padding and Louis, 2006), both of which are outlined below.

Lamura and Gompper (2002) enforce no-slip boundary conditions in the collisional part of the model by including virtual "solid" particles in cells which partially overlap the solid. These virtual particles are included in the collisions among particles. The velocities of the virtual particles are drawn from a Maxwell-Boltzmann distribution of mean zero and temperature $k_B T$. The mean of zero reduces slip while the temperature $k_B T$ causes the virtual particles to act as thermostats.

In the random-reflect boundary condition particles that hit the solid get a new randomly chosen velocity. The new velocity is relative to the surface and consists of a tangential component v_t and normal component v_n, drawn from the following distributions (Inoue et al., 2001; Padding and Louis, 2006):

$$P(v_t) \propto e^{-\beta v_t^2} \tag{2.7}$$

$$P(v_n) \propto v_n e^{-\beta v_n^2} \tag{2.8}$$

Here, $\beta = \frac{m}{2k_B T}$. Since the new velocities are Maxwell-Boltzmann distributed with temperature $k_B T$ and a mean velocity tangential to the surface of 0, this method reduces slip and has the additional advantage that it makes solids act as thermostats. We prefer this method over the bounceback reflection used by Lamura and Gompper (2002) in which particles reverse their velocity when they hit a solid. At small scales, a surface is not smooth and thus random reflection is a better approximation.

When particles move, they may collide with a solid. Because the particles keep moving after a collision, a series of collisions can occur within one time step Δt if there are multiple objects or if the shape of the object is complex. We therefore use the following iterative procedure.

For each particle, the time δt it has spent moving during this time step is set to 0. Then, as long as δt is smaller than the length of a time step Δt (Table 2.1), the particle keeps moving. Its projected movement is calculated from its velocity vector $\mathbf{v}_i$ as follows: $\mathbf{v}_i * (\Delta t - \delta t)$. If this line intersects a solid, a collision occurs at the collision point $\mathbf{x}_{coll}$ and δt is increased by the amount of time it took to move there. The particle is assigned a new random velocity following Eqs. 2.7 and 2.8. If δt is smaller than Δt, it keeps moving, starting from $\mathbf{x}_{coll}$ and checking for collisions in the same manner.

2.2.4 *Flow*

The expected flow profile in an empty channel is known as Hagen-Poiseuille flow. This flow is characterised by a parabolic flow profile in a cross-section of the channel, with the speed in the x-direction on each point of the y-axis given by

$$v_x(y) = \frac{4 v_{max}(W - y)y}{W^2}, \tag{2.9}$$

where v_{max} is the maximum speed, in the centre of the channel of width W.

To create flow we apply a constant force mg in the x-direction to all fluid particles (Allahyarov and Gompper, 2002). In an experiment this force would correspond to a pressure drop per unit length given by $\partial P/\partial x = -\rho mg$. We use a galilean-invariant thermostat (Padding and Louis, 2006) to keep the system temperature constant. Due to the no-slip condition the channel walls exert a shear force, which increases with the flow speed and the viscosity μ. The system is stable when the gravitational force on the fluid is exactly balanced by this shear force. In this steady state the flow is laminar Hagen-Poiseuille flow, with the speed in the centre of the channel v_{max} given by

$$v_{max} = \frac{\rho W^2 g}{8\mu}. \tag{2.10}$$

This method to create flow is different than that used by Lamura and Gompper (2002), who imposed the Hagen-Poiseuille distribution (Equation 2.9) directly on particles in a 'driving' section of their simulation. However, this causes a significant disruption of the flow: in the simulation area directly adjacent to the driving section large vortices are formed along the channel walls, and the density of the fluid increases. Furthermore, the overall flow velocity in the channel does not become uniform, with significantly reduced flow speeds further away from the driving section due to channel friction. We therefore use gravity-driven flow.

If the system starts at rest, the time required to reach this steady state depends on the system size. This was approximately 50,000 time steps for the larger system sizes we examined. However, since we can estimate the final v_{max} using Equation 2.10, we can initialise the system with Hagen-Poiseuille flow of the appropriate speed using a Maxwell-Boltzmann distribution of temperature $k_B T$, with an average speed in the y direction of zero, and an average speed in the x direction according to Equation 2.9. This means that for the empty channel the system does not need time to stabilise.

For a clear wake structure to develop behind a static object in the channel, the simulation must be run until it stabilises. In that case the flow profile far away from the object is still parabolic, but due to the drag of the object it is slower than estimated by Equation 2.10. Tests showed that at the Reynolds numbers we examined the speed is lower by about 60% if an object is present, therefore we initialise the system with Hagen-Poiseuille flow of v_{max} 60% slower than expected for the empty channel. Such an initialisation of the flow field reduces the time required to reach the steady state by approximately 50% compared to starting the simulation from a resting fluid.

2.2.5 *Measurements*

The recirculation length in the regime of steady recirculation (Lamura et al., 2001) is measured as the length of the area of recirculation in the wake of the object. It is defined as the distance from the rear end of the cylinder to the end of the wake. We define the end of the wake as the rearmost point on the central axis where the average flow in the x-direction is zero. We express the recirculation length in terms of the object diameter D.

The drag coefficient C_D (Lamura et al., 2001) is defined as

$$C_D = \frac{2F_x}{\rho_m v^2 D}, \tag{2.11}$$

where F_x is the force on the object in the direction of flow (in $ma_0\delta t^{-2}$) caused by the change of momenta of the colliding particles, ρ_m is the density of the fluid (in ma_0^{-2}) which equals the density of particles ρ due to our choice of parameters (Table 2.1), v (in $a_0\delta t^{-1}$) is the flow speed in the centre of the channel far away from the object and D is the cross-channel width of the object measured in a_0.

The angle of separation is the angle between the central x-axis and the separation point. A separation point is defined as a point close to the surface where the flow velocity tangential to the surface is zero (of course everywhere *on* the surface the average tangential velocity is zero because of the boundary conditions). An object in low-Reynolds flow always has separation points at angles 0 and 180, but at sufficiently high Reynolds numbers two new separation points occur towards the rear of the object. To measure the separation angle of these two new separation points, we draw a line from the centre of the object to the separation point, and measure the angle ϕ between that line and the central x-axis (Fig. 2.2). As can be seen from Fig. 2.2, the precise angle of separation is difficult to determine because the flow is stochastic. We therefore estimate a minimum and maximum separation angle at each side of the object by hand, and use the average of these four values.

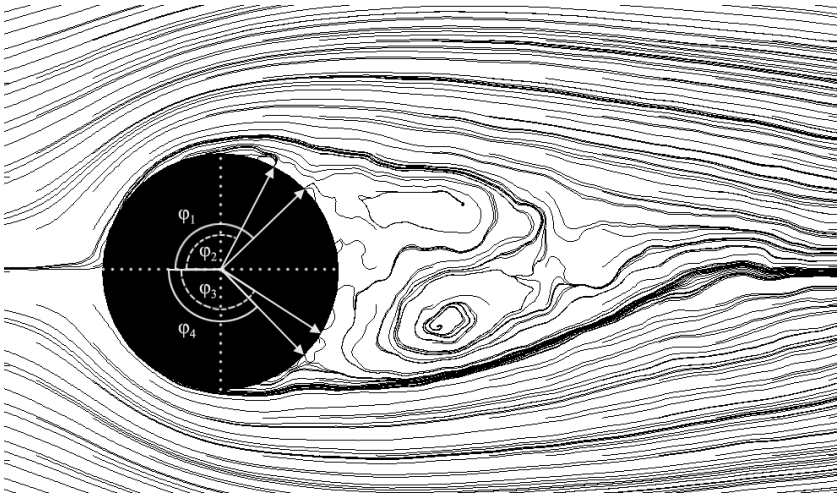

Figure 2.2.: The separation angle ϕ_i. The four lines are estimates of the minimum and maximum separation angle on each side of the object.

All programs were implemented in C++ and simulations were run on single Intel Core2 Duo PCs. Data analysis and visualisation were done with MATLAB ® (The MathWorks, n.d.). The tadpole form was traced from a figure of a cross-section of a bullfrog tadpole (*Rana catesbeiana*) by Liu et al. (1996). The fish shape was traced from a figure of a cross-section of a mullet (*Chelon labrosus*) by Müller et al. (1997). Simulation time for the largest simulation, that of a fish shape at Reynolds number 110, took approximately 10 days.

2.3 RESULTS

When we compare the flow field of the tadpole in our model to that in the numerical model by Liu et al. (1996), it appears to be qualitatively similar as regards the area of low flow

speed around the tail (Fig. 2.3a,b). In further agreement with their results, the addition of leg-like extrusions to it changes neither the flow field nor the drag coefficient (Fig. 2.3c). This confirms the conclusion of Liu and coworkers that the location of leg growth in tadpoles is neutral in terms of drag (Liu et al., 1996).

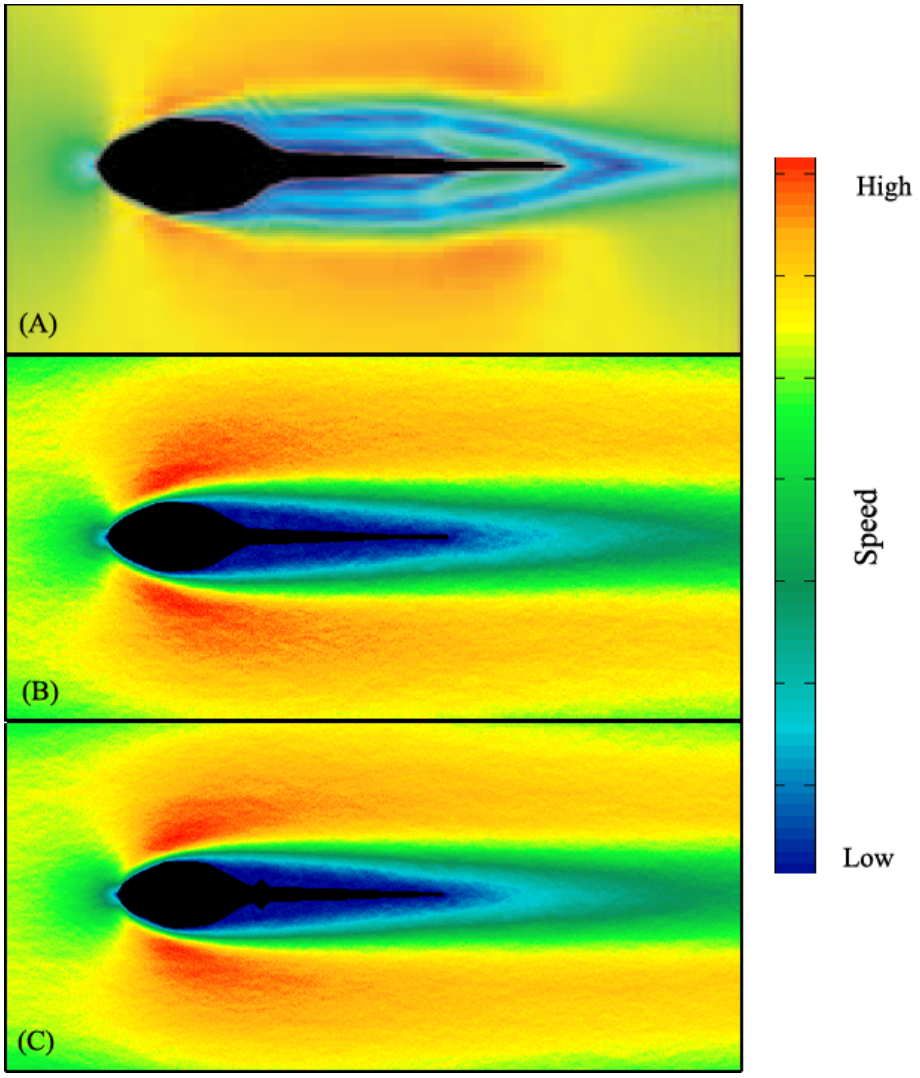

Figure 2.3.: Flow fields around a tadpole shape. (A) from Liu et al. (1996), (B) in our model, (C) in our model with added leg-like protrusions. Colour indicates flow speed, with high speed red and low speed blue. Our simulations are at Reynolds numbers of approximately 105, based on the cross-channel size of the object.

In contrast, when we add such extrusions to a fish shape, the drag coefficient increases by 25%, from 0.97 to 1.22. The drag coefficient is also higher for an S-shaped fish than for a straight one with an increase of 95%, from 0.97 to 1.9, (Table 2.2).

The shape of a tadpole and its drag coefficient resemble those of a circular cylinder with an attached splitter plate (Table 2.2). As regards its drag coefficient (Fig. 2.4a) and recirculation length (Fig. 2.4b), our results of the circular cylinder without attachment resemble the results

Shapes without and with splitter				
Shape	Re(Width)	Re(Length)	C_D	C_D with splitter
Square	80	80	1.8	1.45
Circle	115	115	1.22	1.05
Flat Plate	70	1.75	2.0	1.7
Fishlike shapes without and with legs				
Shape	Re(Width)	Re(Length)	C_D	C_D with legs
Tadpole	110	528	1.01	1.01
Straight fish	110	724	0.97	1.22
Undulated fish	110	724	1.9	N.A.

Table 2.2.: Drag coefficients for various shapes, with and without attached splitter or leg-like protrusions. Reynolds numbers are shown both based on width as is common in physics (width) and on length as is common in biology. All Reynolds numbers discussed in this paper are width-based. All simulations are two-dimensional.

of the model by Lamura and Gompper (2002) as well as empirical data (Coutanceau and Bouard, 1977; Tritton, 1959). Furthermore, the angles of separation of flow (Fig. 2.5) fall within the range of empirical data from Wu et al. (2004).

We test in our model the hydrodynamics of attached splitter plates by measuring the drag of a circular cylinder over a range of Reynolds numbers, both with and without an attached splitter plate. Due to the splitter plate, the drag coefficient of the cylinder becomes higher at low Reynolds numbers due to additional friction drag (Fig. 2.6). At higher Reynolds numbers (Fig. 2.6) however, the splitter plate stabilises the wake and delays the onset of vortex shedding (Fig. 2.7), which lowers the drag. We find that at these Reynolds numbers splitter plates also reduce the drag of a square cylinder and flat plate (Table 2.2).

2.4 DISCUSSION

The results of our simulations show that at intermediate Reynolds numbers the Multi-Particle Collision Dynamics model is suitable to investigate the hydrodynamics of fish-like shapes. Our quantitative measurements agree with data of empirical and model studies. Thus, the model is robust against adjustments of the boundary conditions and the method to drive the flow. Further, flow around shapes of fish and tadpoles qualitatively resembles that of numerical investigations (Liu et al., 1996).

As to the measurements of the recirculation length (Fig. 2.4a), these tend to be too low at higher Reynolds numbers both in our results and in those of Lamura and Gompper (2002). This arises probably because the wake sometimes deviates from the central axis along which it is measured, and this deviation will cause an underestimation. The size of this error is larger if the wake is longer, and therefore it is larger at high Reynolds numbers. This is due to the considerable stochasticity of flow. Another consequence of this stochasticity is that to maximally reveal patterns of flow, drag et cetera, data had to be averaged over an interval of many time steps (to the order of hundreds). This interval was still much shorter than the

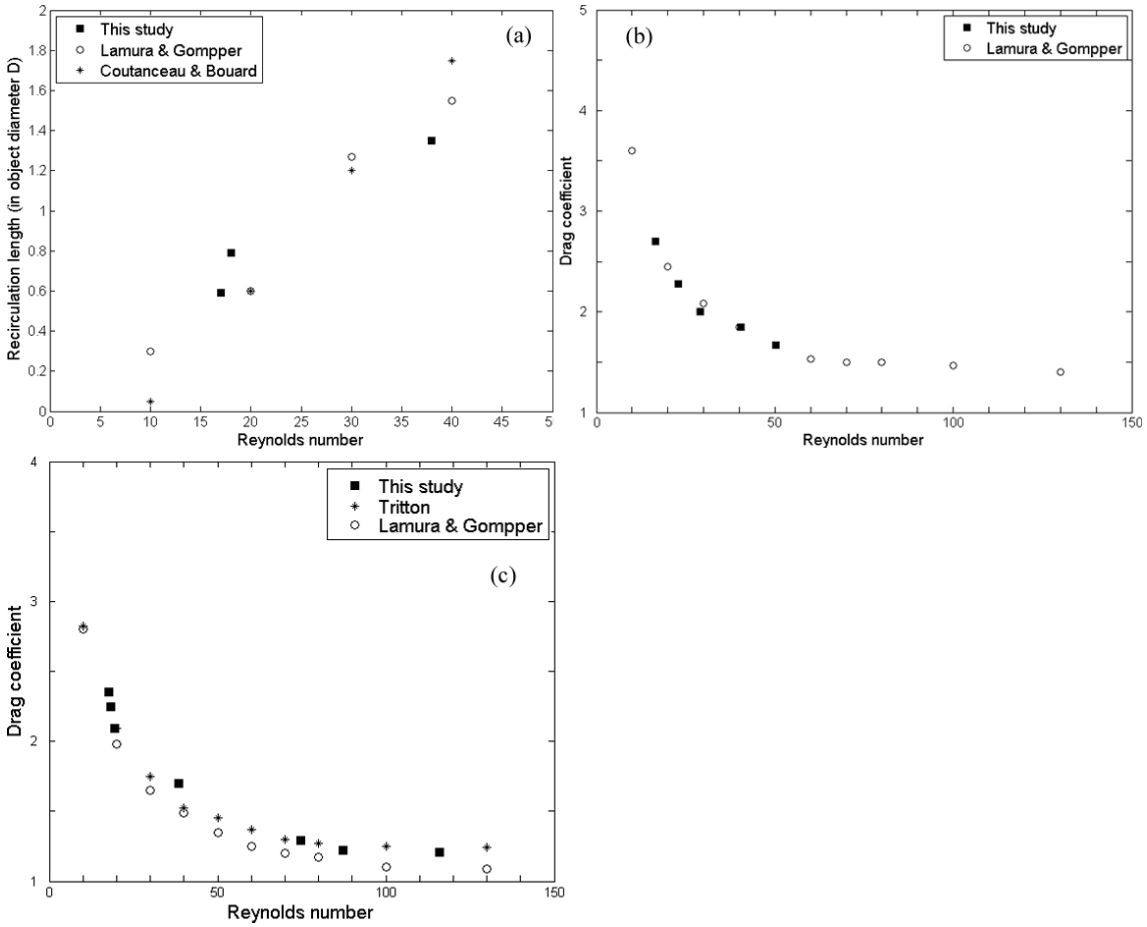

Figure 2.4.: Results of simulations for basic shapes. (*a*): The recirculation length for the circular cylinder as a function of the Reynolds number. Data from Lamura and Gompper (2002) (○), this study(■), Coutanceau and Bouard (1977) (*). Note that steady recirculation only occurs at Reynolds numbers below 45. (*b*): The drag coefficient for the square cylinder as a function of the Reynolds number. Data from Lamura and Gompper (2002) (○), this study(■) (*c*): The drag coefficient for the circular cylinder as a function of the Reynolds number. Data from Tritton (1959) (∗), Lamura and Gompper (2002) (○) and this study(■).

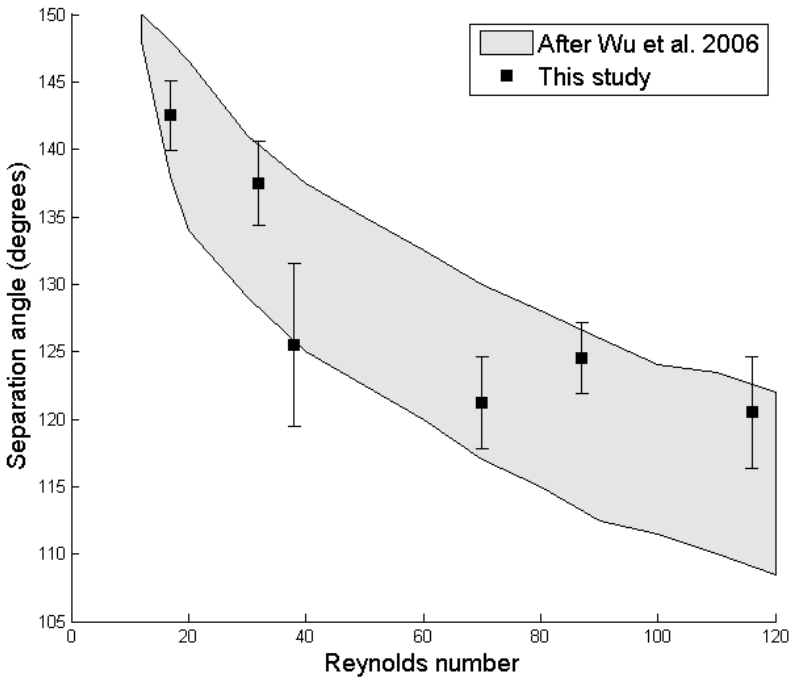

Figure 2.5.: The separation angle for the circular cylinder as a function of the Reynolds number. Data from an overview of experimental data by Wu et al. (2004)(gray area) and mean values ± standard error of this study(■).

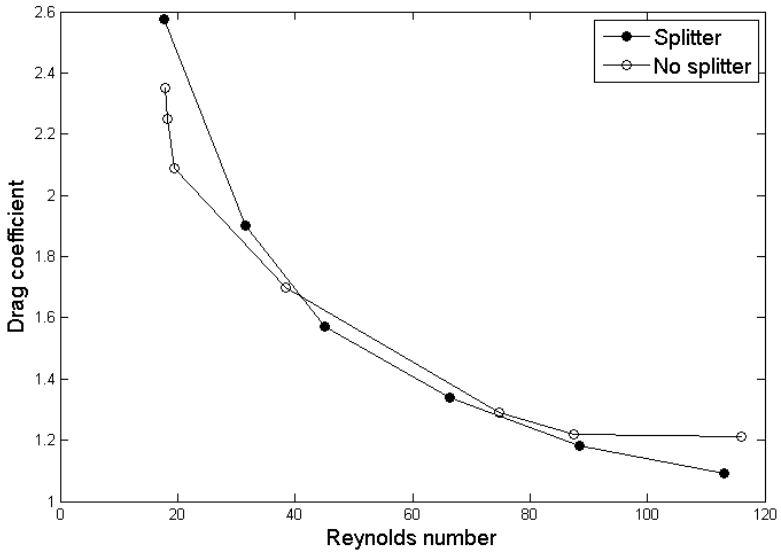

Figure 2.6.: The drag coefficient of the circular cylinder as a function of the Reynolds number. Plotted values are for the cylinder with (●) and without (○) trailing splitter plate.

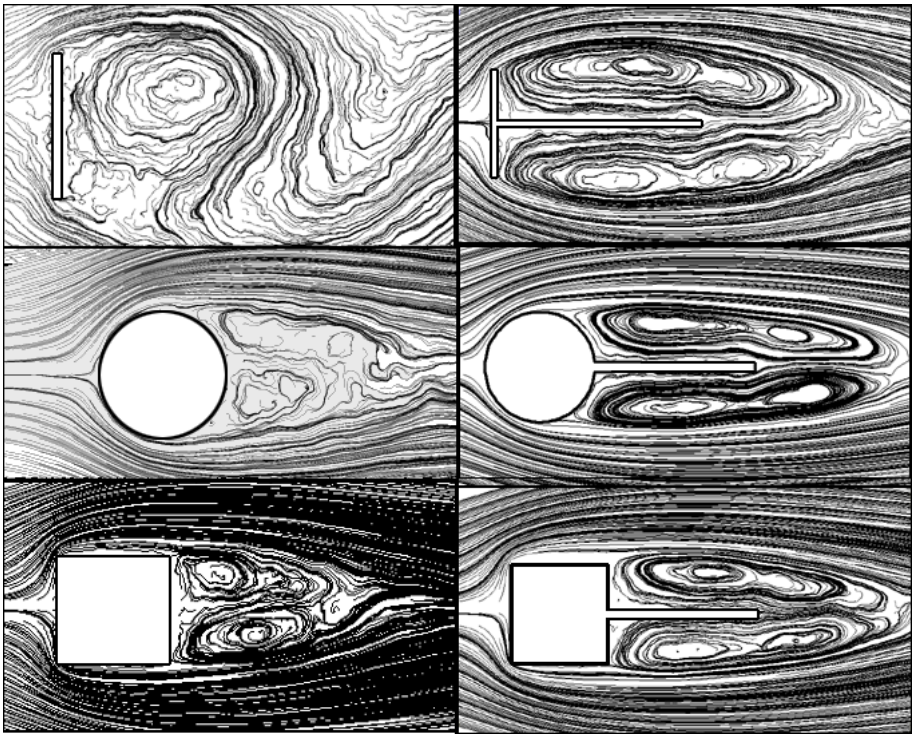

Figure 2.7.: Streamlines for flat plate, circle and square with and without splitter plate attached. The Reynolds number is approximately 80. Note that the flat plate and splitter plates are thicker than the mesh cell size a_0. The cross-channel diameter of the objects is the same in all cases.

cycle of the phenomena we studied. Note that this averaging is common practice in studies of Multi-Particle Collision Dynamics.

It is likely that the width-to-length ratio and blockage ratio of the channel have an effect on flow and drag. We did not study this however, because our future work will concern flow that is not confined between walls.

In future we intend to study the hydrodynamics of the locomotion of fish. Fish swim at Reynolds numbers between 10^3 and 10^5 as measured by biologists, which is much higher than those used in this study. However, the following factors will help us to work in the model in the correct range of Reynolds numbers. First, the Re numbers measured by biologists are based on the length of the fish, those by physicists on its thickness. This reduces the Re number to about one fifth. Second, we may study these undulating fish at somewhat lower Re numbers because real fish swim in in 3D, whereas our model is a representation in 2D. Two dimensions restrict the degrees of freedom of movement and hence, all phenomena – such as recirculation, vortex shedding and turbulence – occur at half (or less) the Reynolds number of that in 3D (Table 2.3). Thus, wakes of fish in our model may develop sooner too.

Flow phenomenon	Re. 2D	Re. 3D
Recirculation	10	25
Vortex shedding	45	280
Turbulence	$1.2 * 10^5$	$4.7 * 10^5$

Table 2.3.: Critical Reynolds numbers for the onset of flow phenomena for circular cylinder (2D) (Wu et al., 2004; Paranthoën et al., 1999; Hoerner, 1965) and sphere (3D) (Taneda, 1956; Hoerner, 1965).

We conclude from our results that the Multi-Particle Collision Dynamics method is suitable for the study of flow around stiff fish-like shapes. We will therefore proceed to investigate its suitability for the study of fish that move.

ACKNOWLEDGEMENTS

H. H. was financed by grant 012682-STARFLAG from the STREP-program "Starflag" in the 6^{th} European framework, awarded to C. K. H.. J. T. P thanks the Netherlands Organisation for Scientific Research (NWO) for financial support.

3

FLUID DYNAMICS OF MOVING FISH[1]

Abstract

The fluid dynamics of animal locomotion, such as that of an undulating fish, are of great interest to both biologists and engineers. However, experimentally studying these fluid dynamics is difficult and time-consuming. Model studies can be of great help because of their simpler and more detailed analysis. Their insights may guide empirical work. Particularly the recently-introduced Multiparticle Collision Dynamics method may be suitable for the study of moving organisms because it is computationally fast, simple to implement, and has a continuous representation of space. As regards the study of hydrodynamics of moving organisms, the method has only been applied at low Reynolds numbers (below 120) for soft, permeable bodies, and static fish-like shapes. In the present paper we use it to study the hydrodynamics of an undulating fish at Reynolds numbers 1100–1500, after confirming its performance for a moving insect wing at Reynolds number 75. We measure 1) drag, thrust and lift forces, 2) swimming efficiency and spatial structure of the wake and 3) distribution of forces along the fish body. We confirm the resemblance between the simulated undulating fish and empirical data. In contrast to theoretical predictions, our model shows that for steadily undulating fish, thrust is produced by the rear 2/3ds of the body and that the slip ratio U/V (with U the forwards swimming speed and V the rearwards speed of the body wave) correlates negatively (instead of positively) with the actual Froude efficiency of swimming. Besides, we show that the common model practice of constraining individuals from accelerating sideways causes them to resemble unconstrained fish with a higher tailbeat frequency.

3.1 INTRODUCTION

The swimming of fish is a topic of broad interest (Videler, 1993), not only to biologists (Abrahams and Colgan, 1985; Herskin and Steffensen, 1998; Svendsen et al., 2003; Walker et al., 2005; Tytell and Lauder, 2008) but also to engineers (Barrett et al., 1999; Bandyopadhyay, 2002). In this context, undulatory swimming is important because it seems to be an efficient mode of locomotion, whether fish swim alone (Barrett et al., 1999) or in groups (Weihs, 1973). However, it is still unknown what influences the efficiency of an undulating fish. It

1 UNDER REVIEW AT PHYSICAL REVIEW E AS: D. A .P. REID, H. HILDENBRANDT, J. T. PADDING, C. K. HEMELRIJK – *"FLUID DYNAMICS OF MOVING FISH IN A TWO-DIMENSIONAL MULTIPARTICLE COLLISION DYNAMICS MODEL"*

has been difficult, both empirically and theoretically, to accurately determine this (Schultz and Webb, 2002). For example, a number of theoretical predictions has not yet been tested, such as 1) that thrust is produced by the kinematics of only the tailtip, 2) that the swimming efficiency is indicated by the slip ratio U/V between the forwards swimming speed U and the rearwards speed of the body wave V. Also untested is the simplifying assumption of many computational models that fish despite being constrained in their acceleration still swim naturally (Lighthill, 1960; Liu et al., 1996; Wolfgang et al., 1999; Sui et al., 2007; Borazjani and Sotiropoulos, 2008, 2009). To test these questions empirically is difficult. Therefore, in the present paper we use a computer model (the so-called Multiparticle Collision Dynamics method) to do so, because of its accuracy in all aspects of hydrodynamics (Malevanets and Kapral, 1998) and its suitability to model biological hydrodynamics (Reid et al., 2009).

Models are needed because of the empirical difficulties of studying the kinematics and hydrodynamics of swimming fish. Empirical measurements of the hydrodynamics are hardly possible yet, and all empirical studies of swimming fish are labour-intensive: they involve filming the fish, and frame-by-frame analysis of swimming kinematics (Gray, 1933) and flows (using particle-seeded water) (Stamhuis and Videler, 1995; Müller et al., 1997, 2000; Tytell and Lauder, 2004; Tytell, 2004). Further, the calculation of Froude efficiency is based on the forces of thrust and drag, which for a steadily swimming fish cancel each other out. To determine these forces accurately, according to Dabiri (2005) not only the velocity field but also the pressure field around the fish should be measured. This is however not possible so far empirically, but can easily be done in models.

Both mathematical and computational models have been used to study the hydrodynamics of swimming fish. The mathematical models greatly simplify both the fish and the fluid: the fish are represented by rods, flat plates or airfoils and the fluid is represented without viscosity (Taylor, 1952; Lighthill, 1960; Wu, 1961; Cheng et al., 1991; Carling et al., 1998; McMillen and Holmes, 2006). Due to these simplifications, even the most influential mathematical theory (the Elongated Body Theory (Lighthill, 1971)) is inaccurate, specifically as regards its use of the slip ratio U/V to indicate swimming efficiency (Cheng and Blickhan, 1994; Barrett et al., 1999; Liao et al., 2003b; Borazjani and Sotiropoulos, 2008, 2009).

Recent increases in computational power have made it possible to use computer models that take into account both viscosity and the detailed shape of fish. These computational models can be divided in two classes, namely numerical methods and particle-based ones.

Earlier numerical methods simulate hydrodynamics of swimming by approximating the Navier-Stokes equations on a spatial grid. In these models, however, the calculations of the interactions between the fluid and the organism are complex (Gilmanov and Sotiropoulos, 2005; Borazjani et al., 2008; Borazjani and Sotiropoulos, 2008, 2009), whether the grid is continually adapted to the shape of the fish as in the older models (Liu et al., 1996; Barrett et al., 1999; Schultz and Webb, 2002; Mittal, 2004) or is kept fixed, as in newer models, e.g. the Immersed Boundary method (Peskin, 2002).

The particle-based methods simulate hydrodynamics through particles that move and collide. From these interactions at the micro-scale, hydrodynamics according to the Navier-Stokes equations emerge at the macro-scale. The particles may be restricted to a grid, such as in the commonly-used Lattice Boltzmann method (Sui et al., 2007), or move freely as in several other methods (Monaghan, 1992; Kajtar and Monaghan, 2008; Malevanets and Kapral,

1998). In case they move freely, the interactions among particles may be smoothed over longer ranges, such as in in the Smoothed Particle Hydrodynamics method (Monaghan, 1992; Kajtar and Monaghan, 2008), or be more local, as in the Multiparticle Collision Dynamics method (Malevanets and Kapral, 1998). Multiparticle Collision Dynamics has been shown to produce hydrodynamics consistent with the Navier-Stokes equations (Malevanets and Kapral, 1999; Kikuchi et al., 2003; Padding and Louis, 2006). It has been used to model biological motion at a microscopic scale (i.e. at Reynolds numbers below 10^{-2}). Examples include groups of swimming sperm cells (Yang et al., 2008), star polymers under shear flow (Ripoll et al., 2006) and tumbling red blood cells (Noguchi and Gompper, 2005), and our recent study of stiff fish-like shapes (Reid et al., 2009).

All worthwhile theoretical models make predictions and simplifying assumptions. Here we investigate the correctness of two predictions and one common simplification in the Multiparticle Collision Dynamics method. The first two originate from the Elongated Body Theory (Lighthill, 1960, 1971, 1975). They are, first, the prediction that thrust of swimming fish is produced only by the kinematics of the tail-tip and second, that the slip ratio U/V indicates swimming efficiency (Lighthill, 1971). Further, the assumption – used in many computational models – that fish that are constrained from accelerating still show natural swimming behaviour (Liu et al., 1996; Wolfgang et al., 1999; Sui et al., 2007; Borazjani and Sotiropoulos, 2008, 2009). To gain more insight in the effects of constraints, we study fish that are constrained from accelerating forwards, sideways or in both directions.

We choose the Multiparticle Collision Dynamics method because it has several advantages. Firstly, it models viscosity. Secondly, it is computationally cheap because it is not continually adapting a grid (Liu et al., 1996; Barrett et al., 1999; Schultz and Webb, 2002; Mittal, 2004; Gilmanov and Sotiropoulos, 2005; Borazjani and Sotiropoulos, 2008, 2009). Thirdly, due to its lack of a grid it is suitable to study complex, moving shapes. Fourthly, it is well suited to parallellisation because there are no long-range interactions among the particles (Monaghan, 1992; Kajtar and Monaghan, 2008)). This means it can be efficiently executed on a modern graphics card.

Computational efficiency is also the reason that we choose to simulate in two dimensions. Besides the obvious gains due to eliminating one dimension of space, the computational efficiency of two-dimensional simulations is also increased because all flow phenomena occur at lower Reynolds numbers than in three-dimensional simulations (Reid et al., 2009). Nevertheless, results of two-dimensional models of swimming fish resemble those of real fish remarkably (Triantafyllou et al., 1993; Pedley and Hill, 1999; Schultz and Webb, 2002; Sui et al., 2007).

We validate our model against empirical and theoretical data of thrust and drag of a flapping model of an insect wing (Wang et al., 2004) and against empirical data of mullets as regards equilibrium swimming speed and the structure and energy of the wake (Müller et al., 1997).

We study undulating fish over a range of tailbeat frequencies, when they are constrained in their acceleration, forwards, sideways or both. We measure their forwards and sideways forces, their slip ratio U/V, their Froude efficiency and the distribution of forces along the body.

3.2 METHODS

3.2.1 *Multiparticle Collision Dynamics*

The model consists of two rectangular environments filled with fluid, one in which an insect wing flaps and another in which a fish undulates. The environment is two-dimensional, homogeneous, contains N identical particles of mass m and has height H and width W for the insect wing and width W and length L_{box} for the fish (Fig. 3.1). The positions $\mathbf{x}_i$ and velocities $\mathbf{v}_i$ of the particles are given by two-dimensional vectors of continuous variables. Every time step Δt the particles first move and then collide with each other. Moving leads to new positions $\mathbf{x}_i$ according to the motion equation $\mathbf{x}_i(t + \Delta t) = \mathbf{x}_i(t) + \mathbf{v}_i(t)\Delta t$.

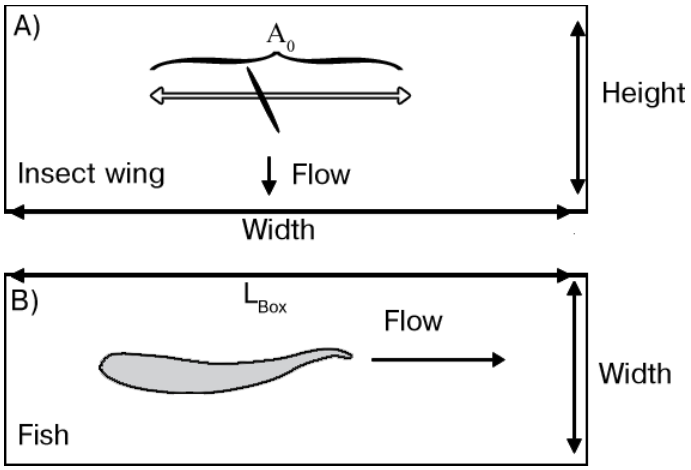

Figure 3.1.: Overview of the system for A) the flapping insect wing and B) the swimming fish. The wing moves along the open arrow, over the distance A_0. The height H and width W of the box (insect wing) and the width W and length L_{box} of the box (fish) are not to scale.

To efficiently simulate collisions between particles, both time and space are coarse-grained by using a square lattice: During the collision step, space is partitioned *temporarily* into cells of size a_0. All particles that are in a particular cell during the collision step are considered to have collided with each other at some moment in the preceding movement step, during which the particles moved in continuous space. To simulate collision, in each lattice cell all particles change their velocities according to $\mathbf{v}_i = \overline{\mathbf{v}} + \Omega \cdot (\mathbf{v}_i - \overline{\mathbf{v}})$. Here $\overline{\mathbf{v}}$ is the mean velocity of the particles in the grid cell and Ω is a stochastic rotation matrix that rotates the velocities by either $+\alpha$ or -α (where α is a fixed system parameter), with equal probability. The rotation direction at a specific moment in time is the same for all particles within a cell but it may differ between time steps. To ensure Galilean invariance we use the method of Ihle and Kroll (2001) and displace the lattice every time step by a vector with x- and y-components which are randomly selected from the uniform interval $[0, a_0)$.

An advantage of the MultiParticle Collision Dynamics method is that several transport properties, such as the shear viscosity and the viscous friction have been analytically

calculated for it (Kikuchi et al., 2003). The most important one for this study is the dynamic viscosity μ, which consists of 2 components:

$$\mu = \mu_{kin} + \mu_{coll}, \tag{3.1}$$

where μ_{kin} is the kinetic component of the viscosity (momentum transported through motion of the particles) and μ_{coll} is the collisional component (momentum transported through interactions between the particles). The equations for the components of the viscosity for the 2D model are (Kikuchi et al., 2003) :

$$\mu_{kin} = \frac{\rho k_B T \Delta t}{a_0^2} \left[\frac{\rho}{(\rho - 1 + e^{-\rho})(1 - \cos 2\alpha)} - \frac{1}{2} \right] \tag{3.2}$$

$$\mu_{coll} = \frac{m(1 - \cos \alpha)}{12 a_0 \Delta t} (\rho - 1 + e^{-\rho}), \tag{3.3}$$

where ρ is the average number of particles per cell, $k_B T$ is the system temperature and Δt is the size of the simulation time step (Table 3.1).

Temperature	$k_B T$	1.0
Lattice cell size	a_0	1.0
Collision rotation angle	α	$\frac{\pi}{2}$
Particle mass	m	1.0
Particles per cell (average)	ρ	8
Time step length	Δt	1.0
Boundary width	B	30
Boundary displacement steepness	n	3
Dynamic viscosity	μ	1.15
Insect wing motion		
Amplitude	A_0	165.0
Chord length	c	58.0
Frequency	f	$4 \cdot 10^{-4}$
Amplitude of rotation	β	$\frac{\pi}{4}$
Fish undulation		
Length	L	900.0
Number of edges	N_E	1024
Wave number	k_L	1.8
Tailbeat frequency	f	$4.8\text{–}6.3 \cdot 10^{-4}$

Table 3.1.: Parameter values used. All values are in simulation units.

3.2.2 *System Boundaries*

The studies we use for comparison assume that the flapping cross-section of a plexiglass model of an insect wing (Wang et al., 2004) and the undulating fish (Müller et al., 1997) are moving in a homogeneous, infinite field. We adapt our boundary conditions in order

to mimic this. To fulfil the criterion of infinite field size, the ordinary periodic boundary conditions suffice. in order to ensure homogeneity of the flow and eliminate irregularities such as vortices, we added a scrambling boundary zone inside the simulation borders (zone B in fig. 3.2). The scrambling eliminates local inhomogeneities of both density and velocity by changing both the position and speed of particles: Each particle in the boundary zone has a chance $p_{displace}$ to randomly move to a new position and have its speed overwritten with a new random one drawn from a Maxwell-Boltzmann distribution with mean 0 and temperature $k_B T$. The probability of displacement smoothly increases from 0 at the inner boundary of the zone to 1 at the outer boundary, following

$$p_{displace} = \left(1 - \frac{Dist}{B}\right)^n, \tag{3.4}$$

where $Dist$ is the distance to the nearest outer boundary and n determines the steepness of the increase of $p_{displace}$ (Fig. 3.2). Displacement is parallel to the nearest system edge: if the particle is close to a vertical border its y-coordinate is randomised, if it is close to a horizontal border its x-coordinate is changed. The zones of vertical and horizontal shuffling connect diagonally in the corners of the simulation. The new coordinate is uniformly distributed over an interval R which lies between these diagonals (Fig. 3.2).

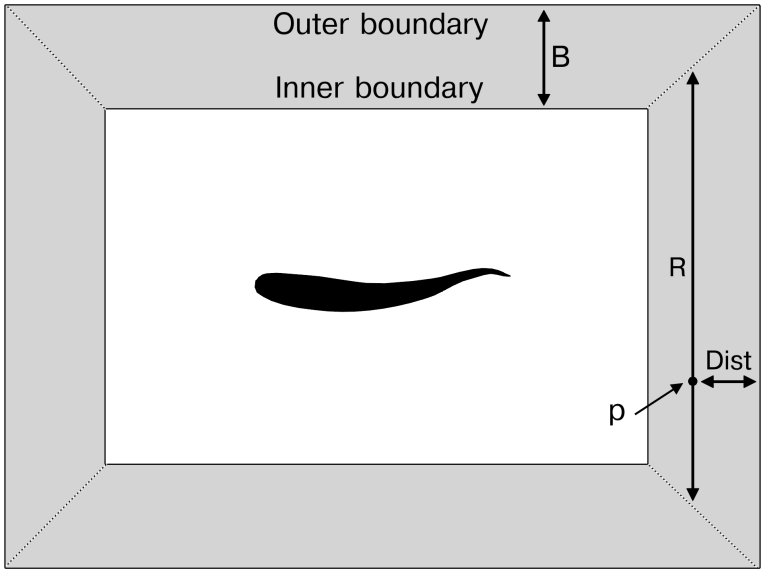

Figure 3.2.: Scrambling boundary condition. Within the boundary zone of thickness B (not to scale), a particle p's probability to be randomly displaced depends on its distance $Dist$ to the outer system edge. Displacement is parallel to the nearest system edge. Dotted lines indicate the boundaries between horizontal and vertical shuffling zones. The new position is along the interval R which lies between these boundaries at distance $Dist$ from the outer system edge.

3.2.3 *Boundary conditions and box size*

Our boundary conditions appear to eliminate the vorticity of the flow of both the insect wing (Fig. 3.3A) and the fish (Fig. 3.3B).

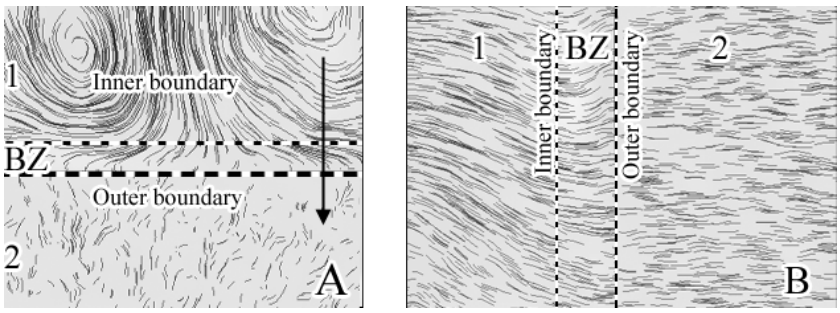

Figure 3.3.: Elimination of vorticity by the boundary zone for A) Wake of the flapping insect wing. B) Wake of the swimming fish (Fig. 3.2). The arrow shows overall flow direction. Black lines are truncated streamlines. Localised flow phenomena are eliminated by the boundary zone (BZ) as fluid travels through it from one part of the simulation (1) to another (2).

However, if the simulation box is too small interactions between the moving organism and the boundary zone may influence our results. To determine the optimal box size, we tested different box sizes for both insect wing and fish. For the insect wing we measured drag and lift and found that the box height must be above 8 chord lengths c to avoid influencing the drag (Fig. 3.4A) but does not influence the lift, and that there were no constraints on width as regards either drag or lift. To be sure to avoid unwanted effects of the edges of the box, we used relatively large boxes of ten by ten chord lengths.

For the undulating fish, we tested the effect of box size on the equilibrium swimming speed. The box length appeared not to affect the speed (Fig. 3.4B), thus we conclude that the boundary conditions correctly eliminate momentum and vorticity. For box width, it appeared that for widths below 1 fish length L the swimming speed of the fish increased, due to the channelling effect (Weihs, 1973) (data available on request). In order to avoid this and leave space for the wake to develop we use a box length of four body lengths and a box width of one body length.

3.2.4 *Particle-Object Collisions*

The fluid and organism interact during both the collision and the streaming step. These interactions exchange momentum between the fluid and organism, and ensure that there is no slip at the interface. This is done by two methods, ie. the fake particle rule during the collision step (Lamura et al., 2001), and the random-reflect rule during the streaming step (Inoue et al., 2001; Padding and Louis, 2006). The fake particle rule is applied to cells which are partially filled by the organism and partially by the fluid. Here we represent the organism by including fake particles in such a number that the number of particles in the cell equals the mean density ρ (Fig. 3.5A) The velocities of these fake particles are drawn

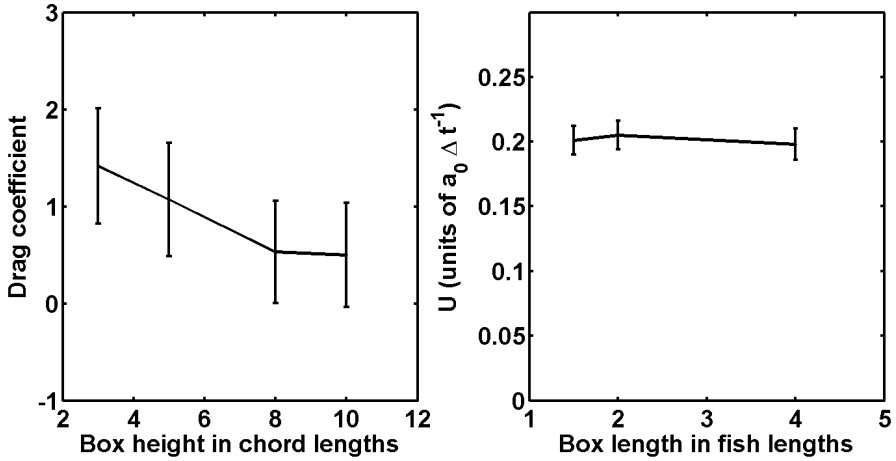

Figure 3.4.: Effects of size of simulation box on A) drag coefficient of the cross section of an insect wing (box size in chord length c of the wing) and B) equilibrium swimming speed (in simulation units) of the undulating fish (box size in fish body length L.

from a Maxwell-Boltzmann distribution with temperature $k_B T$ and a mean velocity which is equal to the local velocity of the organism. Note that the change in momentum due to the rotation of the fake particles is important to include in the hydrodynamical forces on the organism. In case of the fish, omission of this force greatly reduces forward motion (see Fig. S1).

In the random-reflect boundary condition, particles that hit the organism get a new randomly chosen velocity. The new velocity, relative to the surface, consists of a tangential component v_t and normal component v_n, drawn from the following distributions (Inoue et al., 2001; Padding and Louis, 2006):

$$P(v_t) \propto e^{-\beta v_t^2} \tag{3.5}$$

$$P(v_n) \propto v_n e^{-\beta v_n^2}, \tag{3.6}$$

with $\beta = \frac{m}{2k_B T}$. Both methods also have the benefit that they make the organism act as a weak thermostat because they introduce random velocities of the average system temperature $k_B T$.

The organisms in our models are represented as polygons. This means that their outline is composed of a finite series of lines, so-called edges, which meet at points called vertices. Every time step Δt the vertices move according to the specified motion of the object, which represent the flapping of the wing or the undulation of the fish (Eqs. 3.8, 3.10). We use Euler integration, meaning that during a time step the displacement of the vertices is equal to their velocity. The local velocity of any point on the object's surface can be calculated by interpolating the velocities of the two adjacent vertices.

Because the same particle may collide with an object multiple times within one time step Δt, we use the following iterative procedure to determine its trajectory. For each particle, the time δt it has spent moving during the current time step is set to 0. Then, as long as

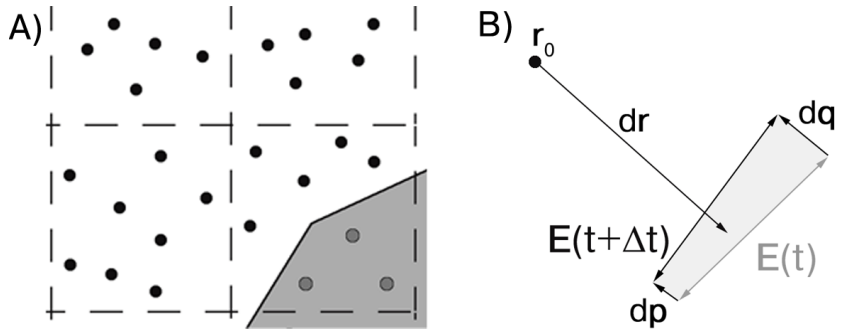

Figure 3.5.: A) "Fake particle" boundary condition. Fake particles (indicated in gray) are included in cells which partially overlap the object (indicated in light gray), and where the number of particles is below the mean fluid density. Mean fluid density ρ is 8 (Table 3.1). B) Schematic overview of the intersection between the path of a moving particle $\mathbf{r}$ and a moving edge $\mathbf{E}$. The precise intersection point depends on the movement speed of both the particle ($d\mathbf{r}$) and of the edge ($d\mathbf{p}$ and $d\mathbf{q}$ for the endpoints of the edge). The area through which the edge E moves during the time step Δt is indicated in gray.

δt is smaller than the length of a time step Δt (Table 3.1), the particle keeps moving. Its movement path is calculated from its velocity vector $\mathbf{v}_i$ as follows: $\mathbf{v}_i \cdot (\Delta t - \delta t)$. If this line intersects one of the edges of an object, a collision occurs at the collision point $\mathbf{x}_{coll}$ and δt is increased by the amount of time it took to move there. The movement path of a particle can be parametrically expressed as a line segment $\mathbf{r}(t) = \mathbf{r}_0 + t d\mathbf{r}$ with $t \epsilon [0, 1]$, where $\mathbf{r}_0$ is its initial position and $d\mathbf{r}$ is its velocity. The motion of the edges of the object is defined by the motion of the vertices at their endpoints. The movement path of the two vertices connected by an edge can also be expressed as two line segments: let $\mathbf{p}(t)$ and $\mathbf{q}(t)$ be the position of the vertices over time, as follows : $\mathbf{p}(t) = \mathbf{p}_0 + t\, d\mathbf{p}$ and $\mathbf{q}(t) = \mathbf{q}_0 + t\, d\mathbf{q}$. We then also define the edge itself as a line segment, pointing from $\mathbf{p}(t)$ to $\mathbf{q}(t)$. Its starting position is $\mathbf{p}(t)$ and its direction $\mathbf{u}(t)$ is $\mathbf{u}(t) = \mathbf{q}(t) - \mathbf{p}(t)$, or more explicitly

$$\mathbf{u}(t) = (\mathbf{q}_0 - \mathbf{p}_0) + t\,(d\mathbf{q} - d\mathbf{p})\,. \tag{3.7}$$

Any point on the edge can be expressed as $\mathbf{E}(s,t) = \mathbf{p}(t) + s\mathbf{u}(t) = s\mathbf{q}(t) + (1-s)\mathbf{p}(t)$.

The movements of particle and edge intersect (Fig. 3.5B) if at any time t' the equality $\mathbf{E}(s,t') = \mathbf{r}(t')$ holds. This gives two equations (one for each component x and y) with two unknowns (s and t'). Solving this leads to a quadratic equation, the roots of which can be found using the quadratic formula. More details can be found in the appendix.

After the collision, the particle gets a new random velocity following Eqs. 3.5 and 3.6, with the local speed of the object surface added to the result. If δt is smaller than Δt, it keeps moving, starting from the point of collision $\mathbf{x}_{coll}$ and may collide several additional times in the same manner.

The force which the fluid exerts on the object during a time step Δt is the opposite of the sum of the change in momenta of all particles that collide with it during that time step, divided by the time step Δt. Note that particles may collide with the body both during the

streaming step (as described above), and during the rotation step (through the fake particle rule).

3.2.5 *Insect Wing*

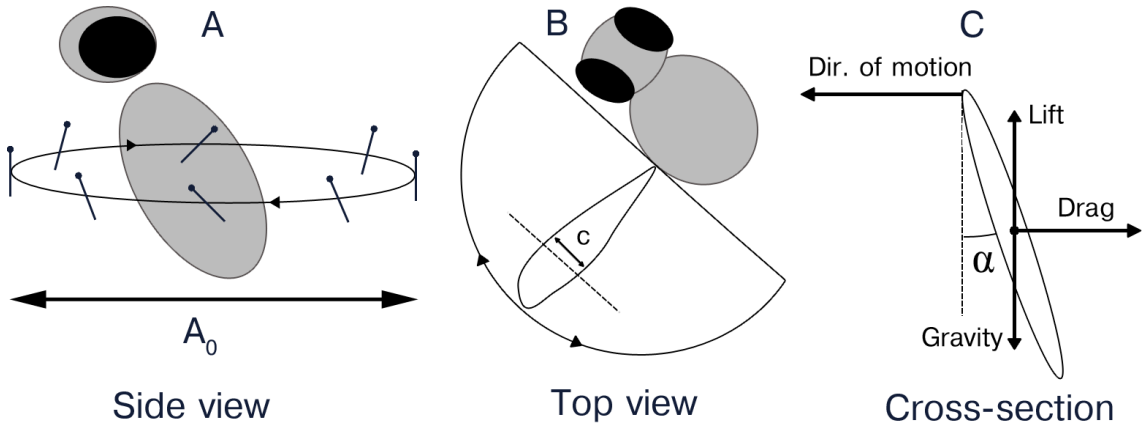

Figure 3.6.: Schematic overview of a hovering fruit fly. A) Side view: a series of snapshots of the moving cross-section of the wing as moves back and forth over distance A_0. The leading edge of the wing is represented by a dot. Movement and rotation of the wing are in phase. The elliptical path of motion is a visual aid: in the simulations the wing does not displace vertically. B) Top view of the insect: the dashed line shows which cross-section (of chord length c) of the wing we simulate. C) Forces on the moving wing. The forces act on the centre of gravity.

Our simulations of the cross-section of an insect wing (Fig. 3.6A,B), based on those by Wang et al. (2004), concern a two-dimensional representation of a transverse cross-section of a horizontally beating upscaled model of a wing of a fruit fly (*Drosophila melanogaster*) as it hovers in place. We represent the cross-section of the wing by an ellipse with a thickness ratio of 0.125 (Fig. 3.6C). We make the wing (with chord length c) move, without it being influenced by the flow around it, as follows. It moves back and forth through the horizontal plane over a distance A_0 while it rotates around its centre of mass (Figs. 3.1A, 3.6A). The position $x(t)$ of the centre of the wing cross-section and the angle $\alpha_w(t)$ between the wing and the y-axis change over time with frequency f according to

$$x(t) = \frac{A_0}{2}\cos(2\pi f t) \tag{3.8}$$

$$\alpha_w(t) = \alpha_{w,0} + \beta\sin(2\pi f t + \phi). \tag{3.9}$$

Here A_0 is the amplitude of the path of the wing, $\alpha_{w,0}$ is the initial angle, β is the amplitude of the angle and ϕ is the phase difference between the functions of position and angle. This phase difference determines the angle of the wing when it reverses its movement. If there is no phase difference the wing is vertical when its movement reverses, and the wing stroke is symmetrical. If rotation is advanced, the wing is already rotating back from the vertical position before it reaches the extremes of its movement path. If rotation is

delayed, the wing has not finished rotating through the vertical as it reaches the extreme of its stroke (Dickinson et al., 1999; Wang et al., 2004). Like in the study of Wang et al. (2004) we compare the effects on drag and lift of symmetrical ($\phi = 0$), advanced ($\phi = \frac{\pi}{4}$) and delayed ($\phi = \frac{-\pi}{4}$) rotation. We measure the force which the fluid exerts on the moving wing, and decompose it into lift and drag components. The insect is hovering, therefore its lift compensates for the gravity. The drag is horizontal and counteracts the wing's motion.

3.2.6 *Fish*

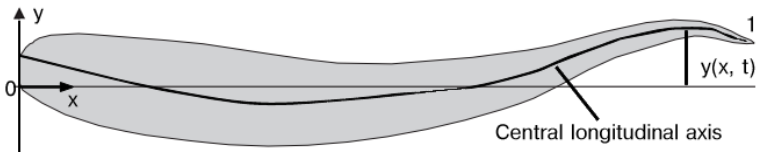

Figure 3.7.: Schematic overview of the deviation from the central axis of the spine of an undulating mullet.

We study the mullet (*Chelon labrosus*) because it swims at a steady speed by undulating its body without using its pectoral fins (Videler, 1993). We simulate an undulating horizontal cross-section of a mullet, traced from the body contours presented by Müller et al. (1997). Because the shape of the fish is more curved at the head than at the tail, we made the polygonal edges at the head of the fish shorter than those of the rear. Note that the undulation of our simulated fish is not influenced by the flow around it. We formulate the characteristics of the propulsive wave along the body of the fish in terms of the lateral movement of its central, longitudinal axis, or spine (Videler and Hess, 1984). To do so, we consider the spine of the straight fish to have an y-value of 0 (Fig. 3.7). We scale the fish in terms of fractions of its body length L, so that $x = 0$ at the front of the fish and $x = 1$ at its rear. For each point x along the spine of the fish, its lateral deviation from the central axis over time is given by

$$y(x,t) = \theta(x)\sin(k_L x - \omega t). \tag{3.10}$$

Here $\theta(x)$ is the amplitude envelope function, which varies nonlinearly along the fish body, $k_L = \frac{2\pi}{\lambda}$ is the wave number, which indicates the number of complete sine waves on the body for a wavelength λ , and $\omega = 2\pi f$ is the angular velocity for the tailbeat frequency f. For undulating mullets the amplitude of the wave is smallest behind the head and increases quadratically towards the tail:

$$\theta(x) = \theta_0 + \theta_1 x + \theta_2 x^2, \tag{3.11}$$

Steady swimming by undulating the body is characterised by two parameters, the Reynolds number Re and the Strouhal number St, which are defined as (Reynolds, 1883; Videler, 1993; Vogel, 1996):

$$Re = \frac{\rho U L}{\mu}, \tag{3.12}$$

$$St = \frac{Af}{V}, \tag{3.13}$$

Where ρ and μ are respectively the density and dynamic viscosity of the fluid, and the remaining parameters describe the fish: L is its length, U its swimming speed, f the frequency of its tailbeat and A is two times the maximum lateral excursion of its tail tip over the tailbeat cycle, which is used as an approximation of the width of its wake.

To give an individual infinite space in which to swim, we move the simulation box along with it. We do so as follows: Whenever the centre of gravity of the fish has moved one cell a_0 away from its original position within the centre of the box, we move the box centre towards that of the fish by one simulation unit a_0. We shift only when it has moved at least one simulation unit, because smaller shifts may cause floating point rounding errors to accumulate. The shift may be horizontal, vertical or both. Subsequently, we apply the periodic boundary condition, thus any particles which left the simulation box through one side are reintroduced at the other side of the simulation, with their velocity overwritten with a random one drawn from a Maxwell-Boltzmann distribution with mean 0 and temperature $k_B T$.

To study the effects of constraint on the acceleration of the fish along its two axes of movement (forwards and sideways), we test the four possible combinations of constraint : 1) free acceleration along all directions ("unconstrained") 2) No sideways acceleration ("sideways constrained") 3) Neither forwards nor sideways acceleration ("all constrained") and 4) No acceleration forwards ("forwards constrained"). If acceleration is unconstrained in at least one direction, we apply along this direction the appropriate component of the net hydrodynamical force to the centre of gravity of the fish. So for instance if a fish is sideways constrained, this implies that the centre of gravity does not accelerate sideways (Fig. 3.8). We consider the fish to have a density equal to that of the fluid, and a mass equal to its surface area times the density ρ. To displace the fish, we use Euler integration and change the position of its centre of gravity by its speed vector.

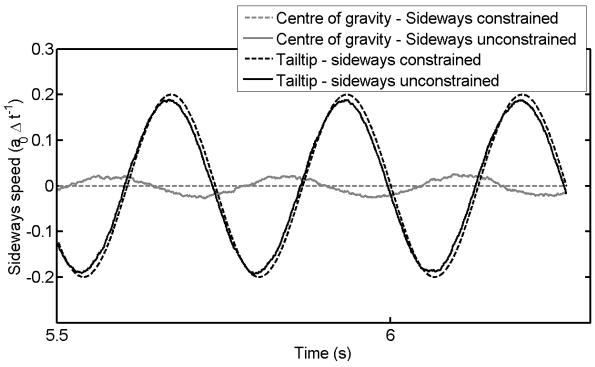

Figure 3.8.: Sideways speed (in simulation units) over time of the centre of gravity of the fish and its tailtip, for fish that either are or are not constrained from sideways acceleration.

To keep the tracking of the forwards and sideways direction of the fish as simple as possible, we choose not to apply the torque to rotate the fish. Preliminary tests showed no effect of this omission on the measured variables.

3.2.7 *Parametrisation and Experimental Setup*

In the Multiparticle Collision Dynamics model, objects should not move faster than approximately 20% of the speed of sound in the fluid, because higher speeds cause significant compressibility effects such as shockwaves. This means that their Mach number $Ma = U/U_{sound}$ should not exceed $1/5$ (Lamura et al., 2001; Lamura and Gompper, 2002). For our parameter settings (Table 3.1), the speed of sound $U_{sound} = \sqrt{2k_BT/m} = \sqrt{2}$ (see (Lamura et al., 2001)). Thus, the maximum velocity of the organisms in our model per simulation time step is $\frac{1}{5} \cdot \sqrt{2} = 0.28a_0/\Delta t$. We conservatively choose a somewhat lower maximum velocity for our default parametrisation, $0.2a_0/\Delta t$. This restriction of the velocity limits our choices for the parametrisation of the moving organisms.

We parametrise our simulation of the flapping cross section of the wing after the experiments with an upscaled model of a Drosophila wing by Wang et al. (2004). We tune the Reynolds number (75) to theirs, via the wing chord length c and wing beat amplitude A_0 and the relation $A_0/c = 2.8$ between them. In our simulation the Reynolds number of the insect wing is $Re = U_{max}c\rho/\mu = 1.29c$, where the wing's maximum speed U_{max} is set to 0.2 as previously explained. Thus for a Reynolds number of 75, the chord length $c = 75/1.29 = 58a_0$ and the wing beat amplitude $A_0 = 2.8 \cdot c = 163a_0$. The experimental insect wing has a chord length of 0.067 m (Sane and Dickinson, 2002), thus our simulation length scale is $a_0 = 0.067/58 = 0.012$ m.

To determine the size of the simulation time step Δt in seconds, we calculate the ratio between the frequency of the wing beat in our simulation f_{sim} and that of the real wing $f_{real} = 0.25$Hz. Because the maximum of the speed function $\frac{\delta}{\delta t}x(t)$ is $U_{max} = A_0 c\pi f_{sim}$, we find that for the maximum speed of 0.2 that we chose due to Mach number constraints $f_{sim} = \frac{0.2}{163\pi} = 3.9 \cdot 10^{-4}\Delta t^{-1}$. Thus, the simulation time step for the insect wing simulations Δt is $1.6 \cdot 10^{-3}$ s (Table 3.2).

Our fish simulations are parametrised to resemble the experimental results of Müller et al. (1997) as regards undulation envelope, and size (Table 3.2). Our model of a fish is $900a_0$ long, which was the maximum that was computationally feasible on our hardware. Thus our simulation unit of distance $a_0 = \frac{0.126}{900} = 1.4 \cdot 10^{-4}$m.

We use the ratio between the swimming speed of the simulated and of the real fish to calculate the length of the simulation time step. The swimming speed is likely to be dependent on the tailbeat frequency (Videler, 1993), which we vary in our simulations. Here we present the time step calculations for the tailbeat frequency of the real mullet; the calculation is the same for other swimming speeds. The swimming speed of the model U_{sim} is intended to be $0.2a_0/\Delta t = 1.4 \cdot 10^{-4}m/\Delta t$, and the real fish swims at 0.176m/s. Therefore $\Delta t = 0.2 \cdot 1.4 \cdot 10^{-4}s/0.176 = 1.5 \cdot 10^{-4}$s (Table 3.2).

We start the simulations without directional flow, by initialising all particles with random velocities drawn from a Maxwell-Boltzmann distribution of mean 0 and temperature k_BT (Table 3.1). Thus, all directional flow in the simulation is caused by the movement of

Insect wing model	
Parameter name	Value
Amplitude	0.187 m
Chord length	0.067 m
Time step	0.0016 s
Frequency	0.25 s^{-1}
Fish	
Parameter name	Value
Length	0.126 m
Time step	0.00015 s
Tailbeat frequency	3.2–4.2 s^{-1}
Tailbeat amplitude	0.0126 m
Undulation amplitude coefficient θ_0	0.02
Undulation amplitude coefficient θ_1	0.08
Undulation amplitude coefficient θ_2	0.16

Table 3.2.: Parametrisation for the cross section of the insect wing model (Wang et al., 2004) and the fish in SI units.

the organisms. Following the experiments of Wang et al. (2004) we simulate 4 full wing beats of the insect wing. For the fish we follow the experiments of Müller et al. (1997) of a fish swimming at steady speed by letting the simulation run until the swimming speed and surrounding flow of the fish reach equilibrium.

3.2.8 *Computational Measurements*

For the flapping insect wing, we measure the forces of drag (horizontal) and lift (vertical). Like Wang et al. (2004), we nondimensionalize these forces by dividing them by the maximal force measured for a steadily moving wing.

For the undulating fish we use the same measurements as the experiments by Müller et al. (1997). They estimate the thrust force F_T indirectly, from the circulation Γ of the vortices in the wake. They use this indirect method because the thrust and drag operate along the same axis in opposite directions, and cancel each other out at a constant swimming speed. The circulation Γ of the vortices in the wake is calculated as $\Gamma = \oint_c \mathbf{v} \cdot d\mathbf{l}$, where c is a closed curve around a vortex, $\mathbf{v}$ is the fluid velocity and $d\mathbf{l}$ is a tangential unit vector along the curve c. From Stokes' theorem, the curve integral can be rewritten as $\Gamma = \mathbf{v}dy' = \iint \omega dA$, with ω being the vorticity and A the surface area of the vortex. In our method, we therefore sum the vorticity over the area of the vortex.

Due to the stochasticity of the method, spatial averaging is needed to obtain a smooth flow field. We employ a Gaussian convolution with a kernel of 50 a_0.

To measure the stability of the wake of the fish, we study an area of 1.5 body lengths behind the swimming fish. We measure the distances in the direction of swimming between subsequent vortices that rotate in the same direction (dx in Fig. 3.9), and the distances perpendicular to the swimming direction between subsequent counter-rotating vortices (dy

in Fig. 3.9). We establish the centre of a vortex by drawing in a screenshot two perpendicular lines through its area of maximal vorticity (the darkest for clockwise or lightest for counterclockwise vortices, respectively), and assuming that the centre lies at the intersection point of the two lines. The average distance we calculate over 10 snapshots taken at random intervals. We also measure the forces on the fish directly.

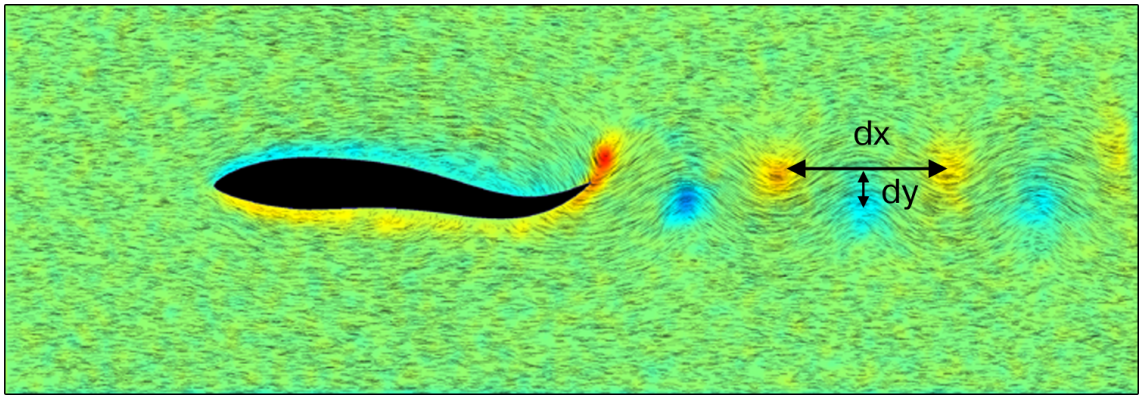

Figure 3.9.: Wake of the swimming fish in our model, with truncated streamlines. Distance between vortices in the swimming direction and perpendicular to it are indicated as dx and dy, respectively. Vorticity is shown by the colour, with blue indicating clockwise and red indicating counterclockwise vorticity.

In our simulations we determine thrust and sideways power as follows. The total forward force F at any moment t is calculated by a summation over the skin edges of the fish (Fig. 3.10):

$$F(t) = \sum_i \mathbf{F}_i \cdot \mathbf{e}_f = \sum_i \left(\mathbf{F}_n^i \cdot \mathbf{e}_f + \mathbf{F}_t^i \cdot \mathbf{e}_f\right), \tag{3.14}$$

where $\mathbf{F}_n^i = (\mathbf{F}_i \cdot \mathbf{n})\,\mathbf{n}$ is the force vector perpendicular to the skin at edge i, $\mathbf{F}_t^i = \mathbf{F}_i - \mathbf{F}_n^i$ is the force vector tangential to the skin and $\mathbf{e}_f$ is a forwards-pointing unit vector. The summations of the first and second element in the last expression thus represent the pressure and viscous contributions, respectively, to the forward force, though it should be noted that if the tangential speed varies strongly around the body the viscous forces may have a small normal component.

To separate the thrust and drag out of this total body force following the method of Borazjani and Sotiropoulos (2008), we decompose the force, depending on whether or not the force is positive (thrust) or negative (drag):

$$T(t) = \sum_i \left[\mathbf{F}_n^i \cdot \mathbf{e}_f H(\mathbf{F}_n^i \cdot \mathbf{e}_f) + \mathbf{F}_t^i \cdot \mathbf{e}_f H(\mathbf{F}_t^i \cdot \mathbf{e}_f)\right] \tag{3.15}$$

$$D(t) = -\sum_i \left[\mathbf{F}_n^i \cdot \mathbf{e}_f H(-\mathbf{F}_n^i \cdot \mathbf{e}_f) + \mathbf{F}_t^i \cdot \mathbf{e}_f H(-\mathbf{F}_t^i \cdot \mathbf{e}_f)\right], \tag{3.16}$$

where H is the Heaviside step function. Thus, for each edge, for both the perpendicular (pressure) and tangential (viscous) force on it, we add the forward component of the force to

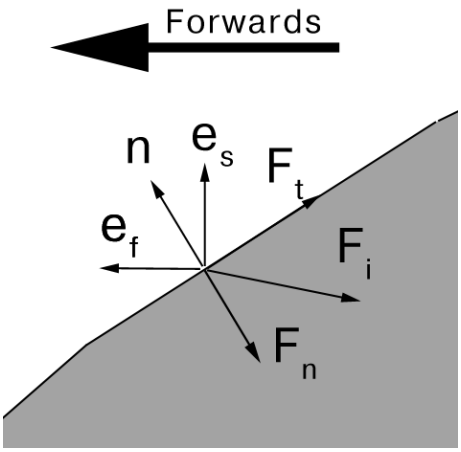

Figure 3.10.: Decomposition of the force F_i on the skin of the fish into pressure (F_n) and viscous (F_t) components (see Methods). The surface normal is indicated as n and the unit vectors pointing forwards and sideways are labelled e_f and e_s.

the thrust if it is positive, and to the drag if it is negative. The sum of thrust and drag is the total force $F(t)$:

$$F(t) = T(t) - D(t). \tag{3.17}$$

We calculate per time step Δt the sideways power P_s which the fish exerts:

$$P_s(t) = \sum_i \mathbf{F}_i \cdot \mathbf{e}_s V^i_{und}, \tag{3.18}$$

where $\mathbf{e}_s$ is a unit vector in the sideways direction, and V^i_{und} is the sideways velocity of edge i.

From these forces, we determine the swimming efficiency. Following Tytell and Lauder (2004) and Borazjani and Sotiropoulos (2008), we use a modified version of the Froude efficiency:

$$\eta = \frac{\bar{T}\bar{U}}{\bar{T}\bar{U} + \bar{P_s}}, \tag{3.19}$$

where $\bar{T}$ is the mean thrust over a tailbeat cycle, $\bar{U}$ is the mean forwards speed of the fish and $\bar{P_s}$ is the mean sideways power it exerts over a tailbeat cycle. Thus, the Froude efficiency η expresses the percentage of the total power which is converted into forwards speed.

To measure the distribution of the forces along the body of the fish, we calculate them for each edge of the polygon that represents the body, and compute the average and standard deviation per segment of the body. Each segment comprises an equal number of edges, and thus is shorter near the head.

All programs were implemented in a combination of C++ and OpenGL shading language, and simulations were run on a single Intel Core2 Quad PC. Single simulations of a 20 tialbeats of a swimming fish took approximately 12 hours on a single PC. Data analysis and visualisation were done with MATLAB ® (The MathWorks, n.d.) except for the vorticity plots which were made in our simulations.

3.3 RESULTS

3.3.1 *Comparison to empirical data*

We verify the correctness of our model on the basis of empirical data of a model of an insect wing (Wang et al., 2004) and of a swimming mullet (Müller et al., 1997).

For our insect wing, the time series of its drag and lift coefficient resemble experimental results of Wang et al. (2004) in all cases: with advanced rotation (Fig. 3.11A), with no phase difference between translation and rotation (Fig. 3.11B) and with delayed rotation (Fig. 3.11C). Of particular interest is the resemblance regarding two peaks of the drag and lift. One peak occurs close to the moment at which the wing has reversed its direction (Fig. 3.11B, indicated with 'w' at 3.1s) while the other happens just after the middle of the wing beat (Fig. 3.11B, indicated with 'r' at 3.3s), as the wing is beginning to slow from its maximum velocity and reverses its rotation. The first peak is most likely due to the wing re-encountering its own wake (a phenomenon known as 'wake capture' (Dickinson et al., 1999)), while the second peak is probably caused by a combination of rotation and deceleration of the wing (Wang et al., 2004). We confirm that the wing produces more lift with advanced rotation and much less lift with delayed rotation when compared to a wing with no phase difference (Table 3.3), similar to experimental data (Dickinson et al., 1999; Sun and Tang, 2002).

Average drag and lift coefficients				
	C_L		C_D	
	Expt	Sim	Expt	Sim
Sym	0.435	0.477	0.69	0.71
Adv	0.519	0.656	0.56	0.61
Delay	0.09	0.02	0.529	0.557

Table 3.3.: Drag and lift coefficients of the flapping insect wing averaged over time for symmetrical rotation ($\phi = 0$), advanced rotation ($\phi = \frac{\pi}{4}$) and delayed rotation ($\phi = -\frac{\pi}{4}$). Experimental results were time-averaged from figures 2–4 of Wang et al. (2004).

Our fish, for the same tailbeat frequency as the real fish, reaches a similar cruising speed (Table 3.4). Also similarly to real fish, our modelled fish produces a wake with a reverse von Kármán vortex street of alternating, counter-rotating vortices, at a fixed distance and angle from each other, with a jet zig-zagging between them (Fig. 3.9, movie online). The wake resembles that of a mullet (Fig. 5 in (Müller et al., 1997)) as regards the stability of its structure, the size of the vortex rings, their angle with the direction of swimming and their circulation, and the the variability of the distances between the vortices (dx and dy in Fig. 3.9), both in the swimming direction and perpendicular to it (Table 3.4).

From the correspondence of our results to empirical data (Wang et al., 2004; Müller et al., 1997) we conclude that our simulations are sufficiently accurate to further investigate the swimming of fish.

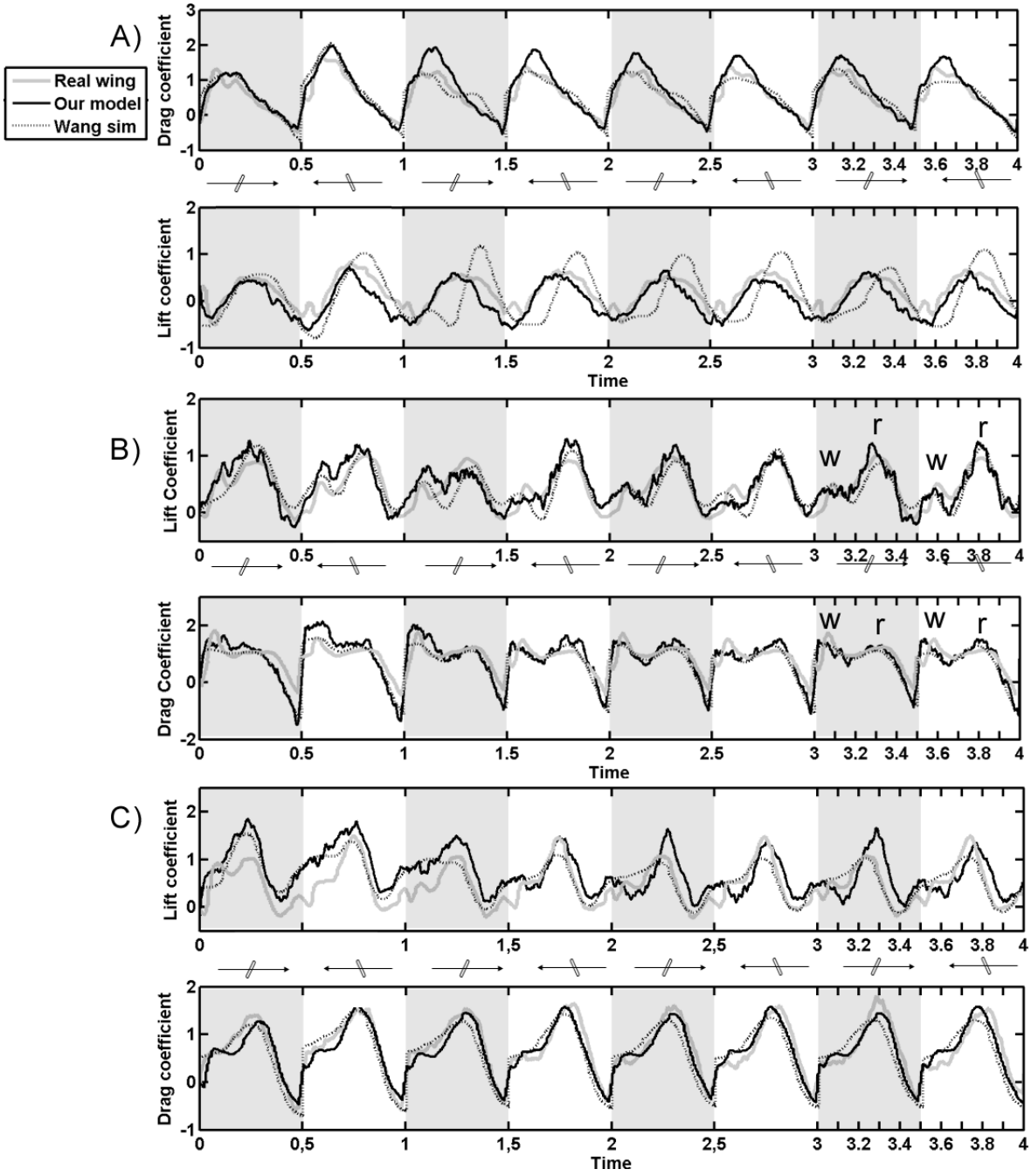

Figure 3.11.: Drag and lift coefficients of a flapping insect wing over time, at $A_0/c = 2.8$. Light gray areas indicate that the wing moves to the right. Real wing data taken from Wang et al. (2004). A) $\phi = -\frac{\pi}{4}$ (delayed rotation) B) $\phi = 0$. Force peaks associated with wake capture and rotational forces are labelled 'w' and 'r', respectively. C) $\phi = \frac{\pi}{4}$ (advanced rotation).

Measure	Simulation value	Experimental value
Swimming speed		
Equilibrium forwards swimming speed U	1.55 Ls^{-1}	1.4 Ls^{-1}
Wake structure and energy		
Ring radius R	104.5 a_0 = 1.45cm	1.9 cm
Ring angle ϕ	$52° \pm 9$	$40° \pm 10$
Circulation Γ	$9.6 \cdot 10^{-4} m^2 s^{-1}$	$7.6 \cdot 10^{-4} m^2 s^{-1}$
Standard deviation of vortex spacing dx, dy	5%, 5%	6%, 6%

Table 3.4.: Results for the equilibrium swimming speed and wake structure and energy of the swimming fish (Fig. 3.17). Experimental results are from Müller et al. (1997). Experimental vortex spacing estimated from their figures. Error ranges are the standard deviations.)

3.3.2 *Model results*

We study the contributions to thrust and drag of forces perpendicular and tangential to the skin. We investigate where on the body thrust and drag are produced, and what the effect is of tailbeat frequency and acceleration constraints on a number of measures such as swimming speed, thrust, drag, exerted sideways power, slip ratio, Froude efficiency and Strouhal number.

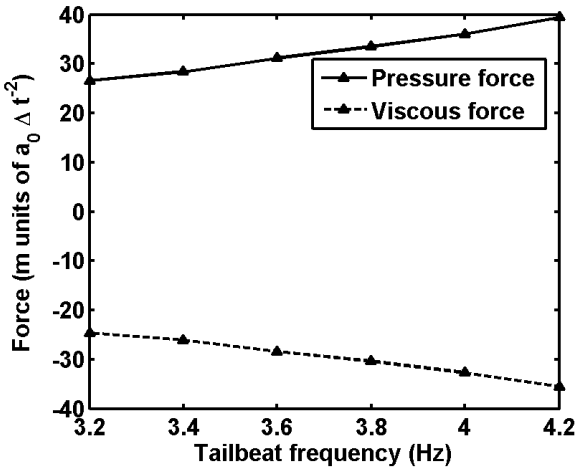

Figure 3.12.: Force in the swimming direction of the freely swimming fish, decomposed into pressure and viscous component. Positive values indicate thrust, negative drag.

Thrust appears to be caused mainly by forces perpendicular to the skin (pressure), and drag is caused by tangential forces (viscosity) (Fig. 3.12). The thrust appears to be produced not only by the tail (segment 8, Fig. 3.13), but by the complete rear 2/3ds of the body (segments 5-8, Figs. 3.13, 3.14). The only area that never produces thrust is the head of the fish, which is responsible for the majority of the drag (segments 1–4, Fig. 3.13) . The part of the body that produces the least drag is just behind the head of the fish (segment 5, Fig. 3.13).

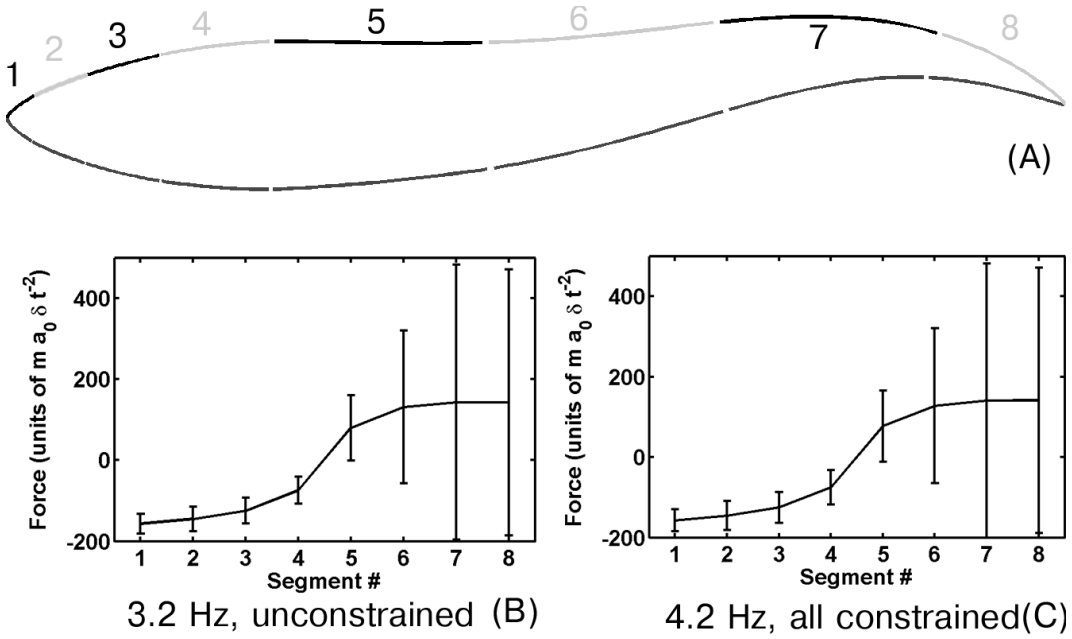

Figure 3.13.: Force in the swimming direction as distributed over several segments of the skin of the fish. Positive values indicate thrust, negative drag. Error bars indicate one standard deviation.

The locations and strengths of the forces on the skin (Figs. 3.14, 3.13) do not differ across the 6 tailbeat frequencies, 3 acceleration constraints and the unconstrained fish (data available on request). This similarity is a consequence of the small size of both the time step Δt and of the segments: differences between different settings can only be detected by averaging over both space and time.

As to the tailbeat frequency in our model, it positively affects forwards swimming speed (Fig. 3.15A), average lateral power (Fig. 3.15B), thrust (Fig. 3.15C) and the slip ratio (Fig. 3.15D), and it decreases the Froude efficiency (Eq. 3.19, Fig. 3.15E). This arises as follows: with increasing tailbeat frequency, the forwards speed increases because of the increased thrust. The Froude efficiency decreases because the sideways power increases more strongly than the forwards speed and thrust do. We explain the higher slip ratio (i.e. the higher swimming speed U relative to the rearwards speed of the body wave V) as resulting from the increased inertia relative to viscosity (i.e. the increased Reynolds number): when its tailbeat reverses, viscous drag slows the fish down less at higher tailbeat frequency. Thus we expect the variability of the swimming speed to decrease with the tailbeat frequency. We confirm this by the significant negative correlation between the tailbeat frequency and the coefficient of variation of the swimming speed ($N = 8$, Spearman's Rho $= -0.88$, $p = 0.007$).

The increased tailbeat frequency influences the wake by increasing the radius of the vortex rings and their angle ϕ with the swimming direction, implying that the wake widens (Figs. 3.16A, B). The circulation in the wake increases significantly for the unconstrained fish (Fig. 3.16C). For each of the sideways-constrained fish (twice $N = 6$, Spearman's Rho

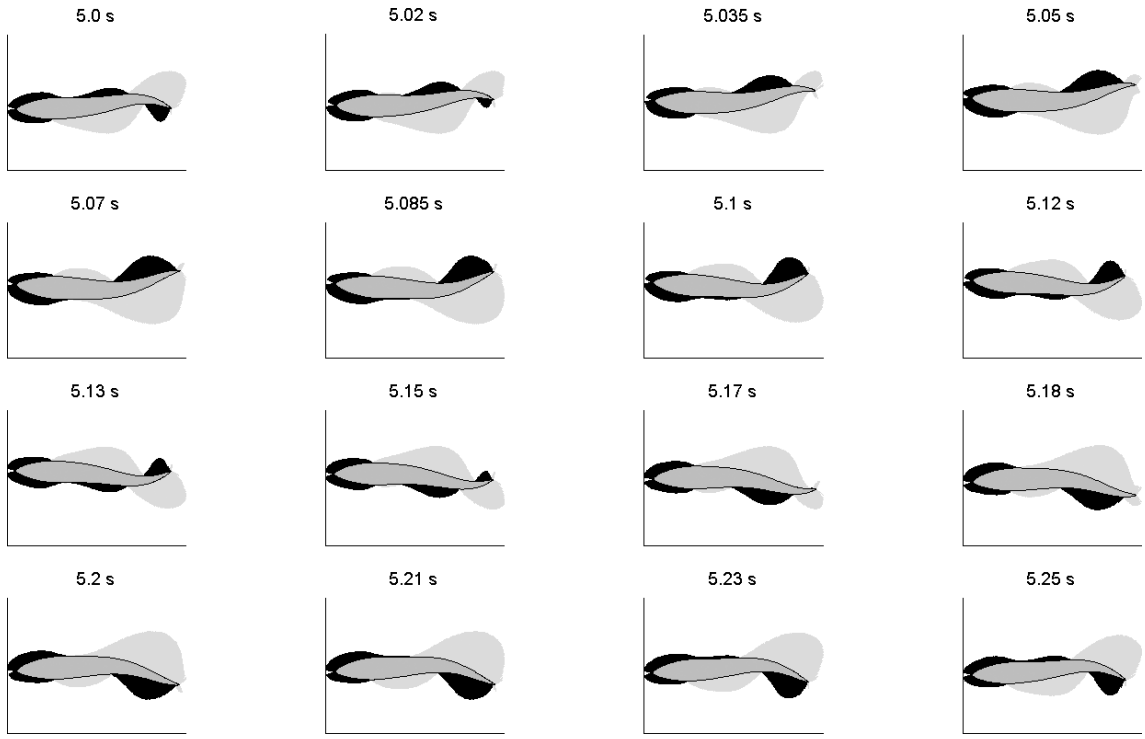

Figure 3.14.: Drag and thrust forces on the skin of the fish over time, for tailbeat frequency of 3.8Hz, unconstrained acceleration. Black indicates drag, gray thrust. Force areas are composed of lines perpendicular to the skin, with the length of the line indicating the relative size of the force on that segment of the skin.

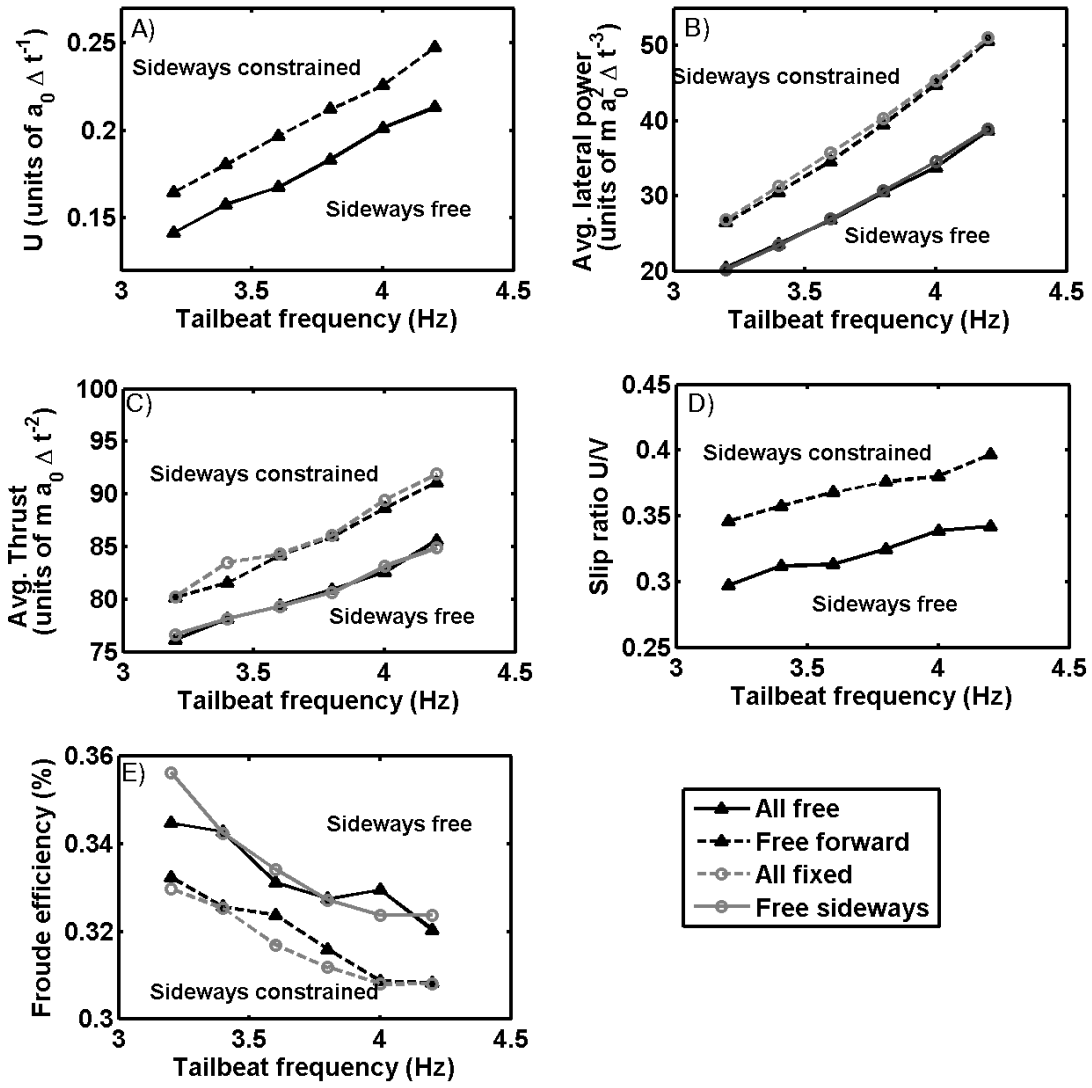

Figure 3.15.: Results of swimming fish that are either constrained or free in their forwards and sideways acceleration, for several tailbeat frequencies. A) Equilibrium forwards swimming speed B) Average lateral power exerted (in simulation units) by the fish C) Average forwards thrust component (in simulation units) D) Slip ratio U/V. E) Froude efficiency of the swimming fish (Eq. 3.19)

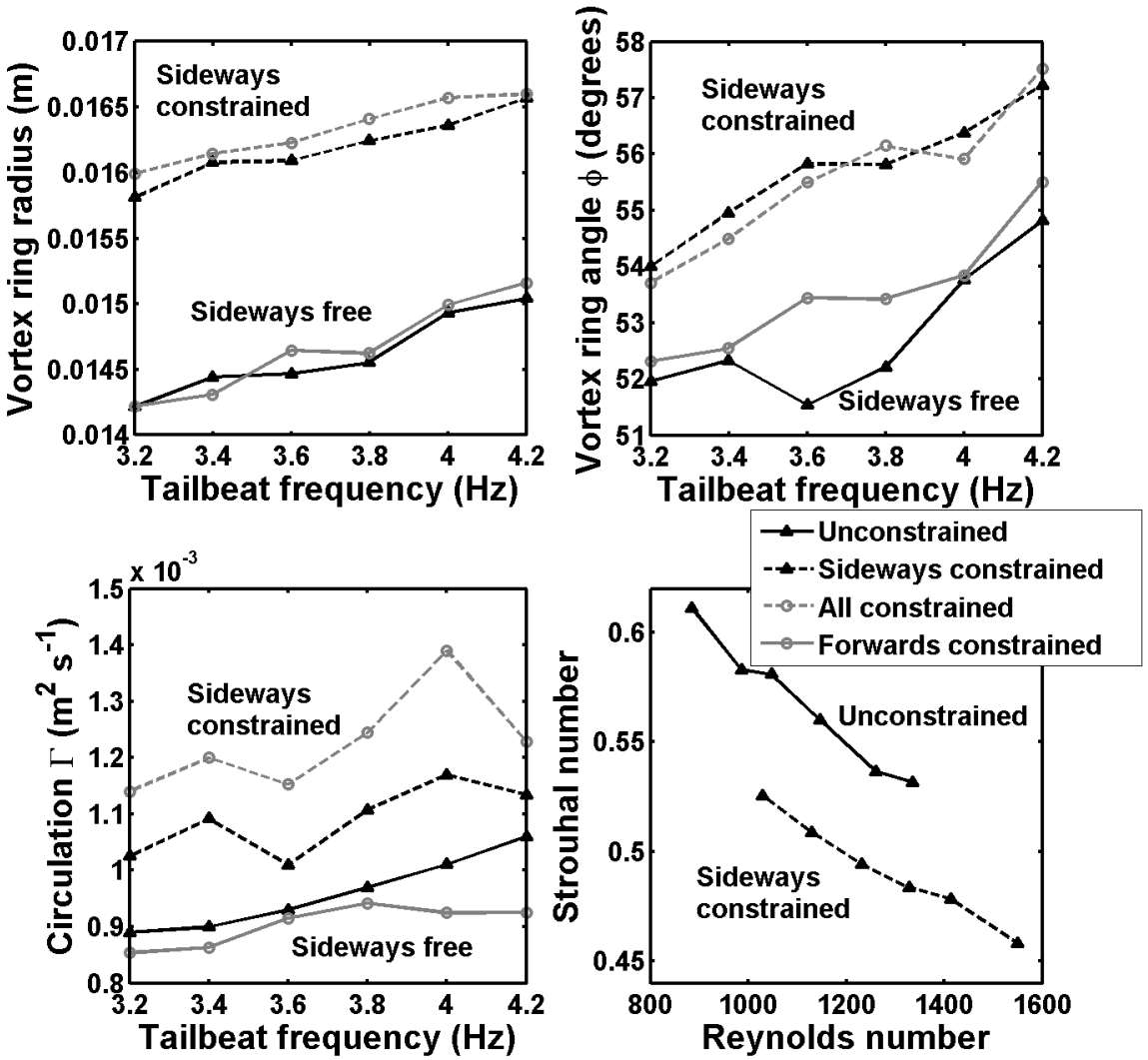

Figure 3.16.: Results of swimming fish that are either constrained or free in their forwards and sideways acceleration, for several tailbeat frequencies. A) Radius of the vortex rings in the wake of the fish B) Angle ϕ of the vortex rings with the forwards swimming direction (Fig. 3.17) C) Circulation Γ in the vortex rings of the wake D) Equilibrium Strouhal number of the swimming fish as a function of the Reynolds number.

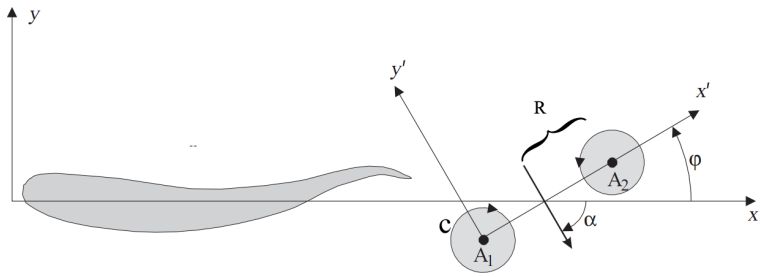

Figure 3.17.: Schematic overview of the wake structure of a mullet, after (Müller et al., 1997).

= 0.77 NS), and for the forwards-only constrained fish (Spearman's Rho = 0.83 NS), however, tailbeat frequency does not significantly influence circulation strength. The Strouhal number is lower for higher tailbeat frequencies (Fig. 3.16D). This implies that the vortices are closer to each other along the swimming direction.

Concerning the effects of constraint of sideways acceleration: Compared to no constraint, it significantly increases the swimming speed (Fig. 3.15A), sideways power (Fig. 3.15B), thrust (Fig. 3.15C) and the slip ratio U/V (Fig. 3.15B), and decreases the Froude efficiency (Fig. 3.15D). For the wake, sideways constraint increases the size, angle and circulation of the vortex rings (Figs. 3.16A-C) and decreases the Strouhal number (Fig. 3.16D). Note that these results are all similar to those of an increased tailbeat frequency. This arises because the sideways constraint increases the sideways velocity of the tail of the fish throughout its tailbeat (Fig. 3.8), because the fish does not accelerate in the direction opposite to where its tail pushes the water.

The effect of forwards constraint is hardly visible (Figs. 3.15, 3.16), except for reducing the circulation if the fish is sideways free and increasing it if the fish is sideways constrained (Fig. 3.16C). Since circulation is derived from the values of vorticity and vortex ring radius which are highly stochastic in our model, the importance of these differences is doubtful.

3.4 DISCUSSION

The resemblance between the fluid dynamics in our model and empirical data of the physical model of a wing of a hovering insect (Wang et al., 2004) and of the undulating fish (Müller et al., 1997) shows the suitability of the Multiparticle Collision Dynamics model for such studies.

Our results disagree with the two theoretical predictions (first, thrust exclusively produced by tailtip and second, slip ratio as an estimator of efficiency) and further show problems with the use of constrained acceleration as a representation of natural swimming. As regards the first point, we show that the rear 2/3ds of the body produces thrust at some point during the swimming cycle. Thus, empirical studies of the swimming of fish should investigate flow along the entire body rather than only focusing on the tail-tip and the wake (Müller et al., 1997; Tytell and Lauder, 2004), as illustrated experimentally by Müller et al. (2001) and Anderson et al. (2001).

As regards the second point, the slip ratio appears not to be an estimator of efficiency. The inverse relationship between it and Froude efficiency in our model is intriguing, because it is opposite of that predicted theoretically (Lighthill, 1960, 1971). So far the relationship between slip ratio and efficiency has only been studied empirically for fish swimming behind pillars, where they appeared to be more efficient (in terms of lower muscle activity) and have a lower slip ratio (Liao et al., 2003b). However, this situation, where the flow was unsteady and undulation was largely passive, cannot really be compared to a fish that swims actively in uniform flow, and therefore more empirical data are needed to test our results. This should be done by measuring of a fish both kinematics and energy expenditure (for example by using respirometers as proposed by Liao (2007)). In the meantime, our results warn against the common practise of using the slip ratio as an estimator of the efficiency of swimming fish (Gillis, 1998; Müller et al., 2002).

Besides, our finding that the slip ratio U/V increases with the tailbeat frequency and Reynolds number is supported by our recent meta-analysis of empirical data (van Weerden et al., 2011).

Further, our results suggest that fish that are constrained not to accelerate sideways produce forces that qualitatively resemble those of unconstrained fish that have a higher tailbeat frequency. Simulation studies that constrain their fish sideways (Sui et al., 2007; Borazjani and Sotiropoulos, 2008) are thus likely to overestimate all the forces and accompanying kinematic and hydrodynamic patterns associated with a particular tailbeat frequency. The general relevance of this needs to be tested in 3D models.

Three of our results are supported by those of other studies, both theoretical and empirical. First, Borazjani and Sotiropoulos (2009) also found a reduction of Froude efficiency with an increase in Reynolds number in their simulations of a swimming eel. Second, the decrease of the Strouhal number with increasing Reynolds number in our model fits both computational results of a swimming mackerel by Borazjani and Sotiropoulos (2008) and experimental data of swimming Pacific salmon of Lauder and Tytell (2006). Third, the increase in swimming speed with higher tailbeat frequency is consistent with empirical data of real fish (Videler, 1993; Gillis, 1998). As regards the consequences of tailbeat frequency for wake structure, our model serves as prediction.

Both in our study of an insect wing and of an undulating fish we compare a 2D model to a 3D experiment, yet we still find similar results. We suppose that in each case there are different reasons for the robustness against a reduction in dimension. For the insect wing, it may indicate that 3D effects, such as spanwise flow along the wing (which can be caused by the leading-edge vortex (Birch and Dickinson, 2001; Lentink et al., 2009; Stamhuis et al., 2002)) are not of great importance at low Reynolds numbers. Indeed, the artificial elimination of spanwise flow in a flapping model of a drosophila wing at a low Reynolds number (75) did not greatly influence the leading-edge vortex (Birch and Dickinson, 2001). However, this robustness may not hold for higher Reynolds numbers, above 1400, because here a strong spanwise flow was found on the same wing (Birch et al., 2004). In the case of the fish, the similarity of our results in a model in two dimensions to those of experiments in 3D may be a consequence of an increase in the effective Reynolds number due to the reduction in dimension. In two dimensions there is one fewer degree of freedom of movement and hence all phenomena – such as recirculation, vortex shedding and turbulence – occur at

less than half the Reynolds number than they do in 3D (Reid et al., 2009). This may cause the similarity in Strouhal number of our results for a relatively low Reynolds number ($1.2 \cdot 10^3$) to experimental data of a mullet by Müller et al. (1997) at a much higher Reynolds number ($30 \cdot 10^3$), and the resemblance of our mullet at Reynolds number 1150 to the three-dimensional carangiform model by Borazjani and Sotiropoulos (2008) at a Reynolds number over 4000. The Froude efficiency in our model appears to be approximately 10% higher than in their 3D model. This may also be a consequence of the two-dimensionality: in 2D there is one fewer direction to waste power in. Further, we cannot exclude that details of results of our model such as the precise distribution of thrust along the body may be influenced by its two-dimensionality. For example, in reality the distribution of the force may be affected by the narrow caudal peduncle of a real fish, but this cannot be represented in a two-dimensional model where the fluid cannot flow over the top or bottom of the fish. However, despite such potential differences between 2D and 3D situations (Kern and Koumoutsakos, 2006), we expect our results to apply qualitatively in three dimensions.

Our model has several weak points. Firstly, mainly due to its high stochasticity, it is necessary to average over either large areas or long intervals to eliminate noise. For example spatial averaging is needed to obtain clear images of the vorticity around the undulating fish (Fig. 3.9). Second, the undulation of the fish was fixed and was not affected by the fluid forces. In future we intend to extend our model with a fish whose undulation is based on internal mechanics as well as being influenced by the surrounding fluid.

In sum, our results indicate the importance of several theoretical and empirical follow-up studies. For low Reynolds simulations it may be possible to model organisms in a simpler manner, by linearising the Navier-Stokes equations (Roper and Brenner, 2009). However, it remains to be tested whether this is also possible for unsteady motion such as the organisms in this study perform. Theoretically it would be of great interest to investigate in our model the swimming efficiency over a wider range of Reynolds numbers, body shapes and swimming styles. It may also be of interest to test whether the extraordinary investment of fish larvae in an increase of their length and hence Reynolds number (Müller and Videler, 1996) comes at the cost of efficiency, or rather increases it. Empirically, the hypotheses concerning the effects of tailbeat frequency on various aspects of the kinematics and hydrodynamics of swimming are greatly in need of further study.

3.5 ACKNOWLEDGEMENTS

We thank John Videler and James C. Liao as well as two anonymous referees for comments on an earlier version. H. H. was financed by grant 012682-STARFLAG from the STREP-program "Starflag" in the 6^{th} European framework, awarded to C. K. H.. J. T. P thanks the Netherlands Organisation for Scientific Research (NWO) for financial support.

3.6 SUPPLEMENT

Supplementary material for this chapter.

Figure 3.18 shows the decomposition of the force in the swimming direction into that caused by the transfer of momentum of the fake particles and that caused by particles colliding with the skin of the fish.

Figure 3.19 shows the forwards speed over time of the undulating fish for several tailbeat frequencies.

Video "Vorticity mullet freeFreeL freq3.8.avi" (Online at `http://www.rug.nl/biol/hemelrijk`) shows a video of the swimming fish.

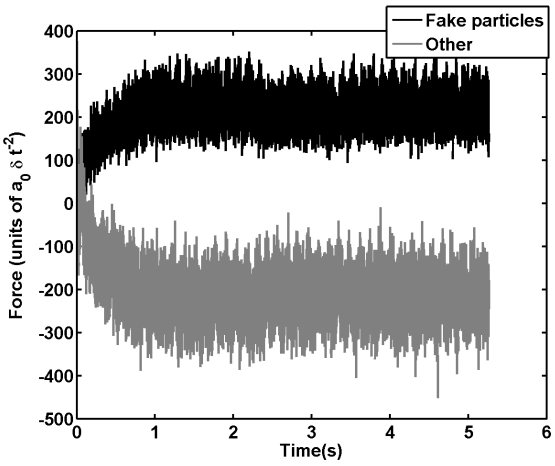

Figure 3.18.: Force of a swimming unconstrained fish with tailbeat frequency 3.8Hz along its swimming direction over time (in simulation units). The force is decomposed into that caused by the inclusion of "fake particles" in the rotation step (black) and that caused by direct collisions of particles with the skin of the fish (gray). Positive force indicates thrust, negative drag.

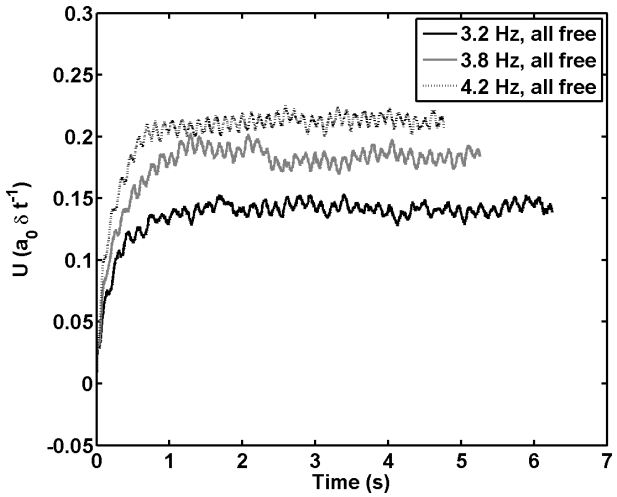

Figure 3.19.: Swimming speed over time of the unconstrained fish, for several tailbeat frequencies..

4

FLUID DYNAMICS OF INFINITE SCHOOLS[1]

Abstract

Several studies have shown fish may save energy by travelling in groups. How these benefits arise has not yet been demonstrated experimentally however, because empirically studying the hydrodynamics of schooling fish is difficult. Theoretical predictions suggest that for optimal efficiency, fish should position themselves in a rigid diamond-shaped structure in two-dimensional layers, with specific inter-individual distances. However, these theoretical predictions concern infinitely large schools and ignore effects of several factors such as of viscosity and of the shape of the fish. For this computer models can be of great help, because in them forces and flows can be directly calculated, and the position and movement of the fish can be imposed. Especially particle-based models of hydrodynamics (where hydrodynamics arise from local interactions between particles that represent the fluid) are useful here because they greatly simplify the interactions between multiple fish and the fluid. In the present paper we study infinitely large schools at a moderately high Reynolds number (1000-1400) in a particle-based model, i.e. the Multiparticle Collision Dynamics method. We investigate four different configurations of infinite schools, namely a diamond-shaped lattice, a rectangular lattice, and (in order to separately determine the effects of lateral and longitudinal neighbours) an infinitely long line and an infinitely wide phalanx. We vary the distance among individuals and we compare of the different school structures and of a single fish the efficiency, swimming speed, thrust and "wasted" lateral power. In our model, fish swim more efficiently when in a school than when alone. Unexpectedly, swimming in an intact wake of a predecessor increases both speed and efficiency. Having lateral neighbours increases efficiency, but at a cost of swimming speed. Remarkably, the benefits are lowest for the specific diamond configuration that was predicted to be optimal.

4.1 INTRODUCTION

The majority of fish species 'school' (that is, they aggregate in groups displaying coordinated, directed movement) at some point in their life history (Shaw, 1978). The prevalence of schooling behaviour indicates that it is likely to confer evolutionary benefits. Suggested

1 SUBMITTED TO JOURNAL OF THE ROYAL SOCIETY INTERFACE AS: D. A .P. REID, H. HILDENBRANDT, J. T. PADDING, C. K. HEMELRIJK – *"A TWO-DIMENSIONAL MODEL OF HYDRODYNAMICS OF INFINITELY LARGE SCHOOLS OF FISH"*

benefits include improved success in foraging, defence against predators and increased hydrodynamical efficiency (Krause and Ruxton, 2002). In the present paper we focus on hydrodynamical efficiency. Empirically the hydrodynamics of schooling fish have so far not been studied, due to the extraordinary effort it would involve to measure it through methods such as Digital Particle Image Velocimetry (Stamhuis et al., 2002). Thus, computer models can be of great use because all kinds of spatial configuration and swimming kinematics can be explored in detail, and be used to theoretically predict how fish in schools might benefit hydrodynamically.

Regarding the hydrodynamical efficiency of schooling, Weihs has made several predictions based on an inviscid theory of hydrodynamics (Weihs, 1973). The first prediction is that for optimal efficiency groups of fish should adopt regular, fixed positions relative to one another, forming two-dimensional layers of diamond-like lattice structures. The lateral distance between neighbours should be two times the width of their wake, and the longitudinal distance between rows (measured from tail to nose) should be at least 0.7 fish lengths (Weihs, 1973, 1975). The second prediction is that lateral neighbours increase an individual's efficiency, and the third that in the diamond lattice structure, lateral neighbours should beat their tails in antiphase to one another. Although his theory raised great interest (having been cited over 70 times according to the ISI Web of Knowledge), empirical evidence is lacking (Partridge and Pitcher, 1979; Abrahams and Colgan, 1985). Nevertheless, fish have been shown to exploit others' wakes to reduce their swimming effort, e.g. individuals in a school consumed less oxygen than single ones and those at the rear of the school had lower tailbeat frequency than those at the front (Belyayev and Zuyev, 1969; Herskin and Steffensen, 1998). Further, schooling individuals preferred positions behind others (Svendsen et al., 2003). Fish have also been shown to exploit the wake behind a pillar both actively through adoption of a special gait (Liao et al., 2003b) and passively, in that dead but flexible fish generated thrust when tethered behind the pillar (Beal et al., 2006).

Weihs' theory is based on simplified hydrodynamics that ignore viscosity and the shape of the fish. The increase of computational power enables modern computer methods to model such features. So far his prediction that the optimal configuration is that of a diamond lattice have not been tested in a computer model that fully models hydrodynamics. To date only a few theoretical studies have investigated hydrodynamical interactions between swimming fish. The spatial arrangements studied were a single fish swimming between the wakes of two predecessors (Deng and Shao, 2006), two and three fish swimming side by side (Zhang and Eldredge, 2010) and an infinitely wide phalanx of side-by-side fish (Dong and Lu, 2007). These studies each found an increase in efficiency for three specific configurations, firstly two side by side fish swimming in anti-phase (Deng and Shao, 2006), secondly a third fish swimming between the wakes of two preceding ones at a longitudinal distance larger than half a body length (Zhang and Eldredge, 2010), and third an infinite phalanx swimming in phase (Dong and Lu, 2007). However, two of the studies were not parametrised biologically, making the value of their results unclear (Deng and Shao, 2006; Zhang and Eldredge, 2010).

None of these theoretical studies investigated specifically the prediction of optimal efficiency of diamond lattice structures (Weihs, 1973). Therefore we do so here. Because no general solution of the Navier-Stokes equations of hydrodynamics has been found, all computer models of them must discretise reality in some way. There are two main methods

of doing so, namely discretising space by means of a grid, and discretising the fluid by representing it as particles. To represent smooth biological shapes in a grid-based method requires continual adaptation of the grid, or a complex coupling between the organism and the grid-based fluid (Gilmanov and Sotiropoulos, 2005; Sui et al., 2007). Therefore we here use the recently-introduced Multiparticle Collision Dynamics method (Malevanets and Kapral, 1998, 1999). In it, particles move in real space (i.e. not on a grid) and exchange momentum in a collision step, resulting in hydrodynamics consistent with the Navier-Stokes equations Malevanets and Kapral (1999); Kikuchi et al. (2003); Padding and Louis (2006). We have verified it against experimental data for static shapes (Reid et al., 2009) and confirmed that simulation of flapping and undulating airfoils at higher Reynolds numbers yielded results resembling experimental data of insect wings and swimming fish (Reid et al., 2011). In the present study we apply Multiparticle Collision Dynamics to the investigation of the hydrodynamical advantages of schooling. We compare the efficiency of several spatial configurations in infinitely large schools of undulating fish and that of a fish swimming alone. We investigate different spatial configurations: one where an individual's neighbours-ahead are at an angle (the diamond lattice structure proposed by Weihs) and one where they are straight ahead (a rectangular lattice structure). We do so for different lateral distances between neighbours. In order to determine the effects of neighbours in different directions (lateral and longitudinal), we compare results to those when there are only neighbours ahead (an infinitely long line) or to the sides (an infinitely wide phalanx). Although later work of Weihs (1975) suggests that lateral neighbours should swim in antiphase, it was impossible to study this on our available hardware because it requires double the computational effort. Therefore in the present paper we investigate only the case of lateral neighbours swimming in phase.

We measure swimming speed, efficiency, forwards thrust and lateral power of the fish.

4.2 METHODS

We here describe a) the hydrodynamical model of the fluid, b) the fluid's interaction with the fish, c) the experimental setup, and d) the measurements.

4.2.1 *The model*

We extend our previous implementation of the Multiparticle Collision Dynamics model with fishlike shapes (Reid et al., 2009, 2011). Below we briefly describe the method (for more details see Reid et al. (2011)), followed by its adaptations for schooling.

The model consists of a rectangular area filled with fluid in which the fish undulate. The environment is two-dimensional, homogeneous, contains N identical particles of mass m and has width W and length L_{box} (Fig. 4.1). The positions $\mathbf{x}_i$ and velocities $\mathbf{v}_i$ of the particles are two-dimensional vectors of continuous variables. Every time step Δt the particles first move (the streaming step) and then collide with each other (the collision step). Moving leads to new positions $\mathbf{x}_i$ according to the motion equation $\mathbf{x}_i(t + \Delta t) = \mathbf{x}_i(t) + \mathbf{v}_i(t)\Delta t$.

To efficiently simulate collisions between particles, in the collision step both time and space are coarse-grained by using a square lattice to temporarily partition the simulation

into cells of size a_0. All particles that are in a particular cell during the collision step are considered to have collided with each other at some moment in the preceding movement step, during which the particles moved in continuous space. To simulate collision, in each lattice cell all particles change their velocities according to $\mathbf{v}_i = \overline{\mathbf{v}} + \Omega \cdot (\mathbf{v}_i - \overline{\mathbf{v}})$. Here $\overline{\mathbf{v}}$ is the mean velocity of the particles in the grid cell and Ω is a stochastic rotation matrix that rotates the velocities by either $+\alpha$ or -α (where α is a fixed system parameter), with equal probability. The rotation direction at a specific moment in time is the same for all particles within a cell but it may differ between time steps. To ensure Galilean invariance we use the method of Ihle and Kroll (2001) and displace the lattice every time step by a vector whose x- and y-components are randomly selected from the uniform interval $[0, a_0)$.

The fish-like shapes in our simulations are represented by polygons and thus composed of a finite series of lines, so-called edges, which meet at points called vertices. We simulate the undulation of the fish by the motion of the vertices each time step Δt according to the undulation equation (Eq. 4.3). We use Euler integration, therefore during a time step the displacement of the vertices is equal to their velocity. The local velocity of any point on the object's surface is calculated by interpolating the velocities of the two adjacent vertices. To determine whether the particles collide with the undulating body during streaming we use a ray–ray intersection algorithm (Appendix A in (Reid et al., 2011)).

The fluid and fish interact during both the collision and the streaming step. These interactions exchange momentum between the fluid and organism, and ensure that there is no slip at the interface. For these interactions we choose two methods that have been shown to ensure minimum slip, i.e. the fake-particle rule during the collision step (Lamura et al., 2001), and the random-reflect rule during the streaming step (Inoue et al., 2001; Padding and Louis, 2006). The fake-particle rule is applied to cells which are partially filled by the fish and partially by the fluid. Because the fish excludes particles the density of particles in these cells is often lower than average. To prevent this and represent the mass of the fish in these cells we include sufficiently many fake particles that the number of particles in each cell at least equals the mean density ρ. The velocities of these fake particles are drawn from a Maxwell-Boltzmann distribution with temperature $k_B T$ and a mean velocity which is equal to the local velocity of the organism. The random-reflect rule implies that particles that hit the organism get a new randomly chosen velocity. The new velocity consists of a tangential component v_t and normal component v_n relative to the surface, drawn from the following distributions (Inoue et al., 2001; Padding and Louis, 2006):

$$P(v_t) \propto e^{-\beta v_t^2} \tag{4.1}$$

$$P(v_n) \propto v_n e^{-\beta v_n^2}, \tag{4.2}$$

with $\beta = \frac{m}{2k_B T}$.

The force which the fluid exerts on the fish during a time step Δt is the opposite of the sum of the change in momenta of all particles that collide with it during that time step, divided by the length of the time step Δt. Note that both during the streaming step (as described above), and during the rotation step (through the fake particle rule) particles may collide with the body. The velocity of the fish is affected by the summed hydrodynamical force on it according to Newtonian mechanics. In the diamond configuration, in order to

keep the position of the fish in the school constant, i.e. in a rigid lattice structure (Weihs, 1973), we apply to each fish the average of the hydrodynamical force of the school.

To represent the movement of fish through infinite space, we move the simulation box along with them. We do so as follows: Whenever the centre of gravity of the fish (or school) has moved one cell a_0 away from its original position within the box, we move the box centre towards that of the fish by one simulation unit a_0 (either vertically, horizontally or both). We shift only by distances of at least one simulation unit, because smaller shifts may cause floating point rounding errors to accumulate.

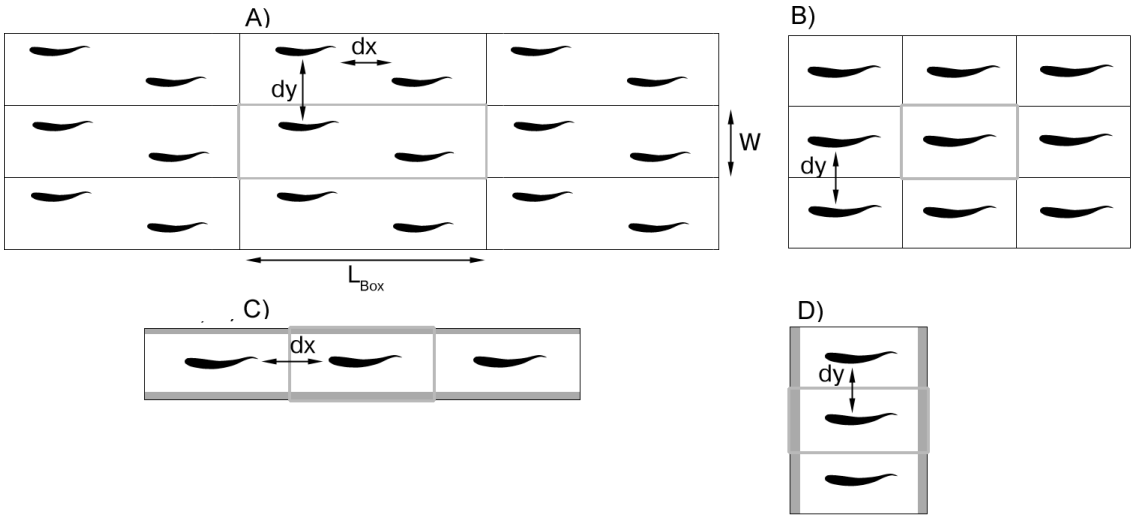

Figure 4.1.: System overview for the spatial configurations. A) diamond lattice, B) Rectangular lattice, C) line and D) phalanx. The light gray outline indicates the actual simulation box and damping areas are indicated in dark gray. Lateral distance dy and forwards distance dx between neighbours depend on the width W and length L_{Box} of the simulation box.

Parametrisation, initial condition and simulation setup

We choose to simulate a mullet (*Chelon labrosus*) for three reasons: first, because it is an obligate schooler, second, because it swims at a steady cruising speed by undulating its body without using its pectoral fins (Videler, 1993), and third, because its swimming kinematics and wake structure have been reported in detail (Müller et al., 1997). We simulate the undulation of a horizontal cross-section of a mullet, traced from the body contours presented by them (Müller et al., 1997). We represent the body as a polygon. To ensure that the curvature at the head is smooth, we use shorter polygonal edges at the head than at the tail. We describe the characteristics of the propulsive wave along the body of the fish in terms of the lateral movement of its central, longitudinal axis, or spine.

We consider the spine of the straight fish to have an y-value of 0 (Fig. 4.2). We scale the fish in terms of fractions of its body length L, so that $x = 0$ at the front of the fish and $x = 1$

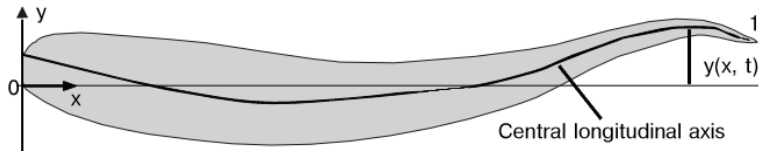

Figure 4.2.: Schematic overview of the deviation from the central axis of the spine of an undulating mullet.

at its rear. For each point x along the spine of the fish, its lateral deviation from the central axis over time is given by

$$y(x,t) = \theta(x)\sin(k_L x - \omega t). \tag{4.3}$$

$$\theta(x) = \theta_0 + \theta_1 x + \theta_2 x^2, \tag{4.4}$$

Here $k_L = \frac{2\pi}{\lambda}$ is the angular wave number, which is based on the length λ of the propulsive wave, $\omega = 2\pi f$ is the angular velocity for the tailbeat frequency f, and $\theta(x)$ is the amplitude envelope function. We use a quadratic function fitted to the experimental results of Videler and Hess (1984), with the amplitude of the wave being smallest behind the head. Note that the undulation of our simulated fish is not influenced by the flow around it.

Our fish are parametrised following the experimental data of a mullet by Müller et al. (1997) as regards length and tailbeat frequency (Table 4.1). Our model of a fish is $900a_0$ long, because this was the maximum that was computationally feasible on our hardware. We fix the units of space and time to the experimental data (Müller et al., 1997). As regards space, the simulation unit of distance a_0 equals the ratio between the length of the real fish (0.126m) and of the simulated fish ($900a_0$), thus $a_0 = \frac{0.126}{900} = 1.4 \cdot 10^{-4}$m.

Parameter name	Value
Length	0.126 m
Time step	0.00015 s
Tailbeat frequency	3.8 s^{-1}

Table 4.1.: Parametrisation of the fish in SI units, after results of Müller et al. (1997).

We use the ratio between the swimming speed of the simulated fish and the real one to calculate the length of the simulation time step Δt. We parametrise the simulations so that the swimming speed of the fish in the model U_{sim} remains below $0.22a_0\Delta t^{-1}$ so as to minimise Mach number effects such as shockwaves (Lamura et al., 2001; Padding and Louis, 2004). The real mullet swims at 0.176m/s. Therefore $\Delta t = 0.2 \cdot 1.4 \cdot 10^{-4}/0.176s = 1.5 \cdot 10^{-4}$s (Table 4.1).

We simulate infinite schools of individuals in four different spatial configurations: a diamond lattice, a rectangular lattice, an infinitely long line and an infinitely wide phalanx. In all cases, the simulation consists of a rectangular area of width W and length L_{Box} with either one or two (in the case of the diamond lattice) fish in it (Fig. 4.1). We use periodic boundary conditions to simulate infinity, thus infinitely duplicating the contents of the box, resulting in a torus topology. To simulate different configurations, we vary the number and positions of fish in the simulation box as well as the boundary conditions.

In case of the diamond and rectangular lattice flow travels freely in all directions, i.e. none of the boundaries is scrambled. In case of the line and phalanx configuration, flow travels freely only across the boundaries that are perpendicular or parallel to the swimming direction, respectively, and we place so-called scrambling zones along the other boundaries (Fig. 4.1C, D). These scrambling zones re-set the velocity of particles to those of random thermal noise and thus remove flow phenomena such as vortices. We used such scrambling zones previously in our simulations of single fish (Reid et al., 2011). Note that we actually simulate only a single fish in the line, phalanx and rectangular lattice, and that therefore the undulation of all fish in those configurations is necessarily in phase. In the case of the diamond lattice we simulate two fish, in the maximum simulation size possible on our hardware. Therefore in the diamond lattice lateral neighbours necessarily swim in phase, and due to time constraints we do not examine the case of diagonal neighbours swimming in antiphase in the present paper. We study schools for different longitudinal distances (dx, measured from the tail of the preceding fish to the nose of the one behind it) between the fish in the line, and different lateral distances (dy, measured between the centres of gravity of two neighbouring fish) in all other cases (Fig. 4.1).

For consistency with the literature on schooling, we describe the inter-fish distances nondimensionally in terms of fish lengths (Weihs, 1973, 1975; Zhang and Eldredge, 2010). In the phalanx and lattice configurations we keep the longitudinal distance fixed at 1 fish length L, because this is the average distance reported for roach (Svendsen et al., 2003). As lateral distances we investigate the one predicted to be optimal for wake exploitation by Weihs (1973) (ie. twice the width of the wake of a fish, which equals 0.4 fish lengths L for our tailbeat amplitude) as well as double and quadruple that. For the line we test longitudinal distances of 1, 2, and 3 fish lengths.

We start the simulations without directional flow, initialising all particles with random velocities drawn from a Maxwell-Boltzmann distribution of mean 0 and temperature $k_B T$ (Table 4.2). Thus, all directional flow in the simulation is caused by the movement of the fish. We run the simulation until the swimming speed and surrounding flow of the fish reach the steady state. Note that, because undulatory swimming is a periodic phenomenon, equilibrium is reached *on average* per tailbeat cycle, not from moment to moment. The swimming speed reaches steady state within ten tailbeats, and flow reaches a steady state after approximately forty tailbeats.

The simulations are implemented in a combination of C++ and OpenGL Shading Language. We use "Single Instruction, Multiple Data" instructions to exploit the inherent data parallelism caused by spatial sorting of the particles, and OpenMP for shared memory multiprocessing on a multi-core CPU. Flow field calculations such as convoluting it with a Gaussian kernel for smoothing and calculating the Jacobian are executed on the graphical card. Because of the limited floating point precision of the graphical card used (Nvidia 8600GT) the actual particle dynamics are calculated entirely on the CPU (Intel Core2 Q6600). We expect an significant performance increase on more recent GPUs that offer the required precision. On the current hardware available, a single run of the largest system (30 million particles) took approximately 5 days.

Fluid		
Temperature	$k_B T$	1.0
Lattice cell size	a_0	1.0
Collision rotation angle	α	$\frac{\pi}{2}$
Particle mass	m	1.0
Particles per cell (average)	ρ	8
Time step length	Δt	1.0
Boundary width	B	$30\ a_0$
Dynamic viscosity	μ	$1.15\ m/(m\Delta t)$
Fish		
Length	L	$900.0\ a_0$
Number of edges	N_E	1024
Wave number	k_L	1.8π
Tailbeat frequency	f	$5.7 \cdot 10^{-4} \Delta t^{-1}$
Tailbeat amplitude	A	$90\ a_0$
Undulation amplitude coefficient 0	θ_0	0.02
Undulation amplitude coefficient 1	θ_1	0.08
Undulation amplitude coefficient 2	θ_2	0.16

Table 4.2.: Parameter values used. All values are in simulation units.

Measurements

Thrust and lateral power are measured as parts of the total body force $\mathbf{F}$ as follows. The total forward force F at any moment t is calculated by a summation of the force over the skin edges of the fish (Fig. 4.3):

$$F(t) = \sum_i \mathbf{F}^i \cdot \mathbf{e}_f = \sum_i \left(\mathbf{F}_n^i \cdot \mathbf{e}_f + \mathbf{F}_t^i \cdot \mathbf{e}_f \right), \tag{4.5}$$

where $\mathbf{F}^i$ is the force on the skin at edge i, $\mathbf{F}_n^i = (\mathbf{F}_i \cdot \mathbf{n})\,\mathbf{n}$ is the force vector perpendicular to the skin on that edge, $\mathbf{F}_t^i = \mathbf{F}_i - \mathbf{F}_n^i$ is the force vector tangential to the skin and $\mathbf{e}_f$ is a forwards-pointing unit vector. The summations of the perpendicular and tangential elements in the last expression thus represent the contributions of pressure and viscosity, respectively, to the forward force. It should however be noted that if the tangential speed varies strongly around the body the viscous forces may have a small normal component.

Because the forwards thrust (T) and rearwards drag (D) operate in opposite directions the total forwards body force F will tend to 0 during steady swimming at equilibrium speed:

$$F(t) = T(t) - D(t). \tag{4.6}$$

To estimate thrust and drag nonetheless, we separate them out spatially along the body by following the method by Borazjani and Sotiropoulos (2008). When summing the force over the body surface, the force on each edge is counted as thrust (T) when it is positive or drag (D) when it is negative:

$$T(t) = \sum_i \left[\mathbf{F}_n^i \cdot \mathbf{e}_f H(\mathbf{F}_n^i \cdot \mathbf{e}_f) + \mathbf{F}_t^i \cdot \mathbf{e}_f H(\mathbf{F}_t^i \cdot \mathbf{e}_f) \right] \tag{4.7}$$

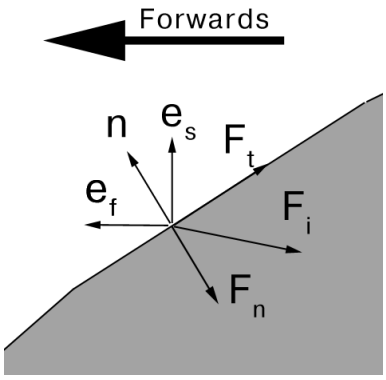

Figure 4.3.: Decomposition of the force F_i on the skin of the fish into pressure (F_n) and viscous (F_t) components (see Methods). The surface normal is indicated as n and the unit vectors pointing forwards and sideways are labelled e_f and e_s.

$$D(t) = -\sum_i \left[\mathbf{F}_n^i \cdot \mathbf{e}_f H(-\mathbf{F}_n^i \cdot \mathbf{e}_f) + \mathbf{F}_t^i \cdot \mathbf{e}_f H(-\mathbf{F}_t^i \cdot \mathbf{e}_f)\right], \tag{4.8}$$

where H is the Heaviside step function. Thus, for each edge, for both the perpendicular (pressure $\mathbf{F}_n$) and tangential (viscous $\mathbf{F}_t$) force on it, we add the forward component of the force to the thrust if it is positive, and to the drag if it is negative.

We calculate per time step Δt the lateral power P_l which the fish exerts:

$$P_l(t) = \sum_i \mathbf{F}_i \cdot \mathbf{e}_s V_{side}^i, \tag{4.9}$$

where $\mathbf{e}_s$ is a unit vector in the lateral direction 4.3, and V_{side}^i is the lateral velocity of edge i.

From these forces, we determine the swimming efficiency. Following Tytell and Lauder (2004) and Borazjani and Sotiropoulos (2008), we use a modified version of the Froude efficiency:

$$\eta = \frac{\bar{T}\bar{U}_{net}}{\bar{T}\bar{U}_{net} + \bar{P}_l}, \tag{4.10}$$

where $\bar{T}$ is the mean thrust over a tailbeat cycle, $\bar{U_{net}}$ is the mean net forwards speed of the fish and $\bar{P_l}$ is the mean lateral power it exerts over a tailbeat cycle. We use the speed from the perspective of the fish $U_{net} = U_{flow} - U_{fish}$. Here, U_{flow} is the speed of the oncoming flow ahead of it (averaged over an area) and U_{fish} is the speed of the fish in the global frame. Note that, since the fish swims in the negative x-direction, the speeds of flow and fish are subtracted rather than summed. The Froude efficiency η expresses the percentage of the total power which is converted into forwards speed.

The relative importance of inertia to viscosity of an organism of length L moving with speed U through a fluid of density ρ and dynamic viscosity μ is characterised by the dimensionless Reynolds number Re:

$$Re = \frac{\rho U L}{\mu}, \tag{4.11}$$

For oscillatory motion such as that of a beating fish tail with frequency f and amplitude A, the amount of oscillatory effort relative to the achieved velocity is characterised by the Strouhal number St:

$$St = \frac{f2A}{U} \tag{4.12}$$

For our simulations only U varies (as a consequence of different spatial configurations) between 0.16 and $0.225 a_0 \Delta t^{-1}$. Hence the Reynolds number lies between $8 \cdot 0.16 \cdot 900/1.15 = 1001$ and 1409 and the Strouhal number lies between $5.7 \cdot 10^{-4} \cdot 180/0.16 = 0.64$ and 0.46 (Table 4.2).

4.3 RESULTS

Compared to single fish, infinitely large schools in our model are more efficient (Fig. 4.4) and faster (except for the most dense diamond lattice) (Fig. 4.5). The increase in efficiency is due to a reduction of both forwards thrust and lateral "wasted" power, while swimming speed is equally high or higher than that of the single fish (Figs. 4.6, 4.7).

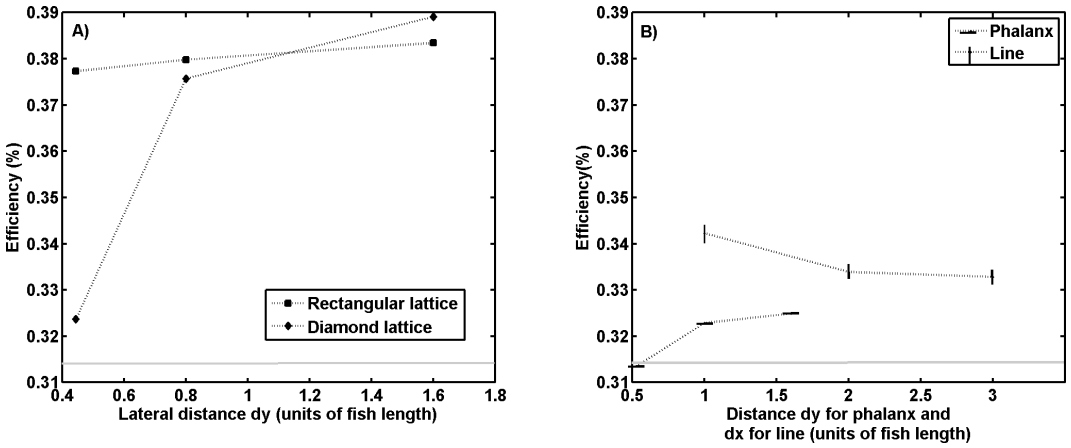

Figure 4.4.: Efficiency η of infinitely-large schools of fish at tailbeat frequency 3.8 Hz. For comparison, the efficiency of a single swimming fish with the same tailbeat frequency is indicated in a gray horizontal line. A): Rectangular and diamond-shaped lattice, with several different distances dy between lateral neighbours. B): Phalanx and line formation, with different inter-fish distances; lateral distance dy for the phalanx and forwards distance dx for the line.

Having neighbours in any direction, be it lateral or longitudinal, appears to be hydrodynamically beneficial for fish. Effects of flow due to individuals ahead become apparent by comparing the line configuration to single fish. Exploiting the wake of a preceding fish increases efficiency (Fig. 4.4B) and swimming speed (Fig. 4.5B), and it decreases thrust (Fig. 4.6B) and lateral power (Fig. 4.7B). This arises because the jet of their predecessor's wakes mostly passes fish laterally (Fig. 4.8). Consequently, fish mostly swim next to the jet. This lowers their thrust, probably because the flow is not laminar, making propulsion more difficult, and lowers their lateral power, which may be due to the decreased pressure in the jet. The effects of lateral neighbours can be inferred from the comparison between the

phalanx and the single fish. An individual profits from the flow of its lateral neighbours in efficiency (by reduced thrust and lateral power), but does not profit in swimming speed, which is reduced (Figs. 4.4B–4.7B). This speed reduction is probably due to an increase in resistance of the whole school to oncoming flow because of the close proximity of lateral neighbours.

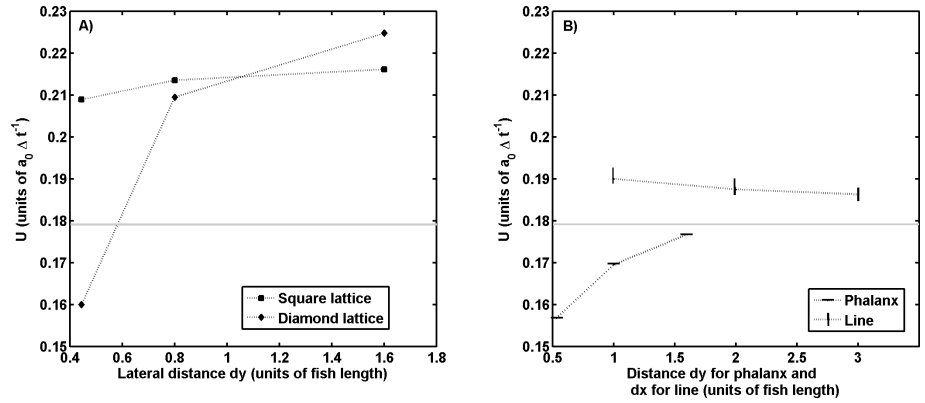

Figure 4.5.: Forwards swimming speed U of infinitely-large schools of fish at tailbeat frequency 3.8 Hz. For comparison, the swimming speed of a single swimming fish with the same tailbeat frequency is indicated in a gray horizontal line. A): Rectangular and diamond-shaped lattice, with several different distances dy between lateral neighbours. B): Phalanx and line formation, with different inter-fish distances; lateral distance dy for the phalanx and forwards distance dx for the line.

In the diamond lattice larger lateral distances result in an increase in the efficiency, swimming speed, thrust and lateral power (Figs. 4.5–4.7). This increase in efficiency is associated with the encounter of a more intact wake structure left by the preceding fish. At smaller lateral distance the neighbours diagonally-ahead disturb the wake structure, both by beating their tails and by compressing the wake between their bodies (Fig. 4.9A, B). In the rectangular configuration there is no such disturbance, and each fish encounters the reverse von Kármán street produced by the preceding fish (Fig. 4.9C). This holds for all lateral distances. Thus, the results of the rectangular lattice are similar at all different lateral distances. Whether the diamond or rectangular lattice configuration is most efficient depends on the lateral distance between neighbours (Fig 4.4A).

In both the rectangular and diamond lattice configurations, the combined hydrodynamical effects of forwards and lateral neighbours are greater than the sum of the separate effects observed in the line and phalanx. For instance, regarding speed, at a lateral distance of $0.8L$ lateral neighbours cause others to slow down to the same degree as neighbours ahead cause them to speed up (Fig. 4.5). Therefore, one might expect individuals in the rectangular lattice to travel at the same speed as a single fish. Instead, they appear to be faster than a single fish. This synergy also holds for efficiency, thrust and lateral power. In the diamond lattice a similar pattern is apparent.

In the line, the rectangular lattice and the loosely-spaced diamond lattice, fish encounter the wake of their predecessor on their nose. This wake includes a jet counter to the swimming

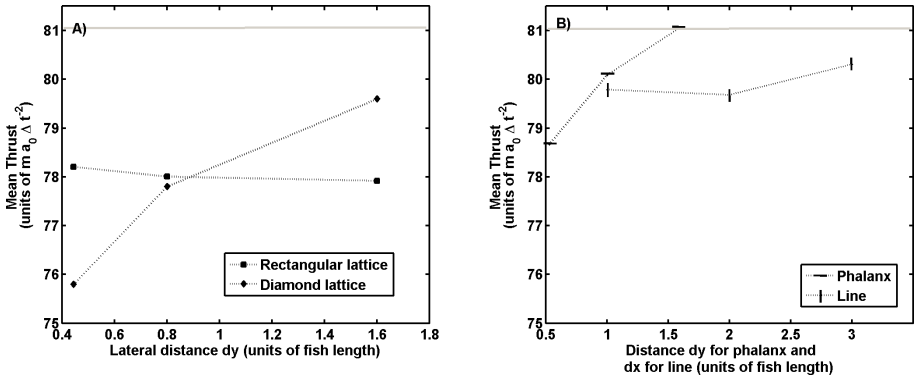

Figure 4.6.: Average thrust $\bar{T}$ of infinitely-large schools of fish at tailbeat frequency 3.8 Hz. For comparison, the thrust of a single swimming fish with the same tailbeat frequency is indicated in a gray horizontal line. A): Rectangular and diamond-shaped lattice, with several different distances dy between lateral neighbours. B): Phalanx and line formations, with different inter-fish distances; lateral distance dy for the phalanx and forwards distance dx for the line.

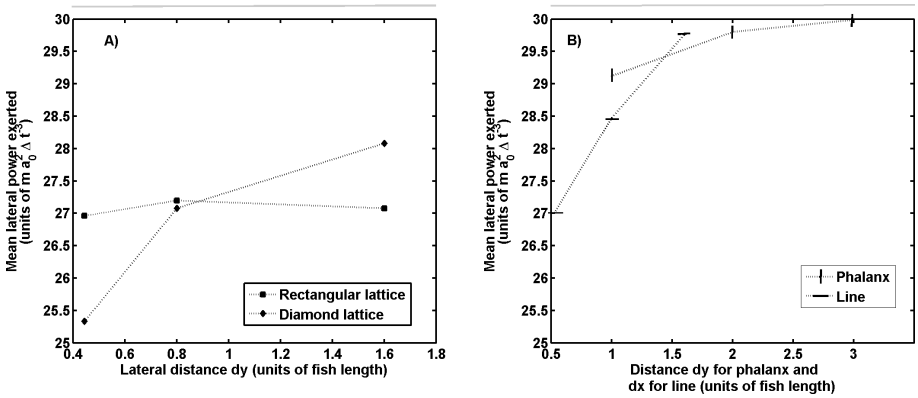

Figure 4.7.: Lateral power P_s of infinitely-large schools of fish at tailbeat frequency 3.8 Hz. For comparison, the lateral power of a single swimming fish with the same tailbeat frequency is indicated in a gray horizontal line. A): Rectangular and diamond-shaped lattice, with several different distances dy between lateral neighbours. B): Phalanx and line formations, with different inter-fish distances; lateral distance dy for the phalanx and forwards distance dx for the line.

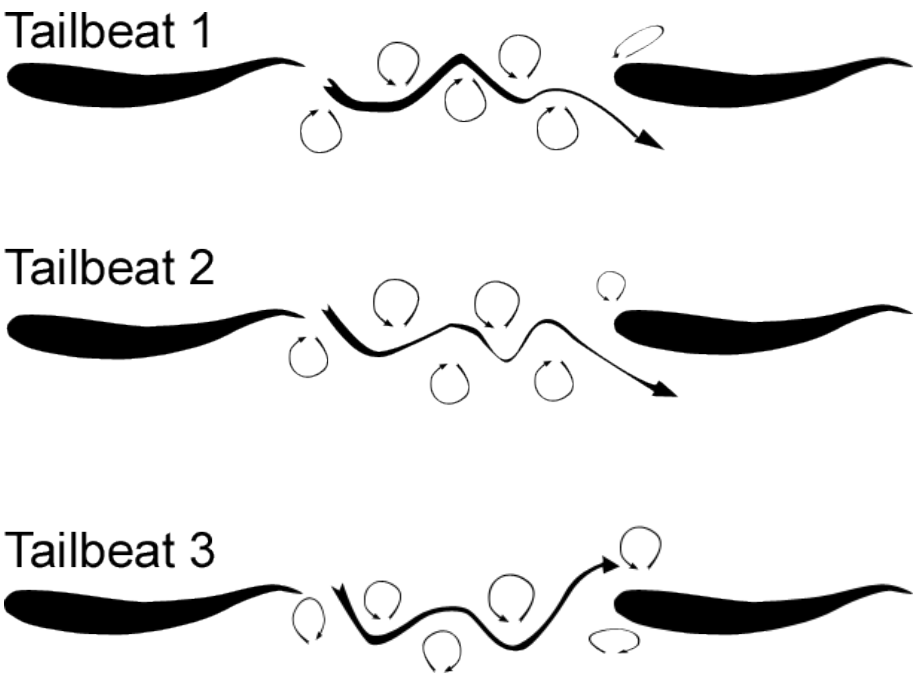

Figure 4.8.: Variability of the structure of the wake in the rectangular lattice, shown over several consecutive tailbeats. Arrows indicate flow direction, and the thickness of the arrow that represents the jet indicates local flow speed.

direction. Remarkably, these formations are faster and more efficient than a single fish because the fish swim besides the jet stream of the wake most of the time. This is remarkable because the fish in our model do not actively attempt to exploit the flows. Their lateral drift is an unintentional consequence of the lateral forces of the wake combined with the lateral undulation: the jet passes by the fish on one side, increasing the fluid's velocity on that side compared to the other side of the fish, hence lowering the pressure there. This causes the fish to drift laterally towards the side with faster flow and lower pressure, and appears to lower the required lateral effort of swimming. This effect is especially apparent in the line formation, where the jet can only have an effect in one lateral direction due to the lack of lateral neighbours. Interestingly, for the line formation there is also a net overall drift due to the direction of the initial tail beat (left or right, Fig. 4.10).

4.4 DISCUSSION

In our model, groups of fish swim faster and more efficiently than single fish, except in a diamond lattice configuration when too closely-packed. From the comparison between phalanx, line and the lattice configurations, a positive effect of having both lateral and longitudinal neighbours on swimming speed and efficiency is apparent that is greater than the sum of the effects of having neighbours in only one direction. In other words, the lateral and forwards effects reinforce each other. Note that the distribution of forces on the skin of

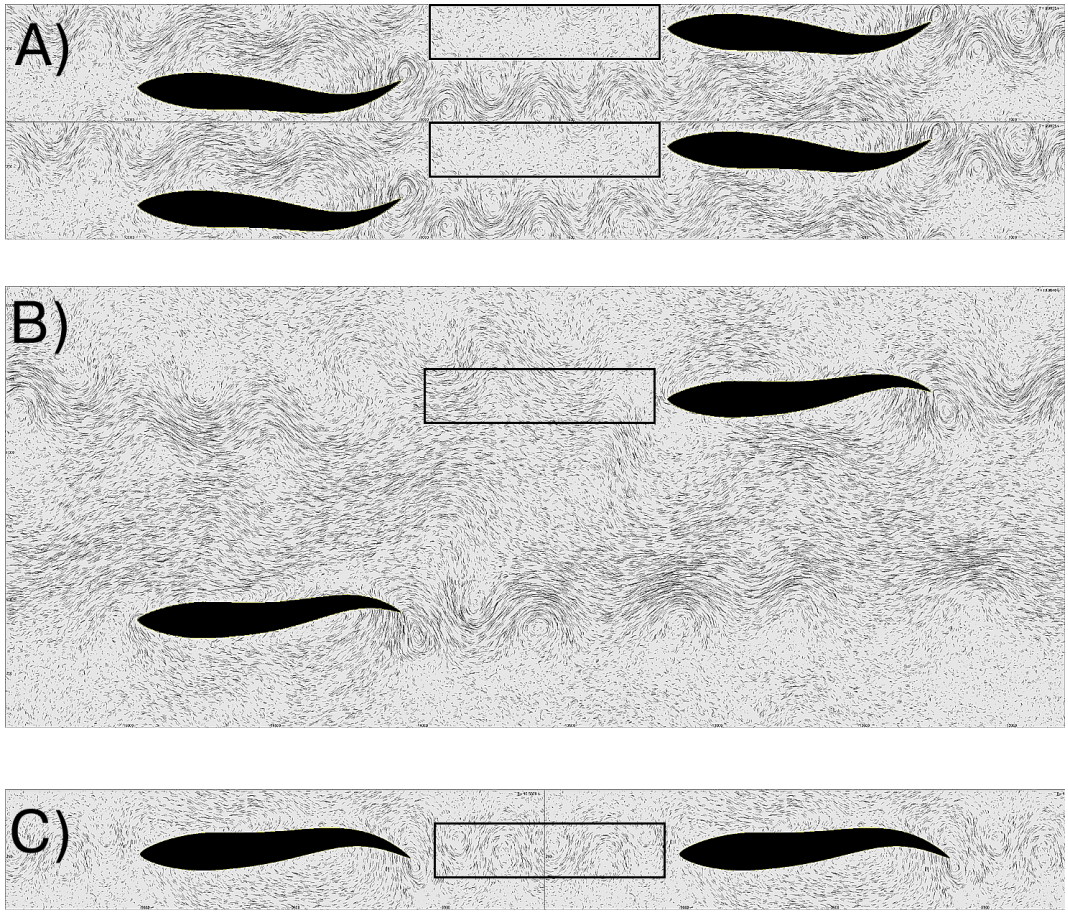

Figure 4.9.: Flow of the infinitely large schools for several configurations. A) Diamond lattice with small lateral distance, B) diamond lattice with large lateral distance and C) rectangular lattice with small lateral distance. Lines are truncated streamlines, with longer lines indicating higher local flow speed. Note the areas ahead of each fish, indicated with a black rectangle. Videos of these configurations can be found at `http://www.rug.nl/biol/hemelrijk`

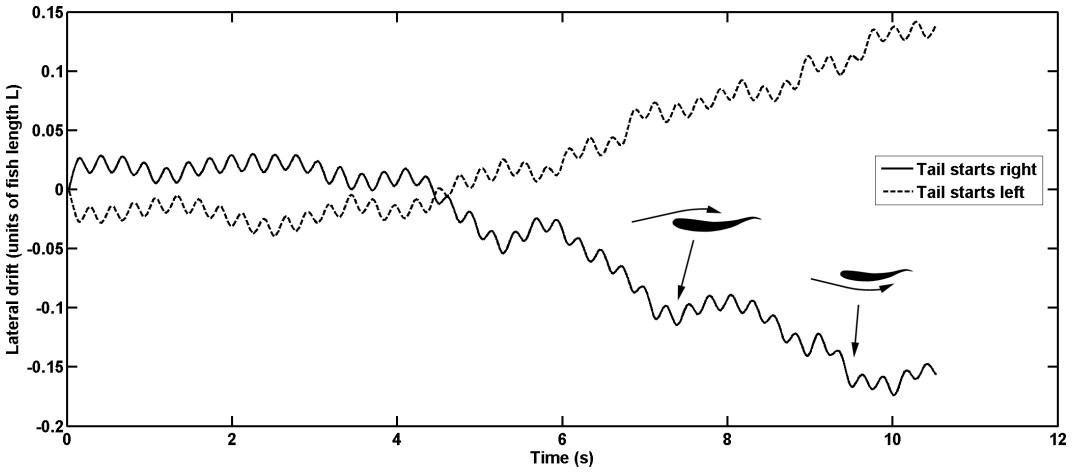

Figure 4.10.: Lateral drift (in fish lengths) over time of the line formation for two different initial conditions of tailbeat phase (left and right). Small inset figures indicate the direction where the jet of the oncoming wake passes each individual at that point in time.

swimming fish is identical in infinitely-large schools to those we previously reported for single fish (see Figs. 13, 14 in Chapter 3).

Our model confirms some of Weihs's predictions and refutes others. It confirms that individuals benefit in efficiency from their lateral neighbours and that a low-velocity area arises between the wakes of lateral neighbours at the lowest lateral distance of 2 times the width of the wake. However, it contradicts the prediction that this particular configuration of a diamond lattice is optimally efficient (Fig. 4.4A). This is especially unexpected because the flow pattern that is supposed to cause this formation to be optimally efficient is present in the model. Indeed, an area of low-velocity fluid occurs ahead of each fish, and the drag-reducing outer edges of each wake pass close by the sides of fish that follow (Fig. 4.9A). The difference in efficiency from Weihs' prediction may be caused by our inclusion of viscosity and the interactions of wakes. This causes for instance the wakes to be compressed as they approach each row of fish and stretched as they pass between the fish. From comparison with the rectangular lattice it is apparent that close lateral proximity alone cannot account for the reduction in efficiency of the dense diamond lattice (Fig. 4.4A). We give three explanations for the lower efficiency of the dense diamond lattice. First, it may be due to the increased drag of the school as a whole, due to each subsequent row in the diamond lattice obstructing the flow that passes through the gap between the preceding fish (Fig. 4.9). In contrast, this is not the case in the rectangular lattice, where flow can pass more freely through subsequent rows. Second, it may arise because individuals are prevented from exploiting the wake of their direct predecessor, due to its disruption by their neighbours diagonally-ahead. Third, it may be caused by lateral neighbours swimming in phase. Weihs suggested that this should cause a strong lateral component to the wakes which would rotate the following individuals, and increase their drag. In our model individuals cannot rotate, and thus drag does not increase in the manner predicted. In fact, drag and thrust are low in the dense diamond

lattice (Fig 4.6A). To shed more insight on this, a diamond lattice with neighbours swimming in antiphase should be studied in the model on better hardware.

At higher lateral distance among individuals, results of the diamond lattice resemble those of the rectangular one (Figs. 4.4A–4.7A). This is because the flow structure is also similar: individuals in both lattices encounter the reverse von Kármán wake of their direct predecessor (Fig. 4.9B).

Our results appear consistent with those of previous models of hydrodynamical interactions between swimming fish. The increase of efficiency compared to a single fish of our phalanx formation fits results of Dong and Lu (2007) and Zhang and Eldredge (2010). Our finding that the diamond lattice increases efficiency but only when lateral distances are higher than 0.4L fits with the results of the model of Deng and Shao (2006).

Unlike in the simulations of Deng et al. (2007), our results do not oscillate when the longitudinal distance between fish changes. This due to two reasons. First, in their results the oscillations were only strong at Strouhal numbers of 0.6 and higher. In our simulations the Strouhal number tends to be relatively low (0.5 on average). Second, in our model, in all settings where fish encounter a wake, the interaction between fish and wake varies strongly from one tailbeat to the next (Fig. 4.8). For a strong distance-dependent oscillation of the dynamics, it would be necessary for the relation of wake and fish to be consistent across tailbeats.

Our model (and that of Weihs) deviates from reality in several ways, e.g. the schools are represented by lattices that are rigid, infinite and two-dimensional. We expect the rigidity to cause an overestimation of forces and swimming speed, because in our previous work we showed that constraints on the acceleration of a fish cause its forces and speed to resemble those of an unconstrained fish with a higher tailbeat frequency. The infinite size of our schools implies that our model is only applicable to the inner part of a school. In our infinite schools flow patterns indicate that fish only interact hydrodynamically with their direct neighbours, because the nearest neighbour disrupts the influence from those further away. Further, because we show that fish profit more from having neighbours in both longitudinal and lateral directions than from having neighbours in either direction alone, real fish should prefer to be in the inner area or at the rear of the school rather than at the front and sides. This inhomogeneous distribution of hydrodynamical benefit is also found in V-formations of flocks of large birds such as geese and pelicans, where the individual at the tip of the 'V' spends more energy than those behind (Weimerskirch et al., 2001; Andersson and Wallander, 2004). This inhomogeneity may reinforce the manner in which individuals in real fish schools are continually changing their positions within the school (Huth and Wissel, 1994). As regards the two-dimensionality of our model, so far results of two-dimensional hydrodynamical models of fish on a qualitative level remarkably resemble results of 3D models as well as empirical data of real fish (Sui et al., 2007; Reid et al., 2009; Borazjani and Sotiropoulos, 2008; Reid et al., 2011). However, in a model it was shown that quantitatively aspects such as the achieved swimming speed of the fish change significantly when the dimensions are changed Kern and Koumoutsakos (2006). Our 2D simulations can therefore only serve as a qualitative prediction of flow in real fish schools.

From our model we may derive an explanation of how an individual can benefit from the wake of another when their undulation frequencies differ, which is apparent in real

fish schools from the lower tailbeat of trailing individuals (Belyayev and Zuyev, 1969; Herskin and Steffensen, 1998; Svendsen et al., 2003). The ability to exploit a wake without synchronisation is indicated in our model both for the line formation by the absence of an effect on exploitation of longitudinal distance (Figs. 4.4B-4.7B) and in the line and rectangular formations by the variation of the encountered wake structure from one tailbeat to another (Fig. 4.8). In both cases fish exploit the wake by swimming just besides the jet of the predecessor.

Our model simplifies reality, for instance the undulation and position of individuals relative to their neighbours is fixed, whereas real fish adapt their gait to exploit vortex wakes (Liao et al., 2003b). Future improvements will involve more natural swimming of individuals, by making their bodies undulate in response to the flows, as well as making them sense flows and dynamically adjust their undulation to optimally exploit them, for example by using the Kármán gait (Liao et al., 2003b). Social responses, such as the common avoidance, alignment and attraction rules (Hemelrijk and Kunz, 2005; Hemelrijk and Hildenbrandt, 2008) will be added to create schooling behaviour that is more natural.

Our results are an important step towards understanding the hydrodynamics of schooling of fish. Unexpectedly, it is beneficial to swim directly behind another fish, as a consequence of the curving of the wake of the predecessor around the follower. Since these benefits of efficiency and speed arise even when the fish are not actively trying to exploit the wake, the benefits of schooling are easier to attain than previously thought, requiring neither precise spacial positioning nor modification of behaviour, for instance by tuning the frequency of undulation.

ACKNOWLEDGEMENTS

Charlotte Hemelrijk is grateful for her startup grant of the University of Groningen belonging to her Rosalind Franklin Fellowship, the grant from the 6th European framework under the STREP-project "Star-Flag" (n12682) in the NEST-programme of "Tackling complexity in science." and that of the Cognitie Pilot project of NWO (051.07.006) by which Hanno Hildebrandt has been paid.

5

A META-ANALYSIS OF FISH SWIMMING[1]

Abstract

The precise mechanics underlying the swimming of fish are of great general interest, both to biologists and to engineers. So far, only one general principle has been reported, namely that swimming speed increases with tail beat frequency. In the present paper, we perform a meta-analysis in order to investigate whether there may exist more of such general principles. Using data of 26 species, we examine the relationships between the swimming speed and several kinematic variables, namely length of the body, frequency and amplitude of the tail beat, and length and speed of the propulsive body wave, and the interrelation of these variables with the hydrodynamically important dimensionless Reynolds number, the Strouhal numbers and the slip ratio U/V (between the forwards swimming speed U and the rearwards speed V of the body wave). Our data reveal several general principles: swimming speed is mainly the result of the speed of the propulsive body wave; it is also significantly (but more weakly) affected by frequency and amplitude of the tail beat, length of the propulsive body wave, and length of the body. Body depth appears to correlate strongly with swimming style, i.e. shallow-bodied fish are anguilliform and deep-bodied fish are carangiform or thunniform. Finally, contrary to common expectation the slip ratio U/V and the Strouhal number depend on the Reynolds number.

5.1 INTRODUCTION

Undulatory swimming is supposed to be an efficient mode of aquatic locomotion, because it is the result of many millions of years of evolution of species that may migrate over thousands of kilometres (Helfman et al., 1997). The general principles governing undulatory propulsion are therefore of great interest to both biologists (for better understanding of the constraints on the evolution of aquatic species) and engineers (for the design of underwater vehicles). However, despite many experimental data of kinematics only a single general principle has been reported, namely that a higher frequency of the tail beat results in faster swimming (Bainbridge, 1958; Webb et al., 1984; Videler, 1993). To search for more principles is the aim of the present meta-analysis.

The kinematics of steady undulatory swimming are largely formulated in terms of the wave that travels rearwards through the body of the fish, with speed $V = \lambda \cdot f$, wavelength

1 SUBMITTED TO JOURNAL OF EXPERIMENTAL BIOLOGY AS: J. F. VAN WEERDEN, D. A .P. REID, C. K. HEMELRIJK – *"A META-ANALYSIS OF FISH SWIMMING"*

λ and frequency f. The amplitude of this wave varies along the fish body, typically being lowest at a point close behind the head of the fish, and maximal at the tail tip (Videler and Hess, 1984). As a result of the wave, water is propelled rearwards and the fish moves forwards at speed U. Because the transmission of speed from the rearwards body wave to the water is not perfect, the forwards speed U is usually lower than that of the body wave V. The ratio U/V (the so-called slip ratio) between the two is often used as an indication of the efficiency of the swimming fish and is supposed to be approximately constant (Webb et al., 1984).

After the discovery of the relationship between tail beat frequency and swimming speed, the kinematics of a number of fish species have been investigated in many studies. However, so far the results of these studies have not been integrated. Studies have reported on the relation between swimming speed and variables such as the tail beat amplitude (Bainbridge, 1958; Webb, 1971; Liao, 2002), the length and speed of the body wave (Gray, 1933; Wardle et al., 1995; Tytell and Lauder, 2004) and the swimming style (i.e. how much of the body undulates) (Breder, 1926; Müller et al., 2001; Blake, 2004). In order to eliminate the effects of fish length on kinematic variables, the variables have often been expressed in fish lengths ('normalised'). The general effectiveness of this standardisation technique is debated, however (Packard and Boardman, 1999; Donley and Dickson, 2000). Based on the Elongated Body Theory, the swimming efficiency is commonly described by the slip ratio U/V (Lighthill, 1971). Experiments with oscillating foils suggest that fish swim most efficiently at an almost constant Strouhal number of 0.25-0.35 (Triantafyllou et al., 1991). These suppositions have so far not been verified empirically however.

In the present study we used online search engines to collect data from the scientific biological literature. We confined our investigation to steadily cruising fish, and collected specifically data of the tail beat (its frequency and amplitude), the body wave (its speed and length) and of the body depth.

We note that the swimming speed is generally incorporated in analyses as a causal variable of the kinematics of the fish (Webb et al., 1984; Long and Nipper, 1996; Liao, 2002; Müller and van Leeuwen, 2004). We assume instead that the kinematics cause the forwards speed, and investigate their relationship with the standard dimensionless measures, i.e. the Reynolds number $Re = UL/\nu$, (with U the forwards swimming speed, L the length of the fish and ν the kinematic viscosity), the slip ratio U/V and the Strouhal number $St = 2Af/U$ (with $2A$ the distance between the maximum lateral excursions of the tail tip and f the tailbeat frequency). We analyse these variables both in absolute units and in fish lengths ('normalised'). Besides, in our calculations of the Reynolds numbers we take the effect of water temperature on the viscosity into account.

5.2 METHODS

In our literature search we used the online search engines ISI web of Knowledge and Google scholar. We searched for data of kinematics of steady, undulatory swimming. We included only those papers that reported data on all of the following variables: the frequency and amplitude of the tailbeat, the length and speed of the body wave, and the length and depth of the body of the fish (Table 5.1). If morphological data were absent, we took them from

Fishbase, World Wide Web electronic publication (2011). To determine the Reynolds number we calculated the correct viscosity for the temperature reported in the paper (Reynolds, 1883).

Measure	Symbol	Units
Fish length	L	cm and TL
Body depth	H	% of TL
Swimming speed	U	cm/s and TL/s
Tailbeat frequency	f	Hz
Tailbeat amplitude	$2A$	cm and TL
Body wave length	λ	cm and TL
Body wave speed	$V = \lambda \cdot f$	cm/s and TL /s
Slip	(U/V)	dimensionless
Strouhal number	$2A \cdot f/U$	dimensionless
Reynolds number	$U \cdot L/\nu$	dimensionless

Table 5.1.: Measures used for analysis.

The size of a fish has commonly been measured in three ways, namely body (or standard) length, fork length and total length (Fig. 5.1). Here we use total length (TL). We analysed the data in both absolute units (cm) and in total fish lengths (TL). Our data contained outliers as regards swimming speed ($\geqslant$ 200 cm/s) and size ($\leqslant$ 2 cm). They comprised not only fish but also axolotls. We studied both the total data set and that with neither outliers nor axolotls.

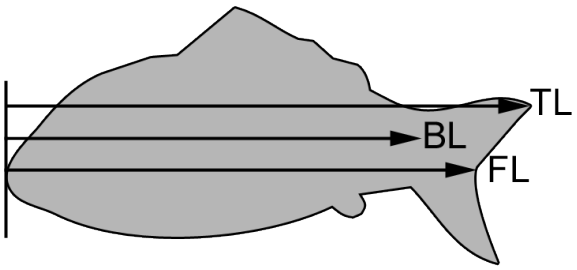

Figure 5.1.: Different ways to measure fish length: Body Length (BL), Fork Length (FL) and Total Length (TL). The present study uses Total Length.

Another method (besides normalisation) to reduce the effect of fish length is to divide the fish into size classes. Individuals of 0-2.5 cm belong to the smallest category and each larger one doubles the length. Because the categories 2.5-5 and 5-10 comprised insufficient data we combined them into one group (Table 5.2).

In most of our analyses we use correlations rather than regressions, because many of the variables are mutually dependent, rather than causal in one direction.

5.3 RESULTS

Twenty-three studies were found that included all required kinematic variables (Table 5.3). They concern 26 species of 24 genera.

Length class	N	slope	R^2	p
2: 3-10 cm	11	1.2	0.16	ns
3: 10-20 cm	18	14.4	0.74	***
4: 20-40 cm	41	24.1	0.47	***
5: $\geqslant$ 40 cm	18	29.2	0.67	***

Table 5.2.: The correlation between tailbeat frequency and swimming speed of several length classes.

The speed of the body wave V appears to be the strongest explanatory variable of the variance in the swimming speed U (Table 5.4). This holds both when expressed in body lengths and in absolute units, and both with and without outliers (Fig. 5.2). Each of the other kinematic variables also appears to significantly influence the swimming speed.

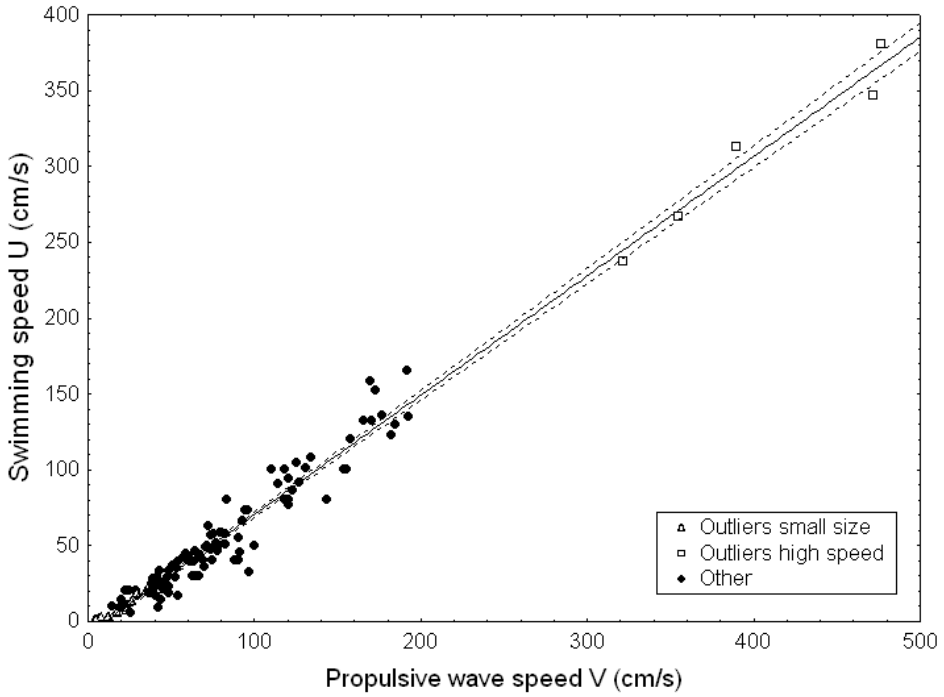

Figure 5.2.: Swimming speed as a function of body wave speed, both in absolute units, for the data including outliers.

The variance of the swimming speed is explained with similar strength by the tail beat frequency as it is by the speed of the propulsive wave, but only when the effect of fish length is reduced, either by normalisation (Table 5.4) or by studying effects per size class (Fig. 5.3).

The unit of measurement appears to influence the relation between the swimming speed U and the fish length L: in absolute units, larger fish swim faster, whereas in fish lengths smaller fish swim faster (Table 5.4).

The correlation of the swimming speed U with the speed of the propulsive wave V is independent of the length L of the fish, which is unexpected because the correlations with

Species	Total nr of data points	Data without extremes	Study
Abramis brama	1	1	Bainbridge (1958)[V]
Ambystoma mexicanum	8	-	D'Aout and Aerts (1997)
Ambystoma mexicanum (juv)	3	-	D'Aout and Aerts (1999)
Ammodytes marinus	4	4	Videler (1993)[V]
Anguilla anguilla	1	1	Hess (1983)[V]
Anguilla anguilla	3	3	Müller et al. (2001)
Anguilla rostrata	1	1	Tytell and Lauder (2004)
Carassius auratus	1	1	Bainbridge (1963)
Chelon labrosus risso	1	1	Müller et al. (2002)
Chelon labrosus risso	1	1	Müller et al. (1997)
Clupea Harengus (larva)	6	-	Fuiman and Batty (1997)
Danio rerio (larva)	2	-	Müller et al. (2008)
Danio rerio (larva)	9	-	Müller and van Leeuwen (2004)
Esox (hybrid)	1	1	Webb (1988)[V]
Euthynnus affinis	4	4	Donley and Dickson (2000)
Gadus morhua	4	4	Videler and Hess (1984)
Gadus morhua	2	2	Webb (2002)
Gambusia affinis	6	6	Langerhans (2009)
Hyperoplus lanceolata	5	5	Videler (1993)[V]
Lepisosteus osseus	7	7	Long and Nipper (1996)
Leuciscus leuciscus	1	1	Bainbridge (1963)
Liza ramada	1	1	Videler (1993)[V]
Micropterus salmoides	5	5	Jayne and Lauder (1995)
Oncorhynchus mykiss	5	-	Jayne and Lauder (1995), from Webb et al. (1984)
Oncorhynchus mykiss	4	4	Webb et al. (1984)[V]
Oncorhynchus mykiss (as Salmo gaidneri)	1	1	Webb (1988)[V]
Pleuronectes platessa	1	1	Webb (2002)
Pollachius virens	9	9	Videler and Hess (1984)[V]
Salmo salar	3	2	Videler (1993)[V]
Sarda chiliensis chiliensis	2	2	Dowis et al. (2003)
Scomber japonicus	8	8	Dickson et al. (2002)
Scomber japonicus	4	4	Donley and Dickson (2000)
Scomber scombrus	9	5	Videler and Hess (1984)[V]
Strongylura marina	3	3	Liao (2002)
Total number of data points	126	88	

Table 5.3.: Collected data of 26 species. Data points may be based on 1 to 10 individuals. [V]: data taken from Videler (1993).

Data	Unit	V	f	2A	λ	L
All	Fish length	(+) 0.94***	(+) 0.93***	(+) 0.42***	(+) 0.16***	(-) 0.15***
Without outliers	Fish length	(+) 0.89***	(+) 0.80***	(+) 0.29***	(+) 0.06*	(-) 0.19***
All	cm	(+) 0.98***	(ns) 0.02	(+) 0.35***	(+) 0.30***	(+) 0.25***
Without outliers	cm	(+) 0.91***	(ns) 0.00	(+) 0.38***	(+) 0.30***	(+) 0.13***

Table 5.4.: Swimming speed U and its correlation with several variables: direction, explained variance (R^2) and significance. *: $p < 0.05$, **: $p < 0.01$, ***: $p < 0.001$. V is the speed of the propulsive body wave, f the tail beat frequency, 2A is the tailbeat amplitude, λ is the length of the propulsive body wave and L is the total length of the fish.

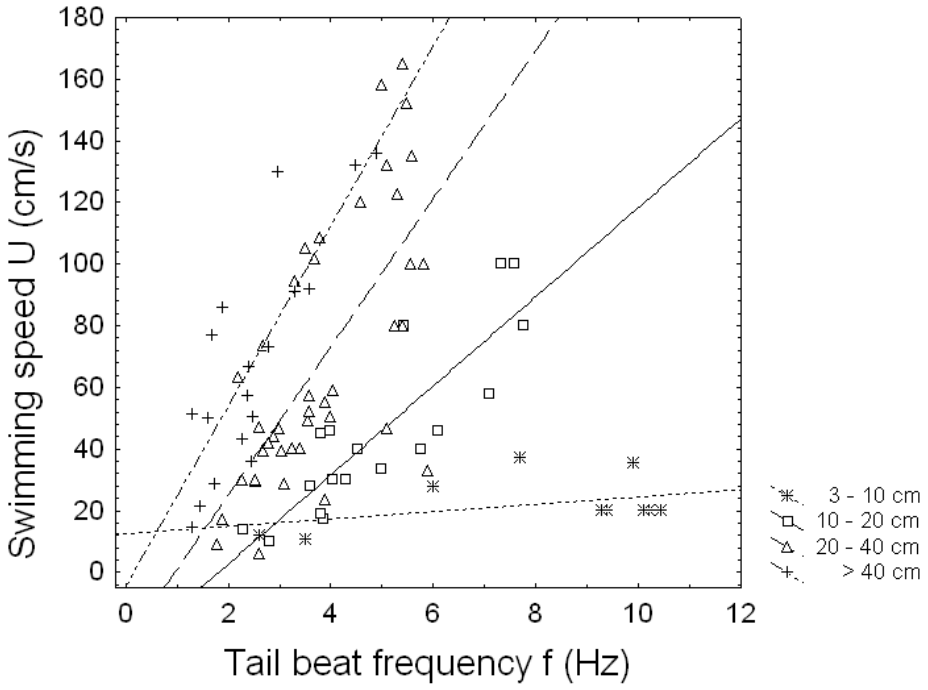

Figure 5.3.: Swimming speed in absolute units as a function of tailbeat frequency of the data without outliers, with the data separated into different length classes (Table 5.2)

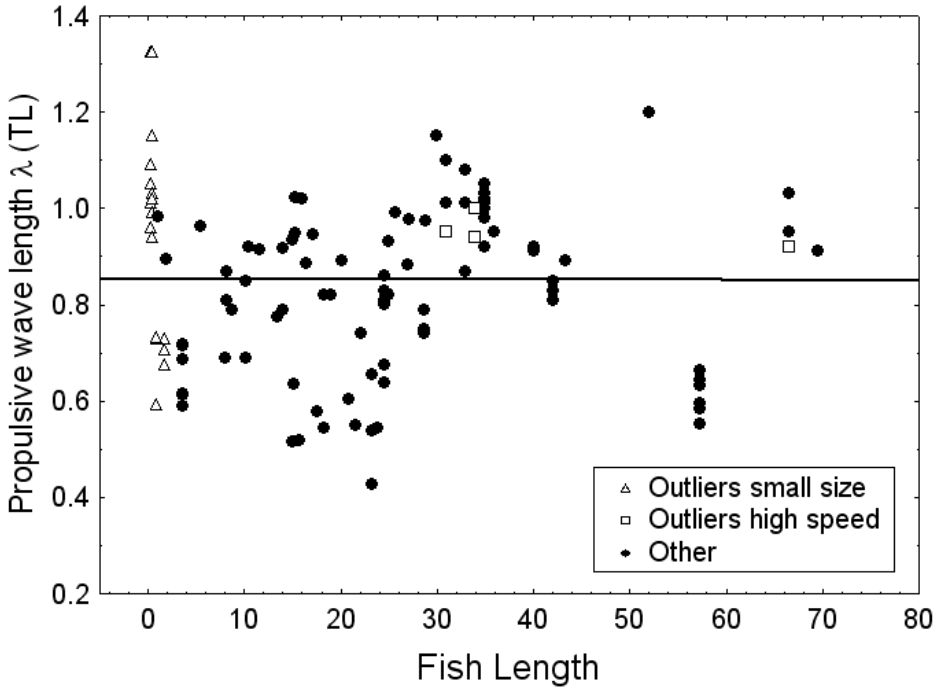

Figure 5.4.: Propulsive wave length λ, as a function of fish length, for the data including outliers.

the swimming speed of both components of V, i.e. tail beat frequency f and propulsive wavelength λ are significantly influenced by the fish length (tail beat frequency $R^2 = 0.283, p < 0.05$, propulsive wavelength: $R^2 = 0.809, p < 0.001$).

Fish length does not correlate with the length of the body wave ($R^2 < 0.001$, $p = 0.98$) (Fig. 5.4)

The data on body depth are bimodally distributed in two classes with depths of 5-8% and 17-30% of the fish length (Fig. 5.5). These classes appear to differ in swimming style: shallow-bodied individuals are anguilliform and deep-bodied individuals are carangiform and thunniform (Breder, 1926; Webb, 1984; *Fishbase, World Wide Web electronic publication*, 2011)). To obtain an approximately equal sample size in both classes, we limit our comparison of fish of different body depths to those that swim at $1 - 3Ls^{-1}$ (Table 5.5). It appears that despite their similarity in body length and in tailbeat frequency, shallow-bodied fish swim slower and have shorter propulsive wavelengths and a slightly higher Strouhal number (i.e. use a higher tail beat frequency to achieve their swimming speed) than deep-bodied ones (Table 5.5).

The slip ratio and Strouhal number both appear to depend on the Reynolds number in a non-linear way (Figs. 5.6, 5.7).

Variable	Mean ± StDev		t-value	p-value
	Shallow	Deep		
Length	21.2 ± 9.32	29.8 ± 13.9	-1.908	0.063
Speed in TL	1.56 ± 0.27	2.0 ± 0.6	-2.166	0.036*
Speed in cm	33.47 ± 15.55	56.7 ± 26.8	-2.713	0.010*
Tailbeat frequency	3.18 ± 0.77	3.4 ± 0.9	-0.716	0.478
Prop. wave length in TL	0.76 ± 0.08	0.9 ± 0.1	-4.724	0.000*
Prop. wave length in cm	16.06 ± 7.67	27.6 ± 14.5	-2.511	0.016*
Prop. wave speed in TL	2.44 ± 0.44	3.1 ± 0.9	-2.431	0.020*
Prop. wave speed in cm	51.31 ± 22.98	86.1 ± 30.8	-3.419	0.001*
Slip ratio U/V	0.65 ± 0.08	0.7 ± 0.1	-0.509	0.613
Strouhal number	0.34 ± 0.09	0.3 ± 0.1	2.974	0.005*
Reynolds number	80483 ± 55325	166595 ± 142119	-1.947	0.058

Table 5.5.: Comparison between shallow-bodied and deep-bodied fish, showing results of Student's t-test. Degrees of freedom were 41 in all cases. There were 11 samples representing shallow-bodied fish and 32 representing deep-bodied ones. *: $p < 0.05$.

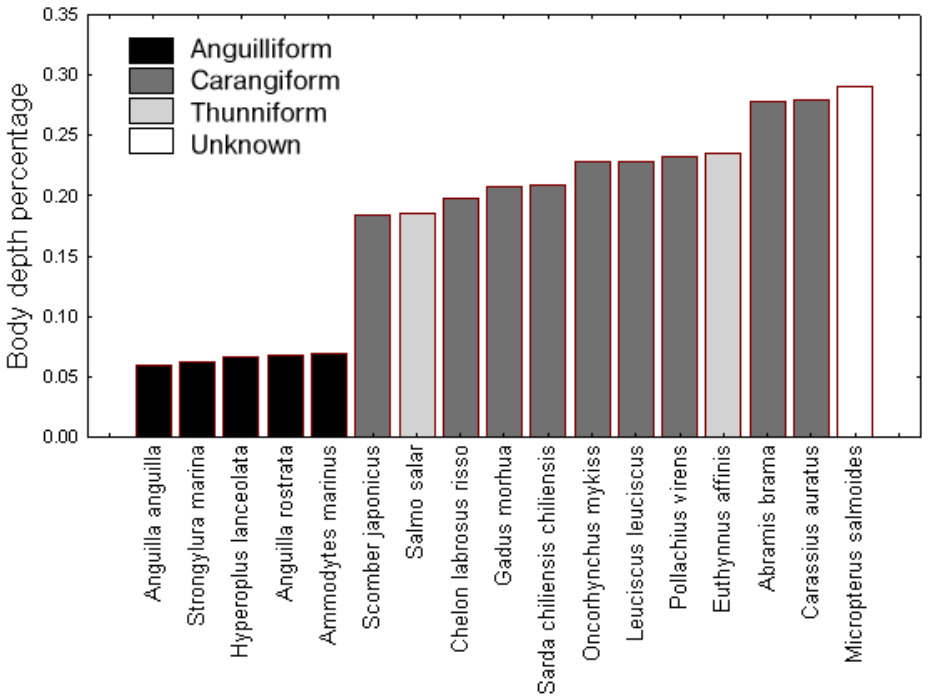

Figure 5.5.: Average body depths for several species of fish, in terms of % of their total length. Colour indicates swimming style.

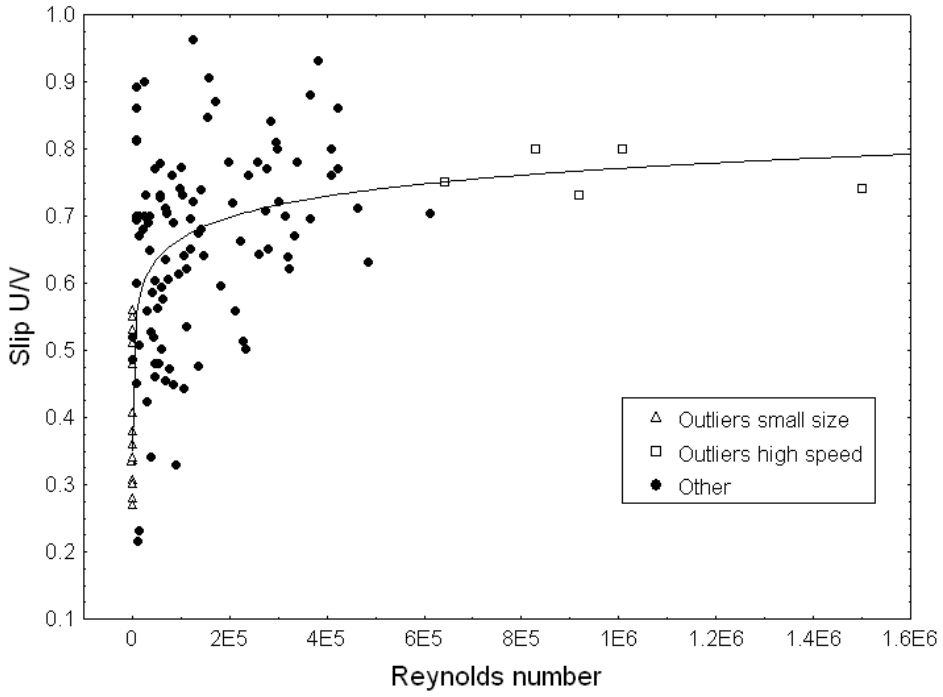

Figure 5.6.: Slip ratio U/V as a function of Reynolds number, for the data including outliers.

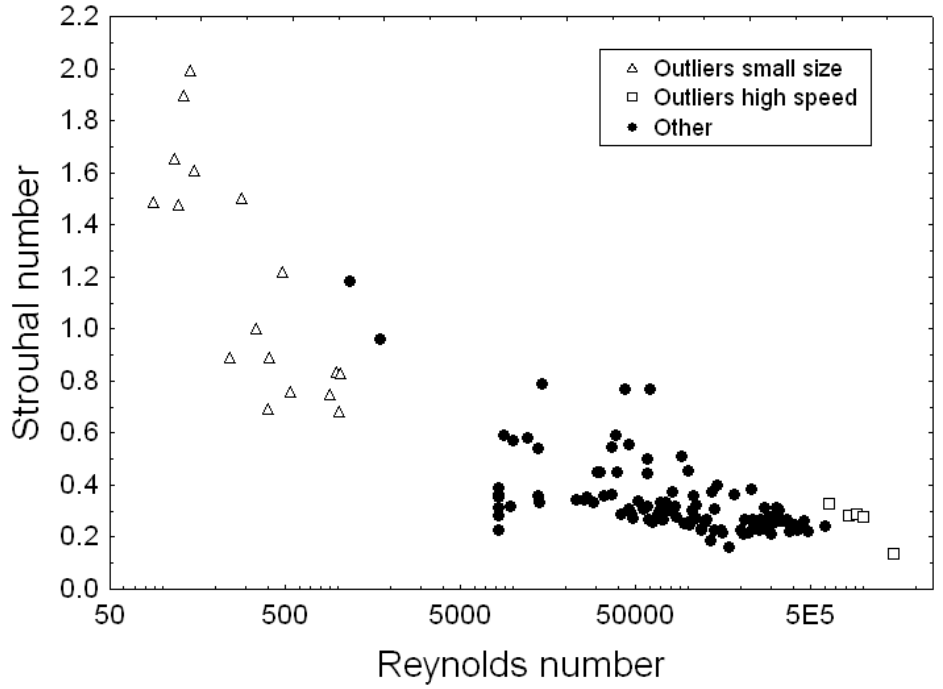

Figure 5.7.: Strouhal number as a function of Reynolds number, for the data including outliers.

5.4 DISCUSSION

Our analysis shows that swimming speed depends almost entirely on the speed of the propulsive body wave, and more so than on any of the other variables (including the tail beat frequency). This finding is independent of the unit of measurement. It confirms the early results for 6 species of Gray (1933). The two components of speed of the propulsive wave (ie. tail beat frequency and wave length) are often used separately for the analysis of swimming speed, but seldom in combination. Our results show however that only the combination of the two truly determines the swimming speed. An appropriate analogy is that of walking: the frequency with which one swings one's legs and the length of one's stride together determine the speed of walking.

Our data concern fish that differ greatly in their size, body depth and swimming style. In spite of this, the relation between the speed of the body wave and swimming speed is consistent throughout the data (Table 5.4, Fig. 5.2). This suggests that the speed of undulatory swimming depends almost entirely on the rearwards speed of the body wave, regardless of differences in other morphological and kinematic factors. This finding can be used by engineers to test whether robotic vehicles resemble swimming of real fish. Assuming that evolution has selected for swimming performance, engineers may optimise their models of undulation by making them fit the relation between swimming speed and propulsive wave speed.

Results of our large dataset differ in two cases from previous results for single species. First, the relation of tail beat amplitude and swimming speed has been shown to reach a plateau for single species (Bainbridge, 1958; Webb, 1975), but this does not happen in our data. Possible explanations for this difference are that in contrast to the other studies in our data animals were not swimming at their maximum speed, and that the maximum tail beat amplitudes differed among species. Second, within a single species the propulsive wave length, both in absolute units and in fish lengths, has been shown to increase with the total fish length (Donley and Dickson, 2000). In our analysis however, this association is absent (Fig. 5.4). Thus we conclude that the propulsive wavelength is characteristic to a particular species: because fish of different species but similar length have different body wave lengths, there is no correlation in our cross-species comparison.

Two of our results may be due to experimental constraints. First, when comparing shallow- and deep-bodied fish, shallow fish are slower than deep ones. This may be due to having their swimming speed artificially biased by the experimenter, through incidentally setting the speed of the flow tank too low because of a belief that anguilliform fish are incapable of fast swimming. Second, large fish may be prevented from swimming at their preferred cruising speed because the tank is too small, which could explain our finding that larger fish swim slower in terms of fish length. Our results thus point to the need to report details of the maximum speed of fish also.

The hypothesis of a single optimal Strouhal number that all fish attempt to attain (Triantafyllou et al., 1993) appears not to be borne out by our data: instead, the Strouhal number of fish appears to be associated with their Reynolds number.

In contrast to earlier findings (Webb et al., 1984), the slip ratio U/V is not constant, but varies with the Reynolds number (Fig. 5.6). It appears that at lower Reynolds numbers the

rearwards motion of the body wave is less effective at propelling an individual forwards. Our computer simulations of hydrodynamics, based on Multiparticle Collision Dynamics, suggest the following explanation (Reid et al., 2009, 2011): when their tail beat reverses, fish may slow down more at lower Reynolds numbers than at higher Reynolds numbers, because the influence of the viscosity is stronger and inertia is lower. This implies a related effect on stride length λ_s (i.e. the distance that a fish travels forwards in a single tailbeat). At lower Reynolds numbers the stride length ($\lambda_s = \lambda U/V$) is shorter, at higher re numbers it is longer.

Further, above this point between Reynolds number 1200 and 2000, the increase of the slip ratio U/V with the Reynolds number slows down (Fig. 5.6). This may reflect the lower influence of viscosity. Due to this lower viscous influence, the swimming efficiency may be higher (Reid et al., 2011). Thus, this point of saturation may be ecologically significant. It is supplementary to the one between swimming styles at a Reynolds number of 200 for developing larvae (Weihs, 1980).

Although the unprecedented size of our data set enables us to clarify the effects of variables on speed that were previously reported only for single species, such as the propulsive wave speed and fish length, still further research would be helpful, especially at the extremely low and high Reynolds numbers where data are still sparse.

Our main conclusion is that more attention should be paid to the speed of the propulsive body wave in relation to swimming speed.

ACKNOWLEDGEMENTS

We are grateful to Jimmy Liao for constructive comments on earlier presentations of our work and to John Videler for comments on the text as well as several informative discussions.

6

DISCUSSION

The preceding chapters describe the most important results of the work done for my doctoral thesis. Chapters 2, 3 and 4 each describe a more advanced version of the computer model and its application to a more complex situation, from static shapes in flow (Chapter 2) to infinite schools of undulating fish (Chapter 4).

The swimming of fish has in the last fifteen years been studied in a variety of computer simulations of hydrodynamics, often with interesting results (Liu et al., 1996; Wolfgang et al., 1999; Kern and Koumoutsakos, 2006; Sui et al., 2007; Borazjani and Sotiropoulos, 2008). Our simulation method is a valuable addition to this field for two main reasons: First, its lack of a spatial grid makes it ideally suited for the study of organisms, especially those that change their shape and relative position. Second, it is extremely fast, without sacrificing hydrodynamical accuracy. All simulations in this thesis were carried out on a single, ordinary desktop PC or laptop, and even the largest simulations took less than a week. It should be noted however that this speed comes at the cost of stochastic noise. The influence of this noise decreases as the system under study becomes larger. This means that the model is most suitable for either high Reynolds numbers, (above 1000) where the noise is largely cancelled out through the law of averages, or extremely low ones (below 1) where Brownian motion is relevant.

Our finding in Chapter 2 that the addition of trailing, tail-like plates to cylinders increases their drag coefficient at low Reynolds numbers, but decreases drag at higher ones, suggests that tails which are flat orthogonally to the direction of undulation are more useful for larger organisms, such as the fish that we study in the subsequent chapters. Further, we argue that the *effective* Reynolds number of a two-dimensional object is higher than that of the corresponding three-dimensional one. In two dimensions the degrees of freedom are reduced and there is no third dimension for energy to dissipate into. This causes all flow phenomena such as the onset of vortex shedding and turbulence to occur at a much lower Reynolds numbers in 2D than in 3D (Table 2.3). We use this finding in Chapters 3 and 4 to explain why our simulations of fish shapes with Reynolds numbers of approximately 1200 are reasonable approximations of real fish swimming at much higher Reynolds numbers (to the order of 10000).

In Chapter 3 we test the effects of the common practice in computer simulations to constrain swimming fish from accelerating. We find that constraining longitudinal acceleration has no effect, but constraining lateral acceleration increase the force which the fish exerts, causing its speed speed and patterns of hydrodynamical forces and flow to resemble those of unconstrained fish with a higher tailbeat frequency. Because constraining the acceleration

of individuals had no qualitative effect for single fish in Chapter 3, we expect that our choice in Chapter 4 to keep the relative positions of individuals in the schools fixed will also not qualitatively affect the patterns of force and efficiency.

The most notable result of our simulations of groups of fish is that the efficiency of the vast majority of spatial configurations and spacings was higher than that of a single fish. This suggests that travelling in groups is likely to save energy for some of its members in many more cases than was originally thought.

Our simulation results are consistent with three findings from our meta-analysis of data of real fish (Chapters 3, 5). Firstly, swimming speed increases linearly with tailbeat frequency as well as with the speed V of the propulsive body wave. Second, the slip ratio U/V at low to intermediate Reynolds number (1000–10000) is strongly dependent on the Reynolds number. Third, rather than there being a single optimal Strouhal number at which fish swim (Triantafyllou et al., 1993), the Strouhal number changes with the Reynolds number. Our simulations of single fish only experimented with different tailbeat frequencies. For a more thorough comparison between simulations and data of real fish it would be necessary to change also parameters such as fish size, tailbeat amplitude and the wavelength of the undulation. This could be used to further validate the model against experimental data. Also of interest would be to study a different body shape and swimming style such as those of an eel against simulations and empirical data (Borazjani and Sotiropoulos (2009); Gillis (1998); Müller et al. (2001), Chapter 5).

Besides further comparison to empirical data, there is of course much work still to be done to improve our understanding of the hydrodynamics of swimming fish, especially in schools. On current hardware it will be possible to study larger groups in our model. This allows for finite school sizes, with individuals that undulate out of phase and with different tailbeat frequencies. The individuals could also be made to swim more naturally, by making their bodies undulate in response to the flows, as well as making them sense flows and dynamically adjust their undulation to optimally exploit them, for example by using the Kármán gait (Liao et al., 2003b). Social responses, such as the commonly-used simulation rules of avoidance, alignment and attraction (Hemelrijk and Kunz, 2005; Hemelrijk and Hildenbrandt, 2008; Hemelrijk et al., 2010) could also be added to create schooling behaviour that is more natural. Or course, for this individuals must be able to move and change their relative positions freely unlike the rigid lattices we studied (Chapter 4). To this end, a control system could be added to the fish so that they curve their body to make turns and change their tailbeat frequency to navigate change their velocity, as has been shown to work in robotic fish (Shao et al., 2008).

The work presented in this thesis has answered several important questions about undulatory swimming and its study in simulations, for example the effects of constraining individuals' acceleration, and the hydrodynamical benefits of travelling in groups. Just as many, if not more, questions remain however. Fortunately, this thesis has also resulted in a simulation tool that will allow many of those questions to be answered in future projects.

A

APPENDIX A : RAY / MOVING LINE INTERSECTION

Let the ray be parametrically expressed in two dimensions as

$$\mathbf{r}(t) = \mathbf{r}_0 + t\,d\mathbf{r}. \tag{A.1}$$

The particle is at $\mathbf{r}_0$ at the beginning of the current time step, which we identify with $t = 0$, and t is continuous time.

Let $\mathbf{p}(t)$ and $\mathbf{q}(t)$ similarly be the position of the endpoints of the moving line over time, as follows :

$$\mathbf{p}(t) = \mathbf{p}_0 + t\,d\mathbf{p} \tag{A.2}$$
$$\mathbf{q}(t) = \mathbf{q}_0 + t\,d\mathbf{q}. \tag{A.3}$$

Any point on the edge can be expressed as $\mathbf{E}(s,t) = s\mathbf{q}(t) + (1-s)\mathbf{p}(t)$, where s is the coordinate along the edge. The movements of particle and edge intersect if at any time t' the equality $\mathbf{E}(s,t') = \mathbf{r}(t')$ holds, in other words

$$s\left(\mathbf{q}_0 + t'\,d\mathbf{q}\right) + (1-s)\left(\mathbf{p}_0 + t'\,d\mathbf{p}\right) = \mathbf{r}_0 + t'\,d\mathbf{r}. \tag{A.4}$$

First we solve for t', focussing on the x component of Eq. A.4

$$t' = -\frac{s\,(q_{0,x} - p_{0,x}) + (p_{0,x} - r_{0,x})}{s\,(dq_x - dp_x) + (dp_x - dr_x)}. \tag{A.5}$$

Then we solve for t', focussing on the y component, with a result similar to the one above but with all subscripts x replaced by y. Equating the two expressions for t', we arrive at a quadratic equation in s:

$$as^2 + bs + c = 0, \tag{A.6}$$

where the coeffients a, b and c can be expressed using the binary perpendicular dot product ($\perp$), which greatly simplifies the coefficients of the quadratic equation and allows the solution to be calculated efficiently (note that $\perp$ is basically the z component of the cross product of vectors in the x-y plane):

$$\perp(\mathbf{A},\mathbf{B}) \equiv A_x B_y - A_y B_x \tag{A.7}$$

$$a = \perp(\mathbf{q}_0 - \mathbf{p}_0, d\mathbf{q} - d\mathbf{p}) \tag{A.8}$$

$$b = \perp(\mathbf{q}_0 - \mathbf{p}_0, d\mathbf{p} - d\mathbf{r}) + \perp(\mathbf{p}_0 - \mathbf{r}_0, d\mathbf{q} - d\mathbf{p}) \tag{A.9}$$

$$c = \perp(\mathbf{p}_0 - \mathbf{r}_0, d\mathbf{p} - d\mathbf{r}) \tag{A.10}$$

Solving the quadratic equation yields two values for s, which, when inserted in Eq. A.5 give two corresponding values for t'. If any of the s lie in the interval $[0, 1]$ and the corresponding t' lies in the interval $[0, \Delta t]$ a collision has occurred. If there are two solutions within this interval, the one with smallest t' occurred first and is picked for further processing.

ACKNOWLEDGMENTS

It has been a great 6 years. They would not have been so great without the wonderful people that I have interacted with during that time. I wish to thank them all here. So, from the bottom of my heart, thank you to my supervisors without whom this project would have been neither possible nor even slightly as good as it ended up being. Thank you to my friends and family without whom I would probably have gone insane. To my colleagues who made coming to work fun and interesting (until the awful new building happened anyway). And to my dear wife and daughter without whom life would not be worth living.

Daan Reid
Groningen
August 24, 2011

BIBLIOGRAPHY

Abrahams, M. V. and Colgan, P. W.: 1985, Risk of predation, hydrodynamic efficiency and their influence on school structure, *Environmental Biology of Fishes* **13**, 195–202.

Allahyarov, E. and Gompper, G.: 2002, Mesoscopic solvent simulations: Multiparticle-collision dynamics of three-dimensional flows, *Physical Review E* **66**, 036702.

Anderson, E. J., McGillis, W. R. and Grosenbaugh, M. A.: 2001, The boundary layer of swimming fish, *Journal of Experimental Biology* **204**, 81–102.

Andersson, M. and Wallander, J.: 2004, Kin selection and reciprocity in flight formation?, *Behavioral Ecology* **15**, 158–162.

Bainbridge, R.: 1958, The speed of swimming of fish as related to size and to the frequency and amplitude of the tail beat, *Journal of Experimental Biology* **35**(1), 109–133.

Bainbridge, R.: 1963, Caudal fin and body movement in propulsion of some fish, *Journal of Experimental Biology* **40**(1), 23–56.

Bandyopadhyay, P. R.: 2002, Maneuvering Hydrodynamics of Fish and Small Underwater Vehicles, *Integrative and Comparative Biology* **42**(1), 102–117.

Barrett, D. S. and Triantafyllou, M. S.: 1995, The design of a flexible hull undersea vehicle propelled by an oscillating foil, *9th Intl Symp. on Unmanned Untethered Submersible Technology*.

Barrett, D. S., Triantafyllou, M. S., Yue, D. K. P., Grosenbaugh, M. A. and Wolfgang, M. J.: 1999, Drag reduction in fish-like locomotion, *Journal of Fluid Mechanics* **392**, 183–212.

Beal, D. N., Hover, F. S., Triantafyllou, M. S., Liao, J. C. and Lauder, G. V.: 2006, Passive propulsion in vortex wakes, *Journal of Fluid Mechanics* **549**, 385–402.

Belyayev, V. V. and Zuyev, G. V.: 1969, Hydrodynamic hypothesis of school formation in fishes, *Journal of Ichthyology* **9**, 578–584.

Birch, J. M. and Dickinson, M. H.: 2001, Spanwise flows and the attachment of the leading-edge vortex, *Nature* **412**, 729–733.

Birch, J. M., Dickson, W. B. and Dickinson, M. H.: 2004, Force production and flow structure of the leading edge vortex on flapping wings at high and low Reynolds numbers, *Journal of Experimental Biology* **207**(7), 1063–1072.

Blake, R. W.: 2004, Fish functional design and swimming performance, *Journal of fish biology* **65**, 1193–1222.

Borazjani, I., Ge, L. and Sotiropoulos, F.: 2008, Curvilinear immersed boundary method for simulating fluid structure interaction with complex 3d rigid bodies, *Journal of Computational Physics* **227**, 7587–7620.

Borazjani, I. and Sotiropoulos, F.: 2008, Numerical investigation of the hydrodynamics of carangiform swimming in the transitional and inertial flow regimes, *Journal of Experimental Biology* **211**(10), 1541–1558.

Borazjani, I. and Sotiropoulos, F.: 2009, Numerical investigation of the hydrodynamics of anguilliform swimming in the transitional and inertial flow regimes, *Journal of Experimental Biology* **212**(4), 576–592.

Borazjani, I. and Sotiropoulos, F.: 2010, On the role of form and kinematics on the hydrodynamics of self-propelled body/caudal fin swimming, *Journal of Experimental Biology* **213**, 19–107.

Breder, C.: 1926, The locomotion of fishes, *Zoologica* **4**, 159–256.

Breuer, M., Bernsdorf, J., Zeiser, T. and Durst, F.: 2000, Accurate computations of the laminar flow past a square cylinder based on two different methods: lattice-boltzmann and finite-volume, *International Journal of Heat and Fluid Flow* **21**, 186–196.

Carling, J., Williams, T. and Bowtell, G.: 1998, Self-propelled anguilliform swimming: simultaneous solution of the two-dimensional navier–stokes equations and Newton's laws of motion, *Journal of Experimental Biology* **201**(23), 3143–3166.

Cheng, J. and Blickhan, R.: 1994, Note on the calculation of propeller efficiency using elongated body theory, *Journal of Experimental Biology* **192**(1), 169–177.

Cheng, J.-Y., Zhuang, L.-X. and Tong, B.-G.: 1991, Analysis of swimming three-dimensional waving plates, *Journal of Fluid Mechanics* **232**, 341–355.

Coutanceau, M. and Bouard, R.: 1977, Experimental determination of the main features of the viscous flow in the wake of a circular cylinder in uniform translation. part 1. steady flow, *Journal of Fluid Mechanics* **79**, 231–256.

Dabiri, J. O.: 2005, On the estimation of swimming and flying forces from wake measurements, *Journal of Experimental Biology* **208**, 3519–3532.

D'Aout, K. and Aerts, P.: 1997, Kinematics and efficiency of steady swimming in adult axolotls (*Ambystoma mexicanum*), *Journal of Experimental Biology* **200**(13), 1863–1871.

D'Aout, K. and Aerts, P.: 1999, The kinematics of voluntary steady swimming of hatchling and adult axolotls (*Ambystoma mexicanum Shaw*, 1789), *Belgian Journal of Zoology* **129**(1), 305–316.

Deng, J. and Shao, X.: 2006, Hydrodynamics in a diamond-shaped fish school, *Conference of Global Chinese Scholars on Hydrodynamics*, pp. 438–442.

Deng, J., Shao, X.-M. and Yu, Z.-S.: 2007, Hydrodynamic studies on two traveling wavy foils in tandem arrangement, *Physics of Fluids* **19**, 113104.

Dickinson, M. H., Lehmann, F.-O. and Sane, S. P.: 1999, Wing Rotation and the Aerodynamic Basis of Insect Flight, *Science* **284**(5422), 1954–1960.

Dickson, K. A., Donley, J. M., Sepulveda, C. and Bhoopat, L.: 2002, Effects of temperature on sustained swimming performance and swimming kinematics of the chub mackerel *scomber japonicus*, *Journal of Experimental Biology* **205**(7), 969–980.

Dong, G.-J. and Lu, X.-Y.: 2007, Characteristics of flow over traveling wavy foils in a side-by-side arrangement, *Physics of Fluids* **19**, 057107.

Donley, J. M. and Dickson, K. A.: 2000, Swimming kinematics of juvenile kawakawa tuna (euthynnus affinis) and chub mackerel (scomber japonicus), *Journal of Experimental Biology* **203**(20), 3103–3116.

Dowis, H. J., Sepulveda, C. A., Graham, J. B. and Dickson, K. A.: 2003, Swimming performance studies on the eastern pacific bonito *sarda chiliensis*, a close relative of the tunas (family scombridae) - ii. kinematics, *Journal of Experimental Biology* **206**(16), 2749–2758.

Drucker, E. G. and Summers, A. P.: 2007, *Moving with fins and limbs: an historical perspective on the study of animal locomotion with paired appendages*, University of Chicago Press, chapter 3.

Eldredge, J. D.: 2007, Numerical simulation of the fluid dynamics of 2D rigid body motion with the vortex particle method, *Journal of Computational Physics* **221**, 626–648.

Engelmann, J., Hanke, W., Mogdans, J. and Bleckmann, H.: 2000, Neurobiology - Hydrodynamic stimuli and the fish lateral line, *Nature* **408**, 51–52.

Falck, E., Lahtinen, J. M., Vattulainen, I. and Ala-Nissila, T.: 2004, Influence of hydrodynamics on many-particle diffusion in 2d colloidal suspensions, *European Physical Journal E* **13**, 267–275.

Fish, F. E.: 2006, The myth and reality of gray's paradox: implication of dolphin drag reduction for technology, *Bioinspiration & Biomimetics* **1**(2), R17.

Fishbase, World Wide Web electronic publication: 2011.
URL: *www.fishbase.org*

Fuiman, L. A. and Batty, R. S.: 1997, What a drag it is getting cold: Partitioning the physical and physiological effects of temperature on fish swimming, *Journal of Experimental Biology* **200**(12), 1745–1755.

Gillis, G. B.: 1998, Environmental effects on undulatory locomotion in the american eel *anguilla rostrata*: kinematics in water and on land, *Journal of Experimental Biology* **201**, 949–961.

Gilmanov, A. and Sotiropoulos, F.: 2005, A hybrid cartesian/immersed boundary method for simulating flows with 3d, geometrically complex, moving bodies, *Journal of Computational Physics* **207**(2), 457–492.

Gray, J.: 1933, Studies in animal locomotion. i. the movement of fish with special reference to the eel., *Journal of Experimental Biology* **10**, 88–104.

Helfman, G. S., Collette., B. B. and Facey, D. E.: 1997, *The Diversity of Fishes*, Blackwell Science.

Hemelrijk, C. K. and Hildenbrandt, H.: 2008, Self-organised shape and frontal density of fish schools, *Ethology* **114**, 245–254.

Hemelrijk, C. K., Hildenbrandt, H., Reinders, J. and Stamhuis, E.: 2010, Emergence of oblong school shape: models and empirical data of fish, *Ethology* **116**, 1099–1112.

Hemelrijk, C. K. and Kunz, H.: 2005, Density distribution and size sorting in fish schools: an individual-based model, *Behavioral Ecology* **16**, 178–187.

Herskin, J. and Steffensen, J. F.: 1998, Energy savings in sea bass swimming in a school: measurements of tail beat frequency and oxygen consumption at different swimming speeds, *Journal of fish biology* **53**, 366–376.

Hess, F.: 1983, Bending movements and muscle power in swimming fish, *in* 12A1-12A3 (ed.), *Proceedings of the Australian Fluid Mechanics Conference*, Vol. 2.

Hildenbrandt, H., Carere, C. and Hemelrijk, C.: 2010, Self-organized aerial displays of thousands of starlings: a model, *Behavioral Ecology* **21**, 1349–1359.

Hoerner, S. F.: 1965, *Fluid-Dynamic Drag; Practical Information on Aerodynamic Drag and Hydrodynamic Resistance*, Hoerner Fluid Dynamics.

Huth, A. and Wissel, C.: 1994, The simulation of fish schools in comparison with experimental data, *Ecological Modelling* **75/76**, 135–145.

Ihle, T. and Kroll, D. M.: 2001, Stochastic rotation dynamics: A galilean-invariant mesoscopic model for fluid flow, *Physical Review E* **63**(2), 020201.

Inoue, Y., Chen, Y. and Ohashi, H.: 2001, Development of a simulation model for solid objects suspended in a fluctuating fluid, *Computer Physics Communications* **142**, 114–116.

Jayne, B. C. and Lauder, G. V.: 1995, Speed effects on midline kinematics during steady undulatory swimming of largemouth bass, *micropterus-salmoides*, *Journal of Experimental Biology* **198**(2), 585–602.

Kajtar, J. and Monaghan, J.: 2008, Sph simulations of swimming linked bodies, *Journal of Computational Physics* **227**(19), 8568–8587.

Kelly, S. D. and Murray, R. M.: 2000, Modelling efficient pisciform swimming for control, *International Journal of Robust and Nonlinear Control* **10**, 217–241.

Kern, S. and Koumoutsakos, P.: 2006, Simulations of optimized anguilliform swimming, *Journal of Experimental Biology* **209**, 4841–4857.

Kikuchi, N., Pooley, C. M., Ryder, J. F. and Yeomans, J.: 2003, Transport coefficients of a mesoscopic model, *Journal of Chemical Physics* **119**, 6388–6395.

Krause, J. and Ruxton, G. D.: 2002, *Living in Groups*, Oxford University Press.

Kwon, K. and Choi, H.: 1996, Control of laminar vortex shedding behind a circular cylinder using splitter plates, *Physics of Fluids* **8**, 479–486.

Lamura, A. and Gompper, G.: 2002, Numerical study of the flow around a cylinder using multi-particle collision dynamics, *European Physical Journal E* **9**, 477–485.

Lamura, A., Gompper, G., Ihle, T. and Kroll, D. M.: 2001, Multi-particle collision dynamics: Flow around a circular and a square cylinder, *Europhysics Letters* **56**, 319–325.

Langerhans, R. B.: 2009, Trade-off between steady and unsteady swimming underlies predator-driven divergence in *g*ambusia affinis, *Journal of Experimental Biology* **22**, 1057–1075.

Lauder, G. V. and Tytell, E. D.: 2006, Hydrodynamics of undulatory propulsion, *Fish Physiology* **23**, 425–468.

Lentink, D., Dickinson, W. B., Leeuwen, J. L. v. and Dickinson, M. H.: 2009, Leading-edge vortices elevate lift of autorotating plant seeds, *Science* **324**, 1438–1440.

Liao, J. C.: 2002, Swimming in needlefish (belonidae): anguilliform locomotion with fins, *Journal of Experimental Biology* **205**(18), 2875–2884.

Liao, J. C.: 2006, The role of the lateral line and vision on body kinematics and hydrodynamic preference of rainbow trout in turbulent flow, *Journal of Experimental Biology* **209**, 4077–4090.

Liao, J. C.: 2007, A review of fish swimming mechanics and behaviour in altered flows, *Philosophical Transactions of the Royal Society B* **362**, 1973–1993.

Liao, J. C., Beal, D. N., Lauder, G. V. and Triantafyllou, M. S.: 2003a, Fish exploiting vortices decrease muscle activity, *Science* **302**, 1566–1569.

Liao, J. C., Beal, D. N., Lauder, G. V. and Triantafyllou, M. S.: 2003b, The kármán gait: novel body kinematics of rainbow trout swimming in a vortex street, *Journal of Experimental Biology* **206**, 1059–1073.

Lighthill, J.: 1960, Note on the swimming of slender fish, *Journal of Fluid Mechanics* **9**, 305–317.

Lighthill, M. J.: 1971, Large-Amplitude Elongated-Body Theory of Fish Locomotion, *Proceedings of the Royal Society of London, Series B* **179**, 125–138.

Lighthill, M. J.: 1975, *Mathematical Biofluiddynamics*, Society for Industrial and Applied Mathematics.

Liu, H., Wassersug, R. J. and Kawachi, K.: 1996, A computational fluid dynamics study of tadpole swimming, *Journal of Experimental Biology* **199**, 1245–1260.

Liu, H., Wassersug, R. and Kawachi, K.: 1997, The three-dimensional hydrodynamics of tadpole locomotion, *Journal of Experimental Biology* **200**, 2807–2819.

Long, J. H. and Nipper, K. S.: 1996, The importance of body stiffness in undulatory propulsion, *American Zoologist* **36**(6), 678–694.

Malevanets, A. and Kapral, R.: 1998, Continuous-velocity lattice-gas model for fluid flow, *Europhysics Letters* **44**, 552–558.

Malevanets, A. and Kapral, R.: 1999, Mesoscopic model for solvent dynamics, *Journal of Chemical Physics* **110**, 8605–8613.

Malevanets, A. and Kapral, R.: 2000, Solute molecular dynamics in a mesoscale solvent, *Journal of Chemical Physics* **112**, 7260–7269.

McMillen, T. and Holmes, P.: 2006, An elastic rod model for anguilliform swimming, *Journal of Mathematical Biology* **53**, 843–886.

Mittal, R.: 2004, Computational modeling in biohydrodynamics: Trends, challenges, and recent advances, *IEEE Journal of Oceanic Engineering* **29**, 595–604.

Monaghan, J. J.: 1992, Smoothed particle hydrodynamics, *Annual Review of Astronomy and Astrophysics* **30**, 543–574.

Müller, U. K., Smit, J., Stamhuis, E. J. and Videler, J. J.: 2001, How the body contributes to the wake in undulatory fish swimming: Flow fields of a swimming eel (*Anguilla anguilla*), *Journal of Experimental Biology* **204**, 2751–2762.

Müller, U. K., Stamhuis, E. J. and Videler, J. J.: 2000, Hydrodynamics of unsteady fish swimming and the effects of body size: Comparing the flow fields of fish larvae and adults, *Journal of Experimental Biology* **203**, 193–206.

Müller, U. K., Stamhuis, E. J. and Videler, J. J.: 2002, Riding the waves: the role of the body wave in undulatory fish swimming, *Integrative and Comparative Biology* **42**, 981–987.

Müller, U. K., van den Boogaart, J. G. M. and van Leeuwen, J. L.: 2008, Flow patterns of larval fish: undulatory swimming in the intermediate flow regime, *The Journal of Experimental Biology* **211**, 196–205.

Müller, U. K., van den Heuvel, B. L. E., Stamhuis, E. J. and Videler, J. J.: 1997, Fish foot prints: Morphology and energetics of the wake behind a continuously swimming mullet (*Chelon labrosus risso*), *Journal of Experimental Biology* **200**, 2893–2906.

Müller, U. K. and van Leeuwen, J. L.: 2004, Swimming of larval zebrafish: ontogeny of body waves and implications for locomotory development, *Journal of Experimental Biology* **207**(5), 853–868.

Müller, U. K. and Videler, J. J.: 1996, Inertia as a 'safe harbour': do fish larvae increase length growth to escape viscous drag?, *Reviews in Fish Biology and Fisheries* **6**, 353–360.

Noguchi, H. and Gompper, G.: 2005, Shape transitions of fluid vesicles and red blood cells in capillary flows, *Proceedings of the National Academy of Sciences* **102**, 14159–14164.

Packard, G. C. and Boardman, T. J.: 1999, The use of percentages and size-specific indices to normalize physiological data for variation in body size: wasted time, wasted effort?, *Comparative Biochemistry and Physiology a-Molecular and Integrative Physiology* **122**(1), 37–44.

Padding, J. T. and Louis, A. A.: 2004, Hydrodynamic and brownian fluctuations in sedimenting suspensions, *Physical Review Letters* **93**, 22601.

Padding, J. T. and Louis, A. A.: 2006, Hydrodynamic interactions and brownian forces in colloidal suspensions: Coarse-graining over time and length scales, *Physical Review E* **74**, 031402.

Paranthoën, P., Browne, L. W. B., Le Masson, S., Dumouchel, F. and Lecordier, J. C.: 1999, Characteristics of the near wake of a cylinder at low Reynolds numbers, *European Journal of Mechanics - B/Fluids* **18**, 659–674(16).

Partridge, B. L. and Pitcher, T. J.: 1979, Evidence against a hydrodynamic function for fish schools, *Nature* **279**, 418–419.

Partridge, B. L. and Pitcher, T. J.: 1980, The sensory basis of fish schools: relative roles of lateral line and vision, *Journal of Comparative Physiology* **135**, 315–325.

Pedley, T. J. and Hill, S. J.: 1999, Large-amplitude undulatory fish swimming: Fluid mechanics coupled to internal mechanics, *Journal of Experimental Biology* **202**, 3431–3438.

Peskin, C. S.: 2002, The immersed boundary method, *Acta Numerica* **11**, 479–517.

Pfeifer, R. and Scheier, C.: 1999, *Understanding Intelligence*, MIT Press, Cambridge, MA, USA.

Pohlmann, K., Grasso, F. W. and Breithaupt, T.: 2001, Tracking wakes: The nocturnal predatory strategy of piscivorous catfish, *Proceedings of the National Academy of Sciences of the United States of America* **98**, 7371–7374.

Reid, D. A. P., Hildenbrandt, H., Padding, J. T. and Hemelrijk, C. K.: 2009, Flow around fishlike shapes studied using multiparticle collision dynamics, *Physical Review E* **79**, 046313.

Reid, D. A. P., Hildenbrandt, H., Padding, J. T. and Hemelrijk, C. K.: 2011, Fluid dynamics of moving fish in a two-dimensional multiparticle collision dynamics model. in review.

Reynolds, O.: 1883, An experimental investigation of the circumstances which determine whether the motion of water shall be direct or sinuous, and of the law of resistance in parallel channels, *Philosophical Transactions of the Royal Society* **174**, 935–982.

Ripoll, M., Mussawisade, K., Winkler, R. G. and Gompper, G.: 2004, Low-Reynolds-number hydrodynamics of complex fluids by multi-particle-collision dynamics, *Europhysics Letters* **68**, 106–112.

Ripoll, M., Winkler, R. G. and Gompper, G.: 2006, Star polymers in shear flow, *Physical Review Letters* **96**, 188302.

Roper, M. and Brenner, M. P.: 2009, A nonperturbative approximation for the moderate reynolds number navier–stokes equations, *Proceedings of the National Academy of Sciences of the USA* **106**(9), 2977–2982.

Sakai, T., Chen, Y. and Ohashi, H.: 2000, Formation of micelle in the real-coded lattice gas, *Computer Physics Communications* **129**, 75–81.

Sane, S. P. and Dickinson, M. H.: 2002, The aerodynamic effects of wing rotation and a revised quasi-steady model of flapping flight, *J Exp Biol* **205**(8), 1087–1096.

Schultz, W. W. and Webb, P. W.: 2002, Power Requirements of Swimming: Do New Methods Resolve Old Questions?, *Integr. Comp. Biol.* **42**(5), 1018–1025.

Shao, J., Wang, L. and Yu, J.: 2008, Development of an artificial fish-like robot and its application in cooperative transportation, *control Engineering Practice* **13**, 569–584.

Shaw, E.: 1978, Schooling fishes, *American Scientist* **66**, 166–175.

Stamhuis, E. J. and Videler, J. J.: 1995, Quantitative flow-analysis around aquatic animals using laser sheet particle image velocimetry, *Journal of Experimental Biology* **198**, 283–294.

Stamhuis, E. J., Videler, J. J., van Duren, L. A. and Müller, U. K.: 2002, Applying digital particle image velocimetry to animal-generated flows: Traps, hurdles and cures in mapping steady and unsteady flows in Re regimes between 10(-2) and 10(5), *Experiments In Fluids* **33**, 801–813.

Sui, Y., Chew, Y.-T., Roy, P. and Low, H.-T.: 2007, A hybrid immersed-boundary and multi-block lattice boltzmann method for simulating fluid and moving-boundaries interactions, *International Journal for Numerical Methods in Fluids* **53**, 1727–1754.

Sun, M. and Tang, J.: 2002, The effects of wings rotation on unsteady aerodynamic performance at low Reynolds numbers, *Journal of Experimental Biology* **205**, 2413–2427.

Svendsen, J. C., Skov, J., Bildsoe, M. and Steffensen, J. F.: 2003, Intra-school positional preference and reduced tail beat frequency in trailing positions in schooling roach under experimental conditions, *Journal of fish biology* **62**, 834–846.

Taneda, S.: 1956, Experimental investigation of the wake behind a sphere at low Reynolds numbers, *Journal of the Physical Society of Japan* **11**, 1104–1108.

Taylor, G.: 1952, Analysis of the swimming of long and narrow individuals, *Proceedings of the Royal Society of London, Series A, Mathematical and Physical Sciences* **214**, 158–183.

The MathWorks: n.d., Matlab r2006a.

Triantafyllou, G. S., Triantafyllou, M. S. and Grosenbaugh, M. A.: 1993, Optimal thrust development in oscillating foils with application to fish propulsion, *Journal of Fluids and Structures* **7**, 205–224.

Triantafyllou, M. S., Triantafyllou, G. S. and Gopalkrishnan, R.: 1991, Wake mechanics for thrust generation in oscillating foils, *Physics of Fluids a-Fluid Dynamics* **3**(12), 2835–2837.

Tritton, D. J.: 1959, Experiments on the flow past a circular cylinder at low Reynolds numbers, *Journal of Fluid Mechanics* **6**, 547.

Tytell, E. D.: 2004, The hydrodynamics of eel swimming, II. Effect of swimming speed, *Journal of Experimental Biology* **207**, 3265–3279.

Tytell, E. D.: 2007, Do trout swim better than eels? challenges for estimating performance based on the wake of self-propelled bodies, *Experiments in Fluids* **43**, 701–712.

Tytell, E. D. and Lauder, G. V.: 2004, The hydrodynamics of eel swimming, I. Wake structure, *Journal of Experimental Biology* **207**, 1825–1841.

Tytell, E. D. and Lauder, G. V.: 2008, Hydrodynamics of the escape response in bluegill sunfish, *Lepomis macrochirus*, *Journal of Experimental Biology* **211**, 3359–3369.

van Duren, L. A., Stamhuis, E. J. and Videler, J. J.: 2003, Copepod feeding currents: flow patterns, filtration rates and energetics, *Journal of Experimental Biology* **206**, 225–267.

van Weerden, F., Reid, D. A. P. and Hemelrijk, C. K.: 2011, A meta-analysis of fish swimming. in review.

Videler, J. J.: 1993, *Fish Swimming*, Chapman and Hall, London, GB.

Videler, J. J. and Hess, F.: 1984, Fast continuous swimming of 2 pelagic predators, saithe (*p*ollachius virens) and mackerel (*s*comber scombrus) - a kinematic analysis, *Journal of Experimental Biology* **109**, 209–228.

Vogel, S.: 1996, *Life in Moving Fluids*, Princeton University Press.

Walker, J. A., Ghalambor, C. K., Griset, O. L., McKenney, D. and Reznick, D. N.: 2005, Do faster starts increase the probability of evading predators?, *Functional Ecology* **19**, 808–815.

Wang, Z. J., Birch, J. M. and Dickinson, M. H.: 2004, Unsteady forces and flows in low reynolds number hovering flight: two-dimensional computations vs robotic wing experiments, *Journal of Experimental Biology* **207**, 449–460.

Wardle, C. S., Videler, J. J. and Altringham, J. D.: 1995, Tuning in to fish swimming waves - body form, swimming mode and muscle function, *Journal of Experimental Biology* **198**, 1629–1636.

Watari, N., Makino, M., Kikuchi, N., Larson, R. G. and Doi, M.: 2007, Simulation of DNA motion in a microchannel using stochastic rotation dynamics, *Journal of Chemical Physics* **126**, 094902.

Webb, P. W.: 1971, The Swimming Energetics of Trout: II. Oxygen Consumption and Swimming Efficiency, *J Exp Biol* **55**(2), 521–540.

Webb, P. W.: 1975, Hydrodynamics and energetics of fish propulsion, *Fisheries Research Board of Canada Bulletin* **190**, 1–159.

Webb, P. W.: 1984, Form and function in fish swimming, *Scientific American* **251**, 72–82.

Webb, P. W.: 1988, Steady swimming kinematics of tiger musky, an esociform accelerator, and rainbow-trout, a generalist cruiser, *Journal of Experimental Biology* **138**, 51–69.

Webb, P. W.: 2002, Kinematics of plaice, *pleuronectes platessa*, and cod, *gadus morhua*, swimming near the bottom, *Journal of Experimental Biology* **205**(14), 2125–2134.

Webb, P. W., Kostecki, P. T. and Stevens, E. D.: 1984, The effect of size and swimming speed on locomotor kinematics of rainbow-trout, *Journal of Experimental Biology* **109**, 77–95.

Wei, T., Legac, P., Fish, F. E., Williams, T., Mark, R. and Hutchison, S.: 2008, Mechanics of mammalian swimming, Presented at March Meeting of the American Physical Society.

Weihs, D.: 1973, Hydromechanics of fish schooling, *Nature* **241**, 290–291.

Weihs, D.: 1975, *Swimming and Flying in Nature*, Plenum Press, New York, chapter Some hydrodynamical aspects of fish schooling, pp. 703–718.

Weihs, D.: 1980, Energetic significance of changes in swimming modes during growth of larval anchovy, *e*ngraulis mordax, *Fishery Bulletin* **77**, 597–604.

Weimerskirch, H., Martin, J., Clerquin, Y., Alexandre, P. and Jiraskova, S.: 2001, Energy saving in flight formation, *Nature* **413**, 697–698.

Wolfgang, M. J., anderson, J. M., Grosenbaugh, M. A., Yue, D. K. P. and Triantafyllou, M. S.: 1999, Near-body flow dynamics in swimming fish, *Journal of Experimental Biology* **202**, 2303–2327.

Wu, M. H., Wen, C. Y., Yen, R. H. O. R., Weng, M. C. and Wang, A. N. B.: 2004, Experimental and numerical study of the separation angle for flow around a circular cylinder at low Reynolds number, *Journal of Fluid Mechanics* **515**, 233–260.

Wu, T. Y.: 1961, Swimming of a waving plate, *Journal of Fluid Mechanics* **10**, 321–344.

Yang, Y., Elgeti, J. and Gompper, G.: 2008, Cooperation of sperm in two dimensions: Synchronization, attraction, and aggregation through hydrodynamic interactions, *Physical Review E (Statistical, Nonlinear, and Soft Matter Physics)* **78**(6), 061903.

Zhang, L. J. and Eldredge, J. D.: 2010, Hydrodynamics of undulatory fish schooling in lateral configurations.
URL: *arXiv:1003.4441v1*